Morphology and properties of sol-gel prepared LDPE silica nanocomposites

by

TSHWAFO ELIAS MOTAUNG (B.sc. Honours)
2002144398

Submitted in accordance with the requirements of the degree

Masters of Science (M.Sc.)

Department of Chemistry

Faculty of Natural and Agricultural Science

at the

UNIVERSITY OF THE FREE STATE (QWAQWA CAMPUS)

SUPERVISOR: PROF AS LUYT

May 2009

DECLARATION

We, the undersigned, hereby declare that the research in this thesis is Mr Motaung's own original work, which has not partly or fully been submitted to any other University in order to obtain a degree.

Motaung TE (Mr)

Luyt AS (Prof)

1. ***Dear PhD. I have heard there are troubles of more than one kind. Some come from ahead and some come from behind. But I've bought a big bat. I'm all ready you see. Now my troubles are going to have troubles with me!***

2. ***Instead of giving myself reasons why I can't, I give myself reasons why I can.***

3. ***If one of my dreams should fall and break into a thousand pieces, I will never be afraid to pick one of those pieces up and begin again. "***

ABSTRACT

Blending of polymers is an effective way to manufacture materials with specific properties. Nanofillers play an important role to enhance the thermal and mechanical properties of the polymers. In our work, LDPE and LDPE-g-MA based nanocomposites were prepared using sol-gel derived nanosilica. LDPE was grafted with maleic anhydride to introduce functional groups that could interact with nanosilica. Oxidized paraffin wax was also introduced into the nano-composites as possible compatibilizer. The thermal, mechanical and thermomechanical properties of the nanocomposites were investigated using differential scanning calorimetry (DSC), thermogravimetric analysis (TGA), tensile testing, and dynamic mechanical analysis (DMA). Fourier transform infrared spectroscopy (FTIR), scanning electron microscopy (SEM) and transmission electron microscope (TEM) were employed to determine the morphologies of the composites. FTIR, TEM and SEM analyses of LDPE-g-MA/silica, LDPE-g-MA/wax and LDPE-g-MA/wax/silica samples showed that there was an interaction between the different components and a reduction in silica agglomeration compared to the LDPE-based samples. Generally, the total sample crystallinity increased with an increase in wax content, but the crystallinities of the composites depended on the interactions between the components and the resulting sample morphology. In the case of LDPE the presence of wax reduced the thermal stabilities of the samples, but the presence of silica had little influence. The presence of wax as well as silica had little influence on the thermal stability of LDPE-g-MA, but the LDPE-g-MA/wax/silica composites showed a reduction in thermal stability with increasing wax content. Changes in the tensile properties with addition of silica nano-particles, and with increasing wax content in the samples, reflected the interactions between the different components and the resulting sample morphologies. The DMA results of all the composites and blends show that the presence of silica nanoparticles and wax, as well as the interactions between the different components, had an observable influence on the sample morphology and mobility of the polymer chains.

OPSOMMING

Vermenging van polimere is 'n effektiewe manier om materiale met spesifieke eienskappe te vervaardig. Nanovullers vervul 'n belangrike rol om die termiese en meganiese eienskappe van polimere te verbeter. In ons werk is LDPE en LDPE-g-MA gebaseerde nano-komposiete berei deur sol-gel bereide nano-silika te gebruik. LDPE is geënt met maleïensuur anhidried om funksionele groepe, wat met silika 'n wisselwerking kan hê, daar te stel. Geoksideerde paraffienwas is ook in die nano-komposiete ingemeng om verenigbaarheid te bewerkstellig. Die termiese, meganiese en termo-meganiese eienskappe van die nano-komposiete is ondersoek deur gebruik te maak van differensiaal skandeer kalorimetrie (DSC), termo-grawimetriese analise (TGA), treksterkte toetsing en dinamies meganiese analiese (DMA). Fourier transform infrarooi spektroskopie (FTIR), skandeer elektron mikroskopie (SEM) en transmissie elektron mikroskopie (TEM) is gebruik om die morfologieë van die komposiete te bepaal. FTIR, TEM en SEM analyses van LDPE-g-MA/silika, LDPE-g-MA/was en LDPE-g-MA/was/silika monsters het getoon dat daar 'n interaksie tussen die verskillende komponente en 'n afname in silica opeenhoping vergeleke met die LDPE-gebaseerde monsters was. Oor die algemeen het die totale monster-kristalliniteit toegeneem met 'n toename in was-inhoud, maar die kristalliniteite van die komposiete het afgehang van die interaksies tussen die komponente en die gevolglike monster morfologie. In die geval van LDPE het die teenwoordigheid van was die termiese stabiliteite van die monsters laat afneem, maar die teenwoordigheid van silika het min invloed gehad. Die teenwoordigheid van was sowel as silika het min invloed op die termiese stabiliteit van LDPE-g-MA gehad, maar die LDPE-g-MA/was/silika komposiete het 'n afname in termiese stabiliteit met toenemende was-inhoud getoon. Veranderinge in die treksterkte eienskappe met die byvoeging van silika nano-deeltjies, en met toenemende was-inhoud in die monsters, het die interaksies tussen die verskillende komponente en die gevolglike monster morfologieë gereflekteer. Die DMA resultate van al die komposiete en mengsels toon dat die teenwoordigheid van silika nano-deeltjies en was, sowel as die interaksies tussen die verskillende komponente, 'n opsigtelike invloed op die monster morfologie en beweeglikheid van die polimeerkettings gehad het.

LIST OF ABBREVIATIONS

CRYSTAF	Crystallization fractionation
DCP	Dicumyl peroxide
DMA	Dynamic mechanical analysis
DSC	Differential scanning calorimetry
FTIR	Fourier transform infrared spectroscopy
HDPE	High density polyethylene
LDPE	Low-density polyethylene
LDPE-g-MA	Maleic anhydride grafted low-density polyethylene
LLDPE	Linear low-density polyethylene
MFI	Melt flow index
OMMT/Org-MMT	Organically modified Montmorillonite
PE	Polyethylene
PE-g-MA	Maleic anhydride grafted polyethylene
PP-g-MA	Maleic anhydride grafted polypropylene
PMMA	Poly(methyl methacrylate)
PP	Polypropylene
SEM	Scanning electron microscopy
TGA	Thermogravimetric analysis
TEM	Transmission electron microscopy
TEOS	Tetraethoxysilane
XRD	X-ray diffraction

TABLE OF CONTENTS

ACKNOWLEDGEMENTS

I really want to thank all who assisted me during the course of the research and preparation of this thesis. In particular, my special thanks are due to:

- My supervisor, Prof AS Luyt for his dedicated, scientific and patient guidance in the analysis of all my results and the difficulty of the project.
- Dr V Djokovic, for assisting with interpretation of DMA results.
- The NRF and the University of the Free State for funding the project.
- My parents (Madinkeng Tshabalala Motaung Sarah, and my late father (John Motaung), grand-parents and my siblings (Ausi Dinkeng, Shakes, Mafina, Mmathasi, Thato and Tumi).
- My close friends (Mr Lulu Samson Mohomane, Mr Mfiso Mngomezulu, Mr Funeral Lefu Nhlapo, Ms Julia Puseletso Mofokeng, Mr Jeremia Sefadi, Mr Thabang. Mokhothu, Mr Bongi Tshabalala, Mr Thabo Phelephe, Mr Tsietsi Tsotetsi, Dr Spirit Molefi, Spirit Nkomo, and Phoka Mohau Mofokeng)
- The former and the current chemistry research group and department in general.
- The blue Golf 4, 1.8 Highline 1999 (Mahoota v/s vatkook "*Phuli Qolo*"). Thanks Ntate Moji (*O ya tseba!!!!*).
- Finally, I thank God.

LIST OF TABLES

LIST OF FIGURES

CHAPTER 1

GENERAL INTRODUCTION

1.1 Background

In recent years, there has been extensive research on nanoparticles incorporated into polymer composites and its influence on the material properties. Some research focused on particle size effects. It was found that the importance of using nanoparticles in composites is that they have special size-dependant specific properties, such as improved flame retardency, better dimensional stability and stiffness, while the favorable properties of the pristine polymer remain preserved in the composites [1-6]. In addition, nanofibers, nanotubes and nanowires have many potential applications such as solid state lubricants, catalysts and components of magnetic devices [7,8].

Incorporating particulate inorganic fillers with very low loading levels into polymeric materials also improves the mechanical, electrical, thermal, chemical resistance, surface appearance, optical clarity and processing properties suitable to replace weighty metals and other composite materials in many applications [9-11]. Nanosized fillers have capabilities to improve these properties even more on account of much larger surface areas and stronger interfacial interaction with the adjacent polymer phase [12,13]. Nanoparticles can be both natural and synthetic. Synthetic nanoparticles are artificially manufactured particles smaller than 100 nm in size. These are also referred to as engineered nanoparticles or nanosized particles. The terms ultrafine particles, nucleation mode particles and engineered nanostructured material are also used. However, natural nanoparticles refer to nanoparticles that are non-artificial such as soot and clay. Soot is used as filler in rubber compounds, primarily in automobile tires. Clays are also used as fillers in polymer-clay nanocomposites [14, 15].

Nanoparticles are produced by various deposition methods like solvent evaporation and sol-gel techniques. Solvent evaporation can be used to synthesize polymer nanoparticles or to incorporate nanoparticles in a polymer matrix [16, 17]. Typical solvent evaporation is based on the emulsification of an organic solution of a polymer in an aqueous phase followed by the evaporation of the organic solvent. This leads to the precipitation of the polymer as

nanoparticles of a few hundred nanometers in diameter. Alternatively, solid nano-particles can be thoroughly dispersed in a polymer solution, followed by solvent evaporation. In our work a sol-gel technique was used for nanoparticles preparation. Sol-gel processing is a wet chemical synthesis approach that can be used to generate nanoparticles by gelation, precipitation, and hydrothermal treatment. Sol-gel processing has recently received increasing attention from both the research community and industry. This is primarily because it is a versatile method for synthesizing ceramics, organic/inorganic hybrids, and nanocomposites in the form of particles, fibres, films or coatings, and monoliths. Sol-gel techniques are associated with low processing temperatures, high transparency and the availability of suitable precursors. Sol-gel derived inorganic-organic (hybrid) molecular composites are used in a wide range of applications, such as laser optics, data storage, antiscratch and antireflective coatings [18-20].

There are many types of nanoparticles (titinia, alumina, silica and others) that can be prepared by sol-gel methods [21-24]. These nanoparticles can be incorporated in a polymer matrix through melt mixing using a twin-screw co-rotating extruder or solution mixing. That led to improved properties of the organic and inorganic components as a result of particle size and dispersion quality [25]. In our work, we used the melt-mixing technique, because it is easier, cheaper, and technologically more feasible than solution mixing. The industrial use of silica is well established. The further processing of silica nanoparticles permits their use in ceramics, chromatography, catalysis, and chemical mechanical polishing. Precursor silica particles have been used in stabilizers, coatings, glazes, emulsifiers, strengtheners, and binders. The need for well-defined silica nanoparticles has increased, as high-tech industries (e.g. computer and biotechnology/pharmaceuticals) provide an increased demand for such materials [26,27]. Silica nanoparticles are effective reinforcements for polymers to give improved notch toughness and enhanced tensile performance, as well as improved thermal properties, of the polymers [27-30].

Silica-polymer hybrids manufactured by a sol-gel process are frequently nanocomposites, with phase sizes on the nanometer scale. However, the use of silica is restricted because of the dispersion quality of the nanofillers, which is the result of agglomeration leading to poor adhesion [33, 34]. It was found that interaction which results in agglomerates may lead to lowering of tensile strength and induction of local stress concentrations in the composites, which results in poor properties [35]. This may be due to the hydrophobic nature of some

polymers like polyethylenes, which gives rise to poorer adhesion between the hydrophilic nanofiller and the matrix, so that the bonds between the polymer matrix and the filler are weak. Better dispersion can be obtained by using one of a number of techniques e.g. *in situ* polymerization of monomers in the presence of nanoparticles, use of compatibilizers, modification of nanoparticles with coupling agents like silane coupling, or graft polymerization. Although most of these techniques provide satisfactory dispersion of the nanoparticles, they are characterized by complex polymerization and processing conditions, which add to the high cost of the nanoparticles [36]. Grafting of polymers is the most favored method because of its ease of operation and low cost. It was found that grafted polyethylenes are effective compatibilizers, show satisfactory corrosion resistance, advanced particle dispersion and better adhesion [37-40].

It is possible to blend a paraffin wax with the polymer to improve its processability Because oxidized paraffin wax is very miscible with polyethylenes, it may also improve the interaction between the hydrophobic polymer and the hydrophilic silica nanoparticles. In previous research, polyethylenes blended with different waxes have been extensively investigated [41-44]. In our work, oxidized paraffin wax was also used as a possible compatibilizer. Oxidized paraffin wax consists of a mixture of solid hydrocarbons that were oxidized in the molten state with air. Previous studies showed that the wax is strongly miscible with polyethylene and has a plasticizing effect on the polymer [45-47].

Low density polyethylene is used in an ever growing range of applications. However, the non-polar characteristics of LDPE give rise to poor adhesion, and therefore it is not very suitable for anticorrosive coating applications. Maleic anhydride-grafted polyethylenes (LDPE-g-MAH) are often used as compatibilizers to overcome problems associated with poor phase adhesion in polymer nanocomposite systems. It was found that grafted polyethylenes are effective compatibilizers, show satisfactory corrosion resistance, advanced particle dispersion, and better adhesion. It also accelerates the nonisothermal crystallization process of PE, contributes to a significant increase in the tensile strength and wear resistance of ultra high molecular weight polyethylene, but it decreases the melting points and crystallinities of composites [37-40,49-51]. In this work, LDPE-g-MAH was used as a matrix, and not as a compatibilizer to try and improve the interaction between the matrix and the filler.

1.2 Objectives

The overall objective of this research was to study the influence of silica on the thermal and mechanical properties of low-density polyethylene (LDPE). Maleic anhydride grafted low-density polyethylene (LDPE-g-MAH) was also used as matrix to see if maleic anhydride grafting would improve the interaction of the matrix with the silica nanoparticles. LDPE was also blended with oxidized paraffin wax to see if functionalized paraffin chains will improve LDPE-silica interaction. LDPE-g-MA was prepared through reactive mixing, and nano-silica, prepared through a sol-gel method, was mixed with respectively LDPE, LDPE-g-MA and LDPE/oxidized paraffin wax blend. The samples were characterized using differential scanning calorimetry (DSC), thermogravimetric analysis (TGA), transmission electron microscopy (TEM), scanning electron microscopy (SEM), dynamic mechanical analysis (DMA), fourier-transform infrared spectroscopy (FTIR) and tensile testing.

1.3 Outline of the thesis

This manuscript comprises of five chapters:

Chapter 1: Background and objectives
Chapter 2: Literature survey
Chapter 3: Experimental
Chapter 4: Results and discussion
Chapter 5: Conclusion

1.4 References

1. Y. Kojima, A. Usuki, M. Kawasumi, A. Okada, Y. Fukushima, T. Kurauchi, O. Kamigaito. Mechanical properties of nylon 6-clay hybrid. Journal of Materials Research (1993) 8:1185-1189.
2. H. Cong, M. Radosz, B.F. Towler, Y. Shen. Polymer-inorganic nanocomposite membranes for gas separation. Separation and Purification Technology (2007) 55:281-291.
3. P. Pandey, R.S. Chauhan. Membranes for gas separations. Progress in Polymer Science (2001) 26:853-893.

4. G. Maier. Gas separations with polymer membranes. Angewandte Chemie International Edition (1998) 37:2960-2974.
5. Ź. Andrić, M.D. Dramićanin, V. Jokanović, T. Dramićanin, M. Mitrić, B. Viana. Luminescent properties of nano-SiO_2:Eu3+/polypropylene composite. Journal of Optoelectronics and Advanced Materials (2006) 8:829-834.
6. G. Kickelbick. Concepts for the incorporation of inorganic building blocks into organic polymers on a nanoscale. Progress in Polymer Science (2003) 28:83-114.
7. F. Liao, S. Park, J.M. Larson, M.R. Zachariah, S.L. Grishick. High-rate chemical vapor deposition of nanocrystalline silicon carbide films by radio frequency thermal plasma. Materials Letters (2003) 57:1982-1986.
8. Y.Q. Zhu, H.W. Kroto, D.R.M. Walton, H. Lange, A. Huczko. A systematic study of ceramic nanostructures generated by arc discharge. Chemical Physics Letters (2002) 365:457-463.
9. L.N. Xu, K.C. Zhou, S.L. Xie, L. Huang, N. Gu. SAMs-dected Metallization and its Application in Fabrication of Core-Shell nanocomposites. Solid State Phenomena (2007) 121-123:731-734.
10. P. Hui, Z.Z. Jun, D. Hong Xin. Preparation and application of a nanocomposite (MPNS/SMA) in leather making. Chinese Chemical Letters (2005) 16:1409-1412.
11. A.H. Rohan, D.J. Pochan. Poly (L-lysine) and clay nanocomposite with desired matrix secondary structure: Effects of polypeptide molecular weight. Journal of Polymer Science: Part B: Polymer Physics (2007) 45:239-252.
12. M.Q. Zhang, M.Z. Rong, H.B. Zhang, K. Friedrich. Structure-property relationships of irradiation grafted nano-inorganic particle filled polypropylene composites. Polymer (2001) 42:167-183.
13. C.H. Jeon, S.H. Ryu, Y.W. Chang. Preparation and characterization of ethylene vinyl acetate copolymer/montmorilllonite nanocomposite. Polymer International (2003) 52:153-157.
14. B. Nowack, T.D. Bucheli. Occurence, behaviour and effect of nanoparticles in the environment. Environmental Pollution (2007) 150:5-22.
15. S. Desgouilles, C. Vauthier, D. Bazile, J. Vacus, J. Grossiord, M. Vellard, P. Couvreur. The design of nanoparticles obtained by solvent evaporation. Langmuir (2003) 19:9504-9510.

16. C. Note, S. Kosmella, J. Koetz. Poly (ethyleneimine) as reducing and stabilizing agent for the formation of gold nanoparticles in w/o microemulsions. Colloids and Surfaces A: Physicochemical and Engeneering Aspects (2006) 290:150-156.
17. Y.S. Bhole, S.D. Wanjale, U.K. Kharul, J.P. Jog. Assessing feasibility of polyarylate-clay nanocomposites towards improvement of gas selectivity. Journal of Membrane Science (2007) 306:277-286.
18. http://www.psrc.usm.edu/mauritz/solgel.html (15 April 2008).
19. http://optoweb.fis.uniroma2.it/opto/solgel/index.html (15 April 2008).
20. C. McDonagh, F. Sheridan, T. Butler, B.D. MacCraith. Characterisation of sol-gel-derived silica films. Journal of Non-Crystalline Solids (1996) 194:72-77.
21. A. Klukowska, U. Posset, G. Schottner, A. J. Frydel, V. Malatesta. Photochromic sol-gel derived hybrid polymer coatings: The influence of matrix properties on kinetics and photodegradation. Materials Science-Poland (2004) 22:188-199.
22. A. Mahlaba, M.C. Debeila, R.E. Mokoena, A. Miguel, P. Vitalii, J.C. Neil, S. Scurrell. The influence of gold on the optical properties of sol-gel derived titania. Materials Science and Engineering (2005) 396:70-76.
23. L.Z. Liu, B. Liang, W. Wang, Q.Q. Lei. Preparation of polyimide/inorganic nanoparticle hybrid films by sol-gel method. Journal of Composite Materials (2006) 40:2175-2183.
24. W.L. Qiu, Y.J. Luo, F.T. Chen, Y. Duo, H. Tan. Morphology and size control of inorganic particles in polyimide hybrids by using SiO_2-TiO_2 mixed oxide. Polymer (2003) 44:5821-5826.
25. K. Konopka, A. Biedunkiewicz, A. Boczkowska, Z. Roslaniec, K.J. Kurzydlowski. Polymer matrix composites with particles of TiC obtained by a sol-gel method. Solid State Phenomena (2005) 106:141-144.
26. V.M. Gun'ko, E.F. Voronin, V.I. Zarko, E.V. Goncharuk, V.V. Turov, S.V. Pakhovchishin, E.M. Pakhlov, N.V. Guzenko, R. Leboda, J.S. Zieba, W. Janusz, S. Chibowski, E. Chibowski, A.A. Chuiko. Interaction of poly(vinyl pyrrolidone) with fumed silica in dry and wet powders and aqueous suspensions. Physicochemical and Engeneering Aspects (2004) 233:63-78.
27. E.F. Voronin, V.M. Gunko, N.V. Guzenko, E.M. Pakhlov, L.V. Nosach, R. Leboda, J. S. Zieba, M.L. Malyshevac, M.V. Borysenko, A.A. Chuiko. Interaction of poly(ethylene oxide) with fumed silica. Journal of Colloid and Interface Science (2004) 279:326-340.
28. M. Preghenella, A. Peroretti, C. Migliaresi. Atomic force acoustic microscopy analysis of epoxy-silica nanocomposites. Polymer Testing (2006) 25:443-451.

29. L.Z. Liu, Y.T. Zhang, B.Liang. Q.Q. Lei. Characterization and preparation of nano-SiO_2/polyimide hybrid films. Journal of Harbin University of Science and Technology (2004) 9:99-101.
30. J.C. Tang, H.C. Yang, S.Y. Chen, Y.W. Chen-Yang. Preparation and properties of polyimide/silica hybrid nanocomposites. Polymer Composites (2007) 10:576-581.
31. P. Lee, S. Lien-Chung Hsu. Preparation and properties of polybenzoxazole-silica nanocomposites via sol-gel process. European Polymer Journal (2007) 43:294-299.
32. Y. Li, S.Y. Fu, Y.Q. Li, P. Qin-Yan, G. Xu, C.Y. Yue. Improvements in transmittance, mechanical properties and thermal stability of silica-polyimide composite films by a novel sol–gel route. Composites Science and Technology (2007) 67:2408-2416.
33. V. Vladimirov, C. Betchev, A. Vassiliou, G. Papageorgiou, D. Bikiaris. Dynamic mechanical and morphological studies of isotactic polypropylene/fumed silica nanocomposites with enhanced gas barrier properties. Composites Science and Technology (2006) 66:2935-2944.
34. K. Dutta, S.K. De. Optical and electrical characterization of polyaniline-silicon dioxide nanocomposite. Physics Letters A (2007) 361:141-145.
35. X. Zhang, W. Xu, X. Xia, Z. Zhang, R. Yu. Toughening of cycloaliphatic epoxy resin by nanosize silicon dioxide. Materials Letters (2006) 60:3319-3323.
36. M.U. Whait, A. Hassan, Z.A.M. Ishak, A.R. Rahmat, A.A. Bakar. Morphology, thermal and mechanical behavior of ethylene octene copolymer toughened polyamide 6/polypropylene nanocomposites. Themoplastic Composite Materials 19 :(2006) 545-566.
37. E. Kontou, M. Niaounakis. Thermo-mechanical properties of LLDPE/SiO_2 nanocomposites. Polymer (2006) 47:1267-1280.
38. N. Watanabe, I. Akiba, S. Akiyama. Compatibilizing effects of poly(styrene-*co*-methacrylic acid) on immiscible blends of polystyrene and poly(ethylene glycol). European Polymer Journal (2001) 37:1837-1842.
39. S.K. Singh, S.P. Tambe, A.B. Samui, V.S. Raja, D. Kumar. Maleic acid grafted low density polyethylene for thermally sprayable anticorrosive coatings. Progress in Organic Coatings (2006) 55:20-26.
40. M. Elsayed, A. Bary, M. Eman. Characterization and application of grafted acrylamide onto LDPE, EVA and LDPE/EVA films using gamma radiation. Radiation Physics and Chemistry (1996) 48:689-693.

41. M. Mirzataheri, J. Morshedian. Electron beam performance in the novel solventless LDPE–NVP surface grafting system. Radiation Physics and Chemistry (2006) 75:236-242.
42. I. Krupa, A.S. Luyt. Thermal properies of uncross-linked an cross-linked LLDPE/wax blends. Polymer Degradation and Stability (2000) 70:111-117.
43. I. Krupa, A.S. Luyt. Thermal and mechanical properties of extruded LLDPE/wax blends. Polymer Degradation and Stability (2001) 73:157-161.
44. I. Krupa, A.S. Luyt. Thermal properties of polypropylene/wax blends. Thermochimica Acta (2001) 372:137-141.
45. S.P. Hlangothi, I. Krupa, V. Djoković, A.S. Luyt. Thermal and mechanical properties of cross-linked and uncrosslinked linear low-density polyethylene–wax blends. Polymer Degradation and Stability (2003) 79:53-59.
46. I. Krupa, A.S. Luyt. Physical blends of LLDPE and an oxidised parrafin wax. Polymer (2001) 42:7285-7289.
47. A.S. Luyt, V.G. Geethamma. Effect of oxidized paraffin wax on the thermal and mechanical properties of linear low-density polyethylene-layered silicate nanocomposites. Polymer Testing (2007) 26:461-470.
48. H. Zhai, W. Xu, H. Guo, Z. Zhou, S. Shen, Q. Song. Preparation and characterization of PE and PE-g-MAH/montmorillonite nanocomposites. European Polymer Journal (2004) 40:2539-2545.
49. H. Yuan, P. Hu. Study of a compatibilized ultra-high molecular-weight polyethylene and polyurethane blend. Journal of Applied Polymer Science (2001) 81:3290-3295.
50. J. Zhou, F. Yan. Mechanical and tribology behavior of compatibilized ultra-high-molecular-weight polythylene/liqiud crystalline polymer composites. Polymer Testing (2004) 23:827-833.
51. G. Liang, J. Xu, W. Xu. PE/PE-g-MAH/Org-MMT nanocomposites. II. Nonisothermal crystallization kinetics. Journal of Applied Polymer Science (2004) 91:3054-3059.

CHAPTER 2

LITERATURE REVIEW

2.1 Introduction

Polymer nanocomposites show very interesting properties (mechanical, thermal, electrical, and magnetic) due to a significant increase in the interfacial area because of the small filler size. These properties broadened the scope of application in areas of plastics and rubber reinforcement, coatings, electronics, catalysis, and diagnostics [1-11]. One way to prepare polymer nanocomposites is through a sol-gel process. This type of preparation has been extensively studied and employed as the most important route in forming new hybrid inorganic-organic materials with improvement in particle dispersion quality [12].

Silica is one of the most important fillers and is mostly used in the modification of plastics and glasses. Its introduction into polymers to create organic-inorganic nanocomposites through a sol-gel process has been widely studied. The most prominent route to prepare these materials is the incorporation of inorganic building blocks in organic polymers through interpenetration of the organic polymers into the voids, or by exfoliation of the inorganic material. Though silica nanocomposites prepared by the sol-gel process have attracted a great deal of attention during the past decade, very few studies were devoted to the investigation of the mechanical properties of these materials.

2.2 Silica properties

The chemical compound, silicon dioxide, is one of the most regularly encountered materials in both daily life and in electronics manufacturing. It is also known as silica or silox with the chemical formula SiO_2. Crystalline silica is present in substantial quantities in sand, sandstone and granite, and often forms a significant proportion of clay, shale and slate. It can also be found in chalk, limestone and other rock and soil, though this is extraordinary. Products such as concrete and mortar also contain crystalline silica [13-16].

Silica preparation through the sol-gel method has been studied by various authors with tetraethoxysilane (TEOS) as silica precursor [17-24]. In these preparations TEOS was mixed

with water and alcohol keeping the ratio of TEOS:water:alcohol constant, and then stirred magnetically for about 8h to get a silica sol. This was then incorporated into the polymer matrix by dissolving the matrix with a suitable solvent and by mechanically mixing the sol into the matrix solution. The incomplete condensation of the Si-OH groups improved the optical, thermal and mechanical properties of the final hybrid material. Sugimoto *et al.* [25] studied PMMA-silica hybrid thin films synthesized through a versatile non-hydrolytic sol-gel process. However in this study the sol-gel technique was not applied, but they used colloidal silica dispersed in ethyl acetate and copolymerized in various ratios with methyl methacrylate. Song *et al.* [26], in a study of PMMA-silica hybrid thin films synthesized *via* a versatile non-hydrolytic sol-gel process, indicated that the remaining Si-OH groups have a negative influence on the transparency and thermal properties of the final hybrid material. It was shown from the study that incompatibility between organic polymers and inorganic oxides fillers such as silica, titania and zirconia is often based on the nature of the interface between the organic and inorganic components.

2.3 PE/clay nanocomposites

The polymer nanocomposites prepared by melt intercalation of polymer chains into the galleries of clay have been extensively investigated, because they often exhibit a wide range of improved properties over their bulk counterparts. A lot of work has been done on polyethylene/clay nanocomposites due to the broad applications field of polyethylene. From various works, it can be seen that the synthesis of polyethylene/clay nanocomposites can be through melt or solution intercalation of the polymer into the organically modified clay layers or by intercalation of clay layers by an initiator or catalyst, followed by *in situ* polymerization of the monomer [27-48].

Investigations of polyethylene/clay nanocomposites by melting and mixing, and by introducing compatibilizers, were studied by various authors. The pre-intercalated compound was mixed with PE at temperatures ranging from 165 to 180 °C for less than 10 minutes. To investigate the effects of clay content on the nanocomposites, nanocomposites with various clay contents were prepared. The compatibilizer quantity was kept constant during mixing for all the nanocomposites. The materials were characterized using X-ray diffraction (XRD), transmission electron microscopy (TEM), and scanning electron microscopy (SEM) for morphology. The X-ray diffraction (XRD) analysis observation depicted partial exfoliation

for small clay contents, and some intercalated layers were observed for higher clay contents. Both scanning electron microscopy (SEM) and transmission electron microscopy (TEM) showed well-dispersed nanoclays in the composites, but agglomerates were also observed in some samples [29,30,34,35,45,40,42-47,49].

There were also studies conducted on PE/clay nanocomposites without the introduction of compatibilizer. All the nanocomposites were prepared using melt blending in a Brabender mixer with temperatures ranging from 165 to 200 °C and operating time intervals 5-25 min. Clay contents ranged from 1 to 10% and rotation speeds from 30 to 60 rpm. Morphologies were characterized by XRD, TEM and SEM. Araújo *et al.* [31] investigated nanocomposites containing high density polyethylene (HDPE) and montmorillonite clay organically modified (OMMT) with quaternary ammonium salts through melt intercalation. They used different modified clays at a constant clay loading of 3%. They modified the clay by mixing it with three different types of salts. The nanocomposites were obtained by melt compounding in a counter-rotating twin screw extruder operating under the above mentioned conditions. From the XRD the authors observed that the quaternary ammonium salts were intercalated between two basal planes of MMT, leading to an expansion of the interlayer spacing and that the obtained PE/P-OMMT nanocomposites were partially intercalated. From both SEM and TEM well-dispersed nanoclays were observed in the composites, but in some samples aggregates were also observed. In most cases the morphology results were almost the same, regardless of clay type and preparation method [31,34-40].

Araújo *et al.* [31] used thermogravimetric analysis (TGA) to investigate the effect of organically modified clay on the thermal stability of HDPE/clay nanocomposites. They compared the degradation behavior of the samples in nitrogen and air atmospheres. There was generally an increase in the thermal stability for all the clay-containing samples. All the composites showed better thermal stability in nitrogen than in air atmosphere. The composites containing modified clay had a lower thermal stability than the HDPE/unmodified clay system. The reaction products as well as the clay itself catalyzed the degradation of the polymer. Polyethylene started to degrade at lower temperatures than the polyethylene nanocomposites, because the clay layers acted as effective diffusion barriers which lowered oxygen diffusion to the polymer matrix. Lee *et* al. [29], however, observed a clear decrease in the thermal stability of HDPE/clay nanocomposites with increasing clay content. Zhang *et al.* [34] had similar results with lauryl clay polyethylene nanocomposites, where the polyethylene

nanocomposites showed a lower onset temperature of degradation than the pristine polyethylene.

Lee *et al.* [29] studied HDPE/clay nanocomposites synthesized by melt intercalation using either PP-g-MA or PE-g-MA as a compatibilizer. Their DSC results showed an increase in melting temperature with increasing clay content, while the degree of crystallinity decreased. Zhai *et al.* [38] studied chemically modified PE with grafted maleic anhydride (MAH) monomer on its backbone. Direct melt intercalation was used to prepare two kinds of nanocomposites, polyethylene (PE)/organic montmorillonite (Org-MMT) and maleic anhydride grafted polyethylene (PE-g-MAH)/Org-MMT nanocomposites. They observed that both PP-g-MA and PE-g-MA compatibilized nanocomposites had higher crystallization temperatures compared to the original matrix. There was also an increase in T_c with increasing clay loading. Tanniru *et al.* [30] observed that for clay reinforced HDPE nanocomposites the crystallinity increased with the addition of clay, but the crystallization temperature remained unaffected.

Lee *et al.* [29] observed that loading the polymer with nanoclays significantly improved the mechanical and barrier properties. For example, with 7% clay loading, the tensile modulus increased by about 49% and the tensile strength by about 15% compared to pure polyethylene. Their dynamic mechanical analysis (DMA) results showed that both the storage and loss moduli of the nanocomposites increased with increasing clay content. The storage modulus of the nanocomposite with 7% clay increased about 45% at room temperature. These results indicate that incorporation of clay in the polyethylene matrix with PP-g-MA as compatibilizer remarkably enhanced the stiffness and showed good reinforcing effects. Tanniru *et al.* [30] also used DMA in their study of clay reinforced HDPE nanocomposites. They observed a shifting of the tan δ peak of the nanocomposite to a lower temperature, while the storage modulus remained unaffected with clay addition. They attributed this to a weak interaction between the polymer and the filler.

2.4 Polyethylene-silica nanocomposites

In recent years, polyethylene-silica nanocomposites have been the subject of research by various authors. Some synthesized silica through a sol-gel process, while others mixed

commercial nano-particles into their composites. They investigated the morphological, thermal and mechanical properties of such nanocomposites as function of silica content.

2.4.1 Morphology

Huang *et al.* [50] studied the characterization of linear low-density polyethylene silica (LLDPE/nano-SiO_2) nanocomposites, containing 2, 3, 4 and 5% of aminetryethoxysilane treated silica. LLDPE-g-MA was introduced as compatibilizer. TEM was used to explain the morphological characteristics. For the composites filled with untreated SiO_2, the filler particles tended to aggregate. The surface treatment of the filler was found to improve the degree of wetting of the fillers by the polymer, and the dispersion of the nano-SiO_2. In the composites containing larger numbers of SiO_2 particles, SiO_2 agglomerates were formed.

Kontou *et al.* [51] studied the pure LLDPE matrix and nanocomposites containing 2, 4, 6, 8 and 10% by weight of SiO_2. They investigated two types of commercial LLDPE, one prepared by metallocene (mLLDPE) and the other by a traditional Zieglar-Natta catalyst (zLLDPE). The silica nanocomposites were treated with dimethyldichlorosilane. SEM was used to explain the morphological behaviour of the composites. All the samples contained agglomerates the size of which varied with silica content. At higher silica content (> 4 %) it was observed that the agglomerates formed in mLLDPE were smaller than those formed in zLLDPE. Increasing the silica content in LLDPE led to larger agglomerates. Other authors also found that, regardless of the sample preparation method, agglomeration size increased with an increase in silica content [52-56].

Jonsomjit *et al.* [57] studied LLDPE nanocomposites. They compared the performance of nano-SiO_2 and nano-ZrO_2 as fillers. The nanocomposites were synthesized *via* the *in situ* polymerization of ethylene/1-octene with a zirconocene/MAO catalyst in the presence of the fillers. In the TEM pictures, the nanoscale fillers appeared as a group of sphere-like particles indicating the agglomeration of the primary particles. The nanoscale fillers were well distributed inside the polymer matrix, but poorly dispersed due to agglomeration.

Mishra *et al.* [58] investigated the influence of nanosilica, synthesized through a sol-gel process and mixed with LDPE and wood flour in the presence and absence of dicumyl peroxide (DCP), on the composite properties. The FT-IR results showed Si-O-Si stretching

around 1085 cm^{-1}, which is a common observation for silica based nanocomposites [59-69]. The SEM micrographs showed white spherical silica nanoparticles uniformly dispersed in the matrix. The sizes of the silica particles were found to be in the range of 10-50 nm, but a few large few agglomerates of 100-200 nm were also formed. The SEM images of the fractured surface of the nanocomposites showed incomplete dispersion of the particles.

Kalfus *et al.* [65] investigated the effect of silica nanofiller on the deformation response and morphology of HDPE, LDPE and isotactic polypropylene (iPP) modified with fumed silica. They demonstrated that the degree of matrix reinforcement was considerably affected by the extent of matrix crystallinity, especially in the temperature range from (T_m-130°C) to T_m. They proposed that this phenomenon may be attributed to the alpha-mechanical relaxation process occurring above the matrix T_g. As a result of adding silica into the molten matrix, the mobility of the chains in contact with the silica particles became reduced. This caused substantial changes in the morphology of these semicrystalline nanocomposites.

2.4.2 Thermal properties

The DSC results of Kontou *et al.* [51] showed that the T_gs of the LLDPE/SiO_2 composites were higher than that of the corresponding LLDPE due to the silica nanoparticles restricting the segmental and long range chain mobility of the LLDPE phase. There was, however, no relationship between T_g and silica concentration. The melting peak of both types of composites was not affected by changes in silica concentration. Furthermore, the melting enthalpy of mLLDPE/SiO_2 increased up to a silica content of 4%, and then decreased. A similar trend was observed to zLLDPE. In another study, Han *et al.* [64] investigated the thermal properties of LDPE/silica nanocomposites. They observed that the thermal stability of the nanocomposites with untreated silica surfaces were less thermally stable than pure LDPE, while the presence of surface treated silica improved the thermal stability.

Mishra *et al.* [58] found that DCP treatment and the presence of silica led to higher thermal stability of nano-silica containing LDPE/wood flour composites. They also observed that the onset and peak temperatures of melting of the composites were similar, even in the presence of nano-silica, which indicated that both wood flour and nanosilica had little influence on the LDPE crystallite size and dispersion. Silica was found to have a negligible effect on the crystallinity of LDPE, while the presence of wood flour improved the LDPE crystallization.

2.4.3 Mechanical and thermomechanical properties

Huang *et al.* [50] studied the dynamic mechanical properties of LLDPE/nano-SiO_2 by means of DMTA and observed that the storage (E') and loss (E") moduli of all the nanocomposites increased with increasing SiO_2 content, and that the α transition peak shifted to lower temperatures with increasing nano-SiO_2 concentration. The E' values of the LLDPE composites filled with aminetriethoxysilane treated SiO_2 were lower than those of the composites with untreated SiO_2 at lower temperatures, but this trend was reversed as temperature increased to room temperature. The E" values of the aminetriethoxysilane treated systems were higher than those of the untreated systems at lower temperatures, and the α transition peak shifted to lower temperatures compared to that of the untreated system. The introduction of the compatibilizer into the LLDPE composites filled with aminetriethoxysilane treated SiO_2 enhanced the E' and the E" values of the composites over the temperature range of -50 to 110 °C and led to a shift of the α transition peak to lower temperatures. At low temperatures, the behaviour of the storage and loss moduli was similar to observations of Kalfus *et al.* [65] on related systems.

In their investigation of LLDPE/SiO_2 nanocomposites, Kontou *et al.* [51] observed that the storage moduli of the composites were higher than those of the corresponding LLDPE, particularly at lower temperatures, and also increased with increasing silica content. This trend was reversed for 8% SiO_2 above the main transition temperature around -40 °C. The loss moduli of the composites were higher than those of the corresponding LLDPE. The position of γ transition peak was not affected by changes in silica content, but its intensity increased with silica content, reaching a maximum at 4% silica content. All the samples exhibited a β transition in the temperature range from -40 to -20°C. The β transition shifted to higher temperatures and increased in intensity with increasing silica content, and its intensity reached a maximum at 4% silica. The increase in the intensity and the shift in the position of the β transition indicated an increase in the size of the interphase and a decrease in the polymer chain mobility up to a silica content of 4% by weight. The presence of the nanofillers resulted in an increase in the elastic modulus and tensile strength of the LLDPE, accompanied by a slight increase in the elongation at break.

Mishra *et al.* [58] observed that the tensile strength of LDPE mixed with wood flour and nano-silica decreased with increasing wood flour content, while the tensile modulus

substantially increased. They also observed that the presence of nanosilica gave rise to lower values for both tensile strength and tensile modulus, but an increase in tensile strength with increasing wood flour content was observed for samples prepared in the presence of DCP. The tensile modulus increased with increasing wood flour content, but it was not substantially influenced by the presence of either nano-silica or by sample preparation in the presence of DCP. DMA analyses of the same samples showed results similar to the tensile testing results.

2.5 Other silica nanocomposites

2.5.1 Morphology

Pandey *et al.* [62] investigated the structure, interaction and thermal properties of polyethylene oxide (PEO) and nanosized silica filler with different concentrations of ammonium thiocynate. They observed FTIR peaks at 914 and 802 cm^{-1} related to silica absorption. XRD results showed that the addition of silica to PEO reduced the intensity of and broadened the main peaks, which was an indication of a reduction in the degree of crystallinity. Optical microscopy of the lamellar microstructure of pure PEO showed a partial amorphous phase with dark boundaries between the spherulites. The SEM results complemented the XRD results.

Bikiaris *et al.* [66] studied isotactic polypropylene silica nanocomposites (iPP/SiO_2) containing 1, 2.5, 5, 7.5, 10 and 15% silica nanoparticles. A poly (propylene-g-maleic anhydride) copolymer (PP-g-MA) containing 0.6% maleic anhydride was added to all nanocomposites at three different concentrations, 1, 2.5 and 5 wt% based on silica content. Fourier-transform infrared (FTIR) results indicated that the surface silica hydroxyl groups of the SiO_2 nanoparticles reacted with the maleic anhydride groups of PP-g-MA, which led to a finer dispersion of the individual SiO_2 nanoparticles in the iPP matrix. At a higher concentration of PP-g-MA two peaks, corresponding to anhydride groups, were observed between 1700 and 1800 cm^{-1}. In the spectrum of SiO_2, there was a strong absorbance at 1110 cm^{-1} attributed to the Si-O groups and a broad peak with a maximum at 3440 cm^{-1} attributed to the surface hydroxyl groups.

Peng *et al.* [67] studied natural rubber (NR)/silica nanocomposites developed by combining self assembly and latex compounding techniques. The SiO_2 nanoparticles were homogenously

distributed throughout the NR matrix as nano-clusters with an average size ranging from 60 to 150 nm when the SiO_2 loading was less than 6.5 wt%. At low SiO_2 contents ($\leq$ 4.0 wt %), the NR and SiO_2 particles were assembled as a core-shell structure by using poly (diallyldimethylammonium chloride) (PDDA) as an inter-medium as illustrated in Figure 2.1, and only primary aggregations of SiO_2 were observed. When more SiO_2 was loaded, secondary aggregations of SiO_2 nanoparticles were gradually generated, and the sizes of the SiO_2 clusters dramatically increased.

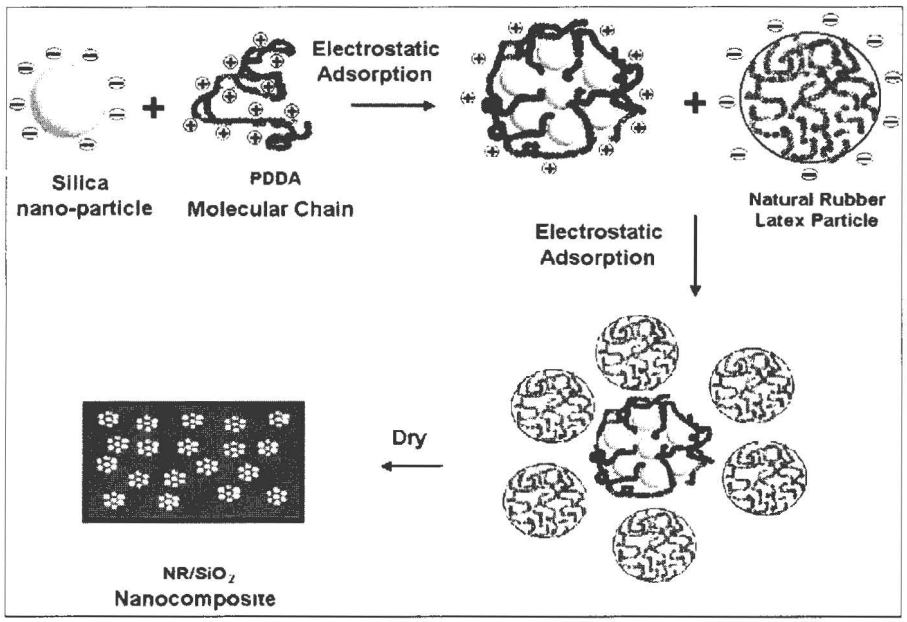

Figure 2.1 Schematic representation of the self-assembly process

Polymer-silica nanocomposites based on poly (2-hydroxyethyl acrylate) (PHEA) were prepared by the simultaneous polymerization of the organic and the silica phases in a sol–gel process with the silica precursor tetraethyl orthosilicate (TEOS). Atomic force microscopy (AFM) in the tapping mode and nanoindentation experiments showed that the structure of the PHEA/silica hybrids strongly depends on the ratio of the two components in the system. The system consisted of aggregated silica particles dispersed in the organic matrix for silica weight fractions lower than 0.15, but above this concentration, the structure was co-continuous with that of the organic matrix, similar to two interpenetrated networks [68].

A high temperature polymer, polybenzoxazole (PBO), was used as the organic phase and the inorganic phase was generated *via* sol-gel reaction from a silica precursor,

phenyltriethoxysilane (PTEOS) in the preparation of a novel organic/inorganic hybrid material through a sol–gel process. The sol-gel reaction was done without the addition of water or catalyst. The TEM and SEM photographs showed that the silica particles were nano-sized and well dispersed in the PBO matrix [69].

Poly(ε-caprolactone) (PCL) based nanocomposites filled with silica nanoparticles were prepared and characterized [70]. In order to promote polymer/inorganic nanofiller compatibility and to increase the interfacial adhesion between the two components, the silica nanoparticle surfaces were functionalized by grafting PCL onto it. The PCL based nanocomposites were prepared through extrusion. TEM and SEM analyses revealed that the silica functionalization provided a useful method of preparation of the nanocomposites with the achievement of a fine, good dispersion and a strong adhesion level. FTIR analysis showed an absorption peak at 1100 cm^{-1} attributed to silica absorption.

Small-angle x-ray scattering (SAXS) experiments were carried out on nanocomposites of poly(vinyl acetate) (PVAc) and fumed silica nanoparticles with different surface areas and chemical treatments [71]. Particle aggregation was found to be independent of the molecular weight of the matrix for a fixed filler concentration and surface treatment. The particle size distributions suggested that particle aggregation was reduced when the native surface hydroxyl groups were blocked by various surface treatments, which also reduced the bonding strength to the polymer matrix. Analysis of the SAS data showed three levels of hierarchy in the organization of silica particles. The first level consisted of small aggregates of silica particles. The second level consisted of polydispersed aggregates resembling mass-fractal objects. This was confirmed by TEM analysis. The polydispersed aggregates further associated to form agglomerates at the third level.

Hernandez *et al.* [68] studied the properties of poly (2-hydroxyethyl acrylate)-silica nanocomposites obtained by a sol-gel process. The silica content was changed from 5 to 10, 15, 20, 25 and 30 wt% by controlling the 2-hydroxyethyl acrylate – tetraethylorthosilicate ratio and by assuming that the sol-gel reactions were complete. They used tetraethoxysilane as precursor and catalyzed the reaction with HCl. The FTIR results showed a peak at around 1085 cm^{-1} which was related to Si-O-Si stretching. There was also an increase in intensity with increasing silica content. The SEM pictures showed a uniform distribution of the particles and aggregates. X-ray microanalysis confirmed the uniformity of the particle

distribution, and density data suggested that all the pores formed during sol-gel have been occupied by the organic polymer matrix chains.

2.5.2 Thermal properties

Vladimirov *et al.* [72] prepared polypropylene/fumed silica nanocomposites through melt mixing using a twin-screw co-rotating extruder. To improve the dispersion degree of the nanoparticles, PP-g-MA was used as a compatibilizer. They plotted the crystallization rate against the silica and PP-g-MA contents. The crystallization rate was expressed as the inverse of the crystallization half time (time needed for the relative crystallinity in an isothermal test to reach 50%), and the results showed that the crystallization rates increased with increasing silica as well as PP-g-MA contents.

Pandey *et al.* [62], in their investigation of PEO/silica/ammonium thiocyanate nanocomposites, showed that an increased amount of silica in the PEO matrix continuously reduced the melting temperature and crystallinity of the host polymer. Zheng *et al.* [63] investigated the decomposition of pure polyethylene terephthalate (PET) and PET/silica nanocomposites through TGA and pyrolysis gas chromatography/mass spectrometry (Py-GC/MS). The PET/silica nanocomposites showed better thermal stability and a higher residual carbon content compared to pure PET, and the activation energies of decomposition was found to increase with increasing amounts of silica nanoparticles.

Peng *et al.* [67] investigated the decomposition of NR/silica nanocomposites in nitrogen and air using TGA. The onset, peak and end temperatures of decomposition all increased with increasing SiO_2 content in both atmospheres up to SiO_2 content of 4.0 wt%, above which the thermal stability did not further improve. The temperature range of the thermal degradation, expressed as $\Delta T = T_p - T_o$, of pure NR was smaller than that of the NR/SiO_2 nanocomposites. The thermal and thermooxidative ageing resistances of the nanocomposites were dominated by the silica nanoparticle distribution, and were influenced by the migration of the inorganic nanoparticles to the surface of the composites at elevated temperatures because of its relatively low surface potential.

In a study of poly (2-hydroxyethyl acrylate) (PHEA)-silica nanocomposites obtained by a sol-gel process, a decrease in thermal stability with an increase in silica content was observed

[68]. Pure PHEA and the nanocomposites exhibited three different degradation steps, but the steps were shifted to lower temperatures in all the nanocomposites. The loss of thermal stability was attributed to additional reactions that took place at temperatures above T_g in the nanocomposite samples. The TGA results in a study of Avella *et al.* [70] showed that the presence of silica nanoparticles increased the thermal stability of the material. That increase in thermal stability was attributed to restricted thermal motion of PCL and to the hindered diffusion of the volatile decomposition products within the nanocomposites due to the finely dispersed silica nanoparticles.

Fragiadakis *et al.* [73] studied poly(dimethylsiloxane) (PDMS) filled with silica nanoparticles prepared by a sol-gel technique. Their DSC results showed a glass transition temperature around -115 °C and a single endothermic melting peak around -40 °C for both pure PDMS and the nanocomposites. The glass transition temperature did not show a significant variation with silica content. The melting temperature decreased with increasing silica content and the melting peak broadened towards lower temperatures. During cooling at 10 °C min^{-1}, the pure PDMS crystallized at a higher temperature than all the composites, which indicated that the rate of crystallization was lower in the presence of the silica particles.

2.5.3 Mechanical and thermomechanical properties

Peng *et al.* [74] studied poly(vinylalcohol)/silica nanocomposites with different silica contents (0.5, 2, 5, 10, and 15%). The samples were synthesized by using a novel self-assembly monolayer technique. The DMA results showed that the onset of the storage modulus increased with SiO_2 content, which was attributed to the rigidity of the silica particles. Two steps in storage modulus curve of PVA were also observed. The first step was associated with the glass transition of the polymer, and the second with the softening of the PVA. The second step became weaker with increasing SiO_2 content, and finally disappeared at SiO_2 content of 10%. At low silica contents the mechanical properties of the composites were dominated by those of PVA, while at higher silica contents the rigidity of the inorganic particles dominated. The loss factor (tan δ) curve for PVA showed a main peak accompanied by a side peak. The main peak corresponded to the glass transition and the side peak to the slip of crystalline molecular chains. The maximum loss factor value of the nanocomposites was lower than that of pure PVA. This meant that the ability for absorbing energy of PVA should be stronger than that of the nanocomposites. Their Q-TMA results indicated that under a constant force, the

elasticity of nanocomposites decreased with SiO_2 content and the softening temperature moves to higher values when SiO_2 is added.

The DMA results of Vladimirov *et al.* [72] showed that higher silica content in polypropylene results in a higher storage modulus. By adding PP-g-MA, an increase in the storage modulus was observed due to the finer dispersion of the filler in the matrix and increased interfacial adhesion. They suggested that the compatibilizer permitted a much more efficient stress transfer from the polymer matrix to the silica nanoparticles. Bikiaris *et al.* [66], in their study of iPP/SiO_2 nanocomposites, observed that the tensile and impact strengths increased with silica content up to 2.5% of silica. Their explanation was that the addition of PP-g-MA copolymer as compatibilizer resulted in a higher adhesion between the iPP matrix and the SiO_2 nanoparticles, due to interaction that takes place between the reactive groups.

The tensile testing results of Peng *et al.* [67] showed that the incorporation of inorganic nanoparticles into the elastomer matrix led to a significant improvement in the mechanical properties of the host elastomer. The tensile strength and modulus increased with silica loading up to 4% SiO_2. With further addition of SiO_2, the tensile strength and modulus gradually decreased due to SiO_2 aggregation. Elongation at break and tear resistance increased with silica content.

Jeon *et al.* [75] studied a sol-gel process where nanometer-scale silica was incorporated into waterborne polyurethanes. These nanocomposites were synthesized from isophoronediisocyanate, poly (tetramethyleneglycol), dimethylolpropionic acid, triethylamine, diethylenetriamine and 3-aminopropyltriethoxysilane as coupling agent. The concentrations of silica used were 0, 2, 5 and 10%. The tensile testing results showed that the modulus and tensile strength increased with increasing nanosilica content, but that the elongation at break decreased. The hardness increased with increasing nanosilica content as a result of the reinforcing effect of dispersed nanosilica. The DMA results of pure polyurethanes showed two broad damping peaks around -45 and 41 °C, which indicated that it had a phase separated morphology. The two peaks corresponded to the glass transitions of the soft and hard domains, respectively. The glass transition temperature of the hard domain decreased with increasing silica content. This implied that the degree of partial phase mixing of soft and hard segment domains increased in the presence of hydrophilic silica. The soft segment domains referred to the segments of the polymer that have glass transition temperatures and the hard

segments domains referred to those rigid segments capable of forming strong intermolecular interactions.

In contrast to what was observed by other authors, Fragiadakis *et al.* [73] observed that for PDMS/silica nanocomposites there was a decrease in storage and loss moduli with increasing silica content at higher temperatures. They associated this with melting in crystalline regions of PDMS. In the same region where E' and E" steeply dropped, they observed a broad peak in the tan δ curve which increased in magnitude with increasing silica content, and which was related to melting. The DMA data showed different behavior compared to DSC, as only one peak was observed in the region of the glass transition, in both the loss modulus and tan δ curves, which shifted by about 10 K towards higher temperatures in the nanocomposites.

Hernandez *et al.* [68], in their study of PHEA/silica nanocomposites, used DMA to explain the polymer dynamics. The DMA measurements showed a stiffness increase in the rubbery state as the silica content was increased. The loss tangent curve of pure PHEA showed two maxima. One corresponded to the main, or α, mechanical relaxation at around 26 °C, and the other one at a lower temperature was associated with a complex side-chain relaxation with small amounts of water. An increase in the silica content decreased the intensity of the α relaxation of the polymer matrix and broadened its shape to the higher temperatures.

2.6 PE modification and compatibilization

Polyolefins are a very important class of commercial polymers applied in a wide range of applications. The individual members of the polyolefin family offer a fairly broad spectrum of structures, properties and applications. This spectrum can be broadened even further by blending individual polyolefins with other polymers or by addition of filler to an individual polyolefin matrix. It was indicated, in previous studies, that blending of commercial polyolefins resulted in materials characterized by poor mechanical properties due to immiscibility and incompatibility between the polymers [76-79]. These were improved by introducing suitable compatibilizers to provide the necessary adhesion between the blend and/or composite constituents. Other studies also indicated that the compatibilizer presence improved particles dispersion, as well as the mechanical and thermal properties of the composites [80,90-93].

2.6.1 Oxidized paraffin wax in polyethylenes

The group of Luyt did a lot of work on polyolefin/wax blends [80-89]. Thermal and mechanical properties were comprehensively studied as function of wax content.

Luyt and Geethamma [80] investigated the possibility of using oxidized paraffin wax as compatibilizer in composites containing LLDPE and layered silicate clays. XRD analysis results showed no exfoliation or intercalation of the clay layers in the absence of wax, whereas an obvious increase in d-spacing was observed when the samples were prepared in the presence of wax. The wax preferably penetrated the clay layers, probably because of stronger interaction between the functional groups on the wax chains and the organic modifier in the clay.

Krupa and Luyt [81] investigated changes in properties of the blends of LLDPE and an oxidized Fischer-Tropsch paraffin wax. The DSC curves of all the blends showed only one endothermic peak in the melting range off LLDPE, despite the fact that the wax showed a double melting peak at lower temperatures. That meant that the wax was miscible with the polymer for all the investigated compositions. The presence of the oxidized wax also did not influence the LLDPE melting temperature. Similar DSC results were found by Luyt and Geethaama [80] and by Luyt and Brüll [82]. The TGA characterization of the blends revealed that the thermal stability of the blends decreased with an increase in wax content, since wax has lower thermal stability than the polymer.

Luyt and Brüll [82] investigated oxidized wax blends with respectively HDPE, LDPE and LLDPE using crystallization analysis fractionation (CRYSTAF) and size exclusion chromatography coupled to FTIR (SEC-FTIR) in order to determine the possibility and extent of co-crystallization of wax with each of the polyethylenes. CRYSTAF showed very little or no co-crystallization of wax with HDPE and LDPE, while there was a strong indication of co-crystallization in the case of LLDPE. SEC-FTIR analyses showed co-elution of wax with LLDPE, indicating some chemical interaction between the oxidized wax and LLDPE.

Djoković *et al.* [86] investigated the influence of the oxidized Fischer-Tropsch paraffin wax on the thermal, mechanical and viscoelastic properties of low density polyethylene (LDPE)-oxidized wax blends. The DSC results showed that the blends had similar melting behaviour

to that of pure LDPE as a result of co-crystallization up to 20% wax content. However, at 30% and higher wax contents, another melting peak appeared at lower temperatures, which was attributed to LDPE and wax crystal separation. In contrast to the observations by Krupa and Luyt [81], the melting temperatures of the blends decreased with an increase in wax content. That was attributed to both a reduction in lamellar thickness and to a narrowing in the lamellar size distribution. The TGA results showed a shift in the onset of decomposition to higher temperatures compared to those of the pure materials for the blends having lower wax contents, despite the lower thermal stability of wax. That was attributed to co-crystallization of the PE and wax chains at these concentrations.

Hato *et al.* [87] investigated the influence of un-oxidized and oxidized Fischer-Tropsch paraffin waxes on the properties of their blends with HDPE, LDPE, and LLDPE. The samples were prepared by melt mixing in a Brabender Plastograph. HDPE blended with both waxes gave rise to complete miscibility for 10 and 20% wax contents. The LDPE blends showed one melting peak for only 10% of both waxes. All the blends of LLDPE with oxidized wax revealed only one endothermic peak, which indicated that the LLDPE and wax were miscible in the crystalline phase for the range of the compositions investigated [85,86].

Krupa and Luyt [81] found an increase in Young's modulus with an increase in wax content, because of the higher modulus of wax. The same behavior was observed by Djoković *et al.* [86]. Novák *et al.* [89] investigated the modification of the polarity of LDPE and HDPE through blending with an oxidized Fischer Tropsch paraffin wax. Young's modulus of the LDPE/wax blends slightly increased with an increase in wax content, whereas that of the HDPE/wax blends slightly decreased. The wax content had no significant influence on the yield point of the HDPE/wax blends, whereas a slight decrease in elongation at yield and an increase in stress at yield were observed for the LDPE/wax blends. This was attributed to an increase in the degree of crystallinity of the blends. Small amounts of wax considerably increased the polar component of the surface free energy of both LDPE and HDPE, and this gave rise to a significant improvement of the strength of the adhesive joints between LDPE and an epoxy-based substrate. This was attributed to the functional groups in the wax that increased the adhesive properties of the polyethylene.

2.6.2 Maleic anhydride grafted polyolefin compatibilization

Modification of polyolefins can be achieved by means of blending, grafting and curing. Polyolefin modification by grafting with maleic anhydride (MAH) in the presence of peroxides as initiators has been extensively researched due to the reactivity of the anhydride functional group [90-96].

Zhou *et al.* [97] studied ultra-high molecular-weight polyethylene (UHMWPE)/liquid crystalline polymer (LCP) composites compatibilized with polyethylene-grafted maleic anhydride (PE-g-MAH) prepared by compression molding. SEM images of the uncompatibilized composites showed obvious signs of phase separation. The interfacial gap between the LCP and the UHMWPE matrix on the fractured sections was clear. These interfacial gaps were attributed to poor interfacial combination between the LCP as the reinforcing agent and the UHMWPE matrix. The fractured section of the composite compatibilized with PE-g-MAH had a fuzzy morphology. This was attributed to a much stronger interphase between LCP and the UHMWPE matrix. However, with an increase in the content of PE-g-MA, the interfacial gaps between LCP and the UHMWPE matrix on the fractured surface became obvious again, which indicated that an excess of compatibilizer led to damage of the interfacial bonding of the matrix and the reinforcer.

Wang *et al.* [98] investigated the effect of the molecular weight of maleated polypropylenes on the compounding of polypropylene/organoclay nanocomposites. Structural analyses from TEM showed a better clay layer dispersion (exfoliation) upon the addition of PP-g-MAH, although clay aggregates were still visible. This observation was confirmed by their XRD results. Similar TEM results were found by Zhai *et al.* [99] and Zhengfa *et al.* [100]. Zhai *et al.* [99] chemically modified HDPE with a grafted maleic anhydride (MAH) monomer on its backbone. Then a direct melt-intercalation method was used to prepare two kinds of nanocomposites, polyethylene (PE)/organic montmorillonite (Org-MMT) and maleic anhydride grafted polyethylene (PE-g-MAH)/Org-MMT nanocomposites. A similar preparation was done by Zhengfa *et al.*[100] using the same polymer.

The DSC results of Zhou *et al.* [97] showed one endothermic melting peak for all the composites, and this was attributed to the same backbone structure of UHMWPE and PE-g-MA. They found that the incorporation of PE-g-MA contributed to a decrease in the melting

points of the composites and also some decrease in their crystallinity. Other authors also observed crystallinity decreases with increasing amounts of PE-g-MAH [101-103]. Zhai *et al.* [99] also used TGA and DSC in the investigation of their compatibilized PE nanocomposites. All the nanocomposites showed higher thermal decomposition and crystallization temperatures when compared to the pure matrix. The TGA results of Wang *et al.* [98] showed that there was an increase in the thermal stability of all the PP-g-MA/clay nanocomposites. The improvement in the thermal stability was attributed to a stronger interaction between the organic and inorganic phases. The individual layers of exfoliated clay platelets acted as an insulator, and the formation of a tortuous path between the layers inhibited the evaporation of volatile degradation products, which enhanced the thermal stability of the clay composites. Similar thermal stability results were obtained by Zhengfa *et al.* [100] and Zhai *et al.* [99].

In a study of the mechanical properties of these composites, Zhou *et al.* [97] found that the inclusion of a PE-g-MAH compatibilizer helped to greatly increase the tensile rupture strength and tensile modulus. These improvements were related to the enhanced cross-linking function of the composites in the presence of the compatibilizer. Wang *et al.* [98] used DMA for further characterization of the composites. All the modified nanocomposites exhibited high storage moduli compared to those of the neat PP. There was no noticeable shift in the glass transitions of the modified systems. Those were attributed to improved interfacial adhesion due to the anhydride group between the reinforcer and the matrix. The presence of the anhydride group in other studies on LDPE showed an improvement in the compatibility between the polymer matrix and inorganic fillers, and enhanced impact strength as well as elongation at break [100,104-110].

2.7 References

1. Y. Kojima, A. Usuki, M. Kawasumi, A. Okada, Y. Fukushima, T. Kurauchi, O. Kamigaito. Mechanical properties of nylon 6-clay hybrid. Journal of Materials Research (1993) 8:1185-1189.
2. W.J. Koros. Gas separation membranes: needs for combined materials science and processing approaches. Macromolecular Symposia (2002) 188:13-22.
3. P. Pandey, R.S. Chauhan. Membranes for gas separation. Progress in Polymer Science (2001) 26:853–893.

4. G. Maier. Gas separation with polymer membranes. Angewandte Chemie International Edition (1998) 37:2960–2974.
5. Ž. Andrić, M.D. Dramićanin, V. Jokanović, M. Matrić, A. Bessiére. Polymer complex solution synthesis of $(Y_xGd_{1-x})2O3:Eu^{3+}$ nanopowders. Optical Materials (2008) 30:1023-1027.
6. K. Jitendra, K. Pandey, R.A. Raghunatha, K. Pratheep, R.P. Singh. An overview on the degradability of polymer nanocomposites. Polymer Degradation and Stability (2005) 88:234-250.
7. X. Xia, S. Cai, C. Xie. Preparation, structure and thermal stability of Cu/LDPE nanocomposites. Materials Chemistry and Physics (2006) 95:122-129.
8. M. Dogling, W.R. Siegel, J. Hong, S.S. Linda, E. Mårtensson, C. Önneby. Influence of the nanoparticle surfaces on the electrical breakdown strength of nanoparticle-filled low-density polyethylene. Journal of Materials Research (2005) 19:857-863.
9. J.I. Hong, L.S. Schalder, R.W. Siegel. Rescaled electrical properties of ZnO/LDPE nanocomposites. Applied Physics Letters (2003) 82:1956-1958.
10. M. Dogling, Y.A. Akplalu, Y. Li, R.W. Siegel, L.S. Schadler. Effect of titinia nanoparticles on the morphology of LDPE. Journal of Polymer Science Part B: Polymer Physics (2005) 43:488-497.
11. M.U. Whait, A. Hassan, Z.A. Mohd Ishak, A.R. Rahmat, A.A. Bakar. Morphology, thermal, and mechanical behaviour of ethylene octene copolymer toughened polyamide 6/polypropylene nanocomposites. Journal of Thermoplastic Composite Materials (2006) 19:545-567.
12. M. Asomoza, M.P. Domínguez, S. Solís, V.H. Lara, P. Bosch, T. López. Hydrolysis catalyst effect on sol-gel silica structure. Materials Letters (1998) 38:249-253.
13. S.B. Jung, T.J. Ha, H.H. Park. Investigation of the properties of organically modified ordered mesoporous silica films. Journal of Colloid and Interface Science (2008) 320:527-534.
14. Y. Xu, D.D.L. Chung. Cement of high specific heat and high thermal conductivity, obtained by using silane and silica fume as admixtures. Cement and Concrete Research (2000) 30:1175-1178.
15. B.G. Fotenteboa, F.M. Abella. Concretes with aggregates from demolition waste and silica fume. Materials and mechanical properties. Building and Environment (2008) 43:429-437.

16. B. Haimson. Micromechanisms of borehole instability leading to breakouts in rocks. International Journal of Rock Mechanics and Mining Science (2007) 44:157-173.
17. S. Yan, J Yin, J. Yang, X. Chen. Structural characteristics and thermal properties of plasticized poly (L-lactide)-silica nanocomposites synthesized by sol-gel method. Materials Letters (2007) 61:2683-2686.
18. B. Samuneva, P. Djambaski, E. Kashcieva, G. Chernev, L. Kabaivanova, E. Emanuilova, I.M.M. Salvoda, M.H.V. Fernandes, A. Wu. Sol-gel synthesis and structure of silica hybrid biomaterials. Journal of Non-Crystalline Solids (2008) 354:733-740.
19. J.Z. Ma, J. Hu, Z.J. Zhang. Polyacrylate/silica nanocomposite materials prepared by sol-gel process. European Polymer Journal (2007) 43:4169-4177.
20. A.S. Hamdy, D.P. Butt. Environmentally compliant silica conversion coatings prepared by sol-gel method for aluminum alloys. Surface and Coating Technology (2006) 201:401-407.
21. K.M.S Khalil, S.A. Makhlouf. High surface area thermally stabilized porous iron oxide/silica nanocomposites via a formamide modified sol-gel process. Applied Surface Science (2008) 254:3767-3773.
22. M.W. Engl, P. Panizza, H. Deleuze, S. Lecommandox, H. Ushiki, R. Backov. Combining sol-gel chemistry and millifluidic toward engineering microporous silica ceramic final sizes and shape: An integrative chemistry approach. Chemical Engineering and Processing (2008) 47:1317-1322.
23. V. Raman, G. Bhatia, A.K. Mishra, S. Bhardwaj, K.N Sood. Synthesis of silica carbide nanofibres from pitch blended with sol-gel derived silica. Materials Letters (2006) 60:3906-3911.
24. L. Zhang, Y. Xu, D. Wu, Y. Sun, X. Jiang, X. Wei. Effect of polyvinylpyrrolidone on the structure and laser damage resistance of sol-gel silica anti-reflective films. Optics and Laser Technology (2008) 40:282-288.
25. H. Sugimoto, K. Daimatsu, E. Nakanishi, Y. Ogasawara, T. Yasumura, K. Inomata. Preparation and properties of poly (methylmethacrylate)-silica hybrid materials incorporating reactive silica nanoparticles. Polymer (2006) 47:3754-3759.
26. X. Song, X. Wang, H. Wang, W. Zhong, Q. Du. PMMA-silica hybrid thin films with enhanced thermal properties prepared via a non-hydrolytic sol-gel process. Materials Chemistry and Physics (2008) 109:143-147.

27. S. Wang, Y. Hu, Q. Zhongkai, Z. Wang, Z. Chen, W. Fan. Preparation and flammability properties of polyethylene/clay nanocomposites by melt intercalation method from Na^+ montorillonite. Materials Letters (2003) 57: 2675-2678.
28. S.W. Kou, W.J. Haung, S.B. Haung, H.C. Kao, F.C. Chang. Synthesis and characterizations of in situ blended metallocene polyethylene/clay nanocomposites. Polymer (2003) 44:7709-7719.
29. J.H. Lee, D. Jung, C.E. Hong, K.Y. Rhee, S.G. Advani. Properties of polyethylene layered silicate nanocomposites prepared by melt intercalation with a PP-g-MA compatibilizer. Composites Science and Technology (2005) 65:1996-2002.
30. M. Tanniru, Q. Yuan, R.D.K. Misra. On significant retention of impact strength in clay reinforced high density polyethylene nanocomposites. Polymer (2006) 47:2133-2146.
31. E.M. Araújo, R. Barbosa, A.W.B. Rodrigues, T.J.A. Melo, E.N. Ito. Processing and characterization of polyethylene/Brazilian clay nanocomposites. Materials Science and Engineering (2007) A445-446:141-147.
32. H. Zhai, W. Xu, H. Guo, Z. Zhou, S. Shen, Q. Song. Preparation and characterization of PE and PE-g-MAH/montmorillonite nanocomposites. European Polymer Journal (2004) 40:2539-2545.
33. H. Lu, Y. Hu, J. Xiao, Q. Kong, Z. Chen, W. Fan. The influence of irradiation on morphology evaluation and flammability properties. Materials Letters (2005) 59:648-651.
34. J. Zhang, D.D. Jiang, C.A. Wilkie. Polyethylene and polypropylene nanocomposites based upon an oligomerically modified clay. Thermochimica Acta (2005) 430:107-113.
35. J. Zhang, C.A. Wilkie. Polyethylene and polypropylene nanocomposites based on polymerically-modified clay containing alkylstyrene units. Polymer (2006) 47:5736-5743.
36. C. Zhao, H. Qin, F. Gong. M. Feng. S. Zhang, M. Yang. Mechanical, thermal and flammability properties of polyethylene/clay nanocomposites. Polymer Degradation and Stability (2005) 87:183-189.
37. A. Lesczczyńska, J. Njuguma, K. Pielichowski, J.R. Banerjee. Polymer/montmorillonite nanocomposites with improved thermal properties. Part II. Thermal stability of montmorillonite nanocomposites based on different polymeric matrixes. Thermochimica Acta (2007) 454:1-22.

38. Q. Wang, Z. Zhou, L. Song. H. Hu, L. Wang. Nanoscopic confinement effects on ethylene polymerization by intercalated silicate with metallocene catalyst. Journal of Polymer Science Part A (2004) 42:38-43.
39. M. Zhanetti, L. Costa. Preparation and combustion behaviour of polymer/layered silicate nanocomposites based upon PE and EVA. Polymer (2004) 45:4367-4373.
40. J. Zhang, D.D. Jiang, C.A. Wilkie. Thermal and flame properties of polyethylene and polypropylene nanocomposites based on an oligomerically-modified clay. Polymer Degradation and Stability (2006) 91:298-304.
41. S.W. Kuo, W.J. Huang, S.B. Huang, H.C. Kao, F.C. Chang. Synthesis and characterizations of in situ blended metallocene polyethylene/clay nanocomposites. Polymer (2003) 44:7709-7719.
42. A. Durmus, A. Kasgoz, C.W. Macosko. Linear low density polyethylene (LLDPE)/clay nanocomposites. Part I: Structural characterization and quantifying clay dispersion by melt rheology. Polymer (2007) 48:4498-4502.
43. Y. Peneva, E. Tashev, L. Minkova. Flammability, microhardness and transparency of nanocomposites based on functionalized polyethylenes. European Polymer Journal (2006) 42:2228-2235.
44. R. Barbosa, E.M. Araújo, T.J.A. Melo, E.N. Ito. Comparison of flammability behaviour of polyethylene/Bazilian clay nanocomposites and polyethylene/flame retardants. Materials Letters (2007) 61:2575-2578.
45. J. Zhang, C.A. Wilkie. Preparation and flammability properties of polyethylene-clay nanocomposites. Polymer Degradation and Stability (2003) 80:163-169.
46. T. Mandalia, F. Bergaya. Organo clay mineral-melted polyolefin nanocomposites effect of surfactant/CEC ratio. Journal of Physics and Chemistry of Solids (2006) 67:836:845.
47. J.T. Xu, Q. Wang, Z.Q. Fan. Non-isothermal crystallization kinetics of exfoliated and intercalated polyethylene/montmorillonite nanocomposites prepared by in situ polymerization. European Polymer Journal (2005) 41:3011-3017.
48. C. Zhao, H. Qin, F. Gong, M. Feng, S. Zhang, M. Yang. Mechanical, thermal and flammability properties of polyethylene/clay nanocomposites. Polymer Degradation and Stability (2005) 87:183-189.
49. S.S. Ray, M. Okamoto. Polymer/layered silicate nanocomposites: a review from preparation to processing. Progress in Polymer Science. (2003) 28:1539-1641.
50. Y. Huang, S. Jiang, L. Wu, Y. Hua. Characterization of LLDPE/nano-SiO_2 composites by solid-state dynamic mechanical spectroscopy. Polymer Testing (2004) 23:9-15.

51. E. Kontou, M. Niaounakis. Thermo-mechanical properties of LLDPE/SiO_2 nanocomposites. Polymer (2006) 47:1267-1280.
52. C.C. Peng, A.Göpfert, M Drechsler, V. Abetz. "Smart" silica-rubber nanocomposites in virtue of hydrogen bonding interaction. Polymers For Advanced Technologies (2005) 16:770–782.
53. R. Sengupta, A. Bandyopadhyay, S. Sabharwal, T.K. Chaki, A.K. Bhowmick. Polyamide-6,6/in situ silica hybrid nanocomposites by sol–gel technique: synthesis, characterization and properties. Polymer (2005) 46:3343-3354.
54. T. Mitsuru, H. Masaki, J.C. Lee, T. Kunihiko. Organic/inorganic nanocomposites prepared by mechanical smashing of agglomerated silica ultrafine particles in molten thermoplastic resin. Polymers for Advanced Technologies (2006) 17: 981-990.
55. D.S. Kim, H.B. Park, J.W. Rhim, Y.M. Lee. Preparation and characterization of crosslinked PVA/SiO_2 hybrid membranes containing sulfonic acid groups for direct methanol fuel cell applications. Journal of Membrane Science (2004) 240:37-48.
56. W. Cheng, Z. Wang, C. Ren, H. Chen, T. Tang. Preparation of silica/polycrylamide/ polyethylene nanocomposites via in situ polymerization. Materials Letters (2007) 61:3193-3196.
57. B. Jongsomjit, J. Panpranot, P. Praserthdam. Effect of nanoscale SiO_2 and ZrO_2 as the filler on the microstructure of LLDPE nanocomposites synthesized via *in situ* polymerization with zirconocene. Materials Letters (2007) 61:1376-1379.
58. A.K. Mishra, A.S. Luyt. Effect of sol-gel derived nano-silica and organic peroxide on the thermal and mechanical properties of low-density polyethylene/wood flour composites. Polymer Degradation and Stability (2008) 93:1-8.
59. S. Kalele, R. Dey, N. Hebalkar, J. Urban, S.W. Gosavi, S.K. Kulkarni. Synthesis and characterization of silica-titania core- shell particles. Journal of Physics (2005) 65:787-791.
60. G.H. Padrón, R. Rodríguez, V.M. Castañro. In-situ thiol-modified silica nanoparticles. The Internet Journal of Nanotechnology (2005) 1:1-7.
61. B. Yan. Sol-gel preparation and luminescence of silica/polymer hybrid material incorporated with terbium complex. Materials Letters (2003) 57: 2535-2539.
62. K. Pandey, M.M. Dwivedi, M. Tripathi. Structure, interaction and thermal study in electrolyte of polyethylene oxide/silica/ammonium thiocynate nanocomposites. Polymer Composites (in press).

63. J. Zheng, P. Cui, X. Tian, K. Zheng. Pyrolysis studies of polyethylene terephthalate/ silica nanocomposites. Journal of Applied Polymer Science (2007) 104:9-14.
64. Z. Han, C. Diao, Y. Li, H. Zhao. Thermal properties of LDPE/silica nanocomposites. Annual Report Conference on Electrical Insulation and Dielectric Phenomena (2006) 310-312.
65. J. Kalfus, J. Jancar, J. Kucera. Effect of weakly interacting nanofiller on the morphology and viscoelastic response of polyolefins. Polymer Engineering and Science (2008) 48:889-894.
66. D.N. Bikiaris, A. Vassilion, E. Pavlidou, G.P. Karayannidis. Compatibilisation effects of PP-g-MA copolymer on iPP/SiO_2 nanocomposites prepared by melt mixing. European Polymer Journal (2005) 41:1965-1978.
67. Z. Peng, L.X. Kong, S.D. Li, Y. Chen, M.F. Huang. Self-assembled natural rubber/silica nanocomposites: Its preparation and characterization. Composites Science and Technology (2007) 67:3130-3139.
68. J.C.Z. Hernández, M.S. Sánchez, J.L.G. Ribelles, M.M. Pradas. Polymer-silica nanocomposites prepared by sol-gel technique: Nanoindentation and tapping mode AFM studies. European Polymer Journal (2007) 43:2775-2783.
69. P.I. Lee, S.L.C. Hsu. Preparation and properties of polybenzoxazole-silica nanocomposites via sol-gel process. European Polymer Journal (2007) 43:294-299.
70. M. Avella, F. Bondioli, V. Cannillo, E.D. Pace, M.E. Errico, A.M. Ferrari, B. Focher, M. Malinconico. Poly (ε-caprolactone)-based nanocomposites: Influence of compatibilization on properties of poly (ε-caprolactone)-silica nanocomposites. Composites Science and Technology (2006) 66:886-894.
71. R.A. Narayanan, P. Thiyagarajan, A.J. Zhu, B.J. Ash, M.L. Shofner, L.S. Schadler, S.K. Kumar, S.S. Sternstein. Nanostructural features in silica-polyvinyl acetate nanocomposites characterized by small-angle scattering. Polymer (2007) 48:5734-5741.
72. V. Vladimirov, C. Betchev, A. Vassiliou, G. Papageorgiou, D. Bikiaris. Dynamic mechanical and morphological studies of isotactic polypropylene/fumed silica nanocomposites with enhanced gas barrier properties. Composites Science and Technology (2006) 66:2935-2944.
73. D. Fragiadakis, P. Pissis, L. Bokobza. Glass transition and molecular dynamics in poly(dimethylsiloxane)/silica nanocomposites. Polymer (2007) 46:6001-6008.
74. Z. Peng, L.X. Kong, S.D. Li. Non-isothermal crystallisation kinetics of self-assembled polyvinylalcohol/silica nanocomposite. Polymer (2005) 46:1949-1955.

75. H.T. Jeon, M.K. Jang, B.K. Kim, K.H. Kim. Synthesis and characterization of waterborne polyurethane-silica hybrids using sol-gel process. Colloids and Surfaces A: Physicochemical and Engineering Aspects (2007) 302:559-567.

76. I.A. Hussein, T. Hameed. Influence of branching characteristics on thermal and mechanical properties of Ziegler-Natta and metallocene hexane linear low density polyethylene blends with low density polyethylene. Journal of Applied Polymer Science (2005) 97:2488-2498.

77. S.C. Tjong. Structural and mechanical properties of polymer nanocomposites. Materials Science and Engineering (2006) 53:73-197.

78. R. Chen, Q. Wu, F. Zhu, S. Lin. Syndiotactic polystyrene-b-atactic polypropylene block copolymer alloy as compatibilizer for syndiotactic polystyrene/isotactic polypropylene blends. Journal of Applied Polymer Science (2002) 89:1596-1605.

79. C.W. Macosko, H.K. Jeon, T.R. Hoye. Reaction at polymer-polymer interfaces for blend compatibilization. Progress in Polymer Science (2005) 30:939-947.

80. A.S. Luyt, V.G. Geethamma. Effect of oxidized paraffin wax on the thermal and mechanical properties of linear low-density polyethylene–layered silicate nanocomposites. Polymer Testing (2007) 26:461-470.

81. I. Krupa, A.S. Luyt. Physical properties of blends of LLDPE and an oxidized paraffin wax. Polymer (2001) 42:7285-7289.

82. A.S. Luyt, R. Brüll. Investigation of polyethylene-wax blends by CRYSTAF and SEC-FTIR. Polymer bulletin (2004) 52:177-183.

83. S.P. Hlangothi, I. Krupa, V. Djoković, A.S. Luyt. Thermal and mechanical properties of cross-linked and uncross-linked linear low-density polyethylene-wax blends. Polymer Degradation and Stability (2003) 79:53-59.

84. H.S. Mpanza, A.S. Luyt. Comparison of different waxes as processing agents for low-density polyethylene. Polymer Testing (2006) 25:436-442.

85. I. Krupa, G. Miková, A.S. Luyt. Phase change materials based on low-density polyethylene/paraffin wax blends. European Polymer Journal (2007) 43:4695-4705.

86. V. Djoković, T.N. Mtshali, A.S. Luyt. The influence of wax content on the physical properties of low-density polyethylene-wax blends. Polymer International (2003) 52:999-1004.

87. M.J. Hato, A.S. Luyt. Thermal fractionation and properties of different polyethylene/wax blends. Journal of Applied Polymer Science (2007) 104:2225-2236.

88. I. Krupa, A.S. Luyt. Thermal and mechanical properties of extruded LLDPE/wax blends. Polymer Degradation and Stability (2001) 73:157-161.

89. I. Novák, I. Krupa, A.S. Luyt. Improvement of the polarity of polyethylene with oxidized Fischer-Tropsch paraffin wax and its influence on the final mechanical properties. Journal of Applied Polymer Science (2005) 95:1164-1168.

90. A. Bhattacharya, B.N. Misra. Grafting: a versatile means to modify polymers. Techniques, factors and applications. Progress in Polymer Science (2004) 29:767–814.

91. S.H.P. Bettini, J.A.M. Agnelli. Grafting of maleic anhydride onto polypropylene by reactive extrusion. Journal of Applied Polymer Science (2002) 85:2706–2717.

92. S.H.P. Bettini, J.A.M. Agnelli. Grafting of maleic anhydride onto polypropylene by reactive processing. I. Effect of maleic anhydride and peroxide concentrations on the reaction. Journal of Applied Polymer Science (1999) 74:247–255.

93. S.H.P. Bettini, J.A.M. Agnelli. Grafting of maleic anhydride onto polypropylene by reactive processing. II. Effect of rotor speed and reaction time. Journal of Applied Polymer Science (1999) 74:256–263.

94. G. Moad. The synthesis of polyolefin graft copolymers by reactive extrusion. Progress in Polymer Science (1999) 24:81–142.

95. K.H. Wang, M.H. Choi, C.M. Koo, Y.S. Choi, I.J. Chung. Synthesis and characterization of maleated polyethylene/clay nanocomposites. Polymer (2001) 42: 9819-9826.

96. A. Priola, R. Bongiovanni, G. Gozzelino. Solvent influence on the radical grafting of maleic anhydride on low density polyethylene. European Polymer Journal (1994) 30:1047-1050.

97. J. Zhou, F. Yan. Mechanical and tribological behavior of compatibilized ultra-high-molecular-weight polyethylene/liquid crystalline polymer composites. Polymer Testing (2004) 23:827-833.

98. Y. Wang, F.B. Chen, K.C. Wu. Effect of the molecular weight of maleated polypropylenes on the compounding of polypropylene/organoclay nanocomposites. Journal of Applied Polymer Science (2005) 97:1667-1680.

99. H. Zhai, W. Xu, H. Gou, Z. Zhou, S. Shen, Q. Song. Preparation and characterization of PE and PE-g-MAH/montmorillonite nanocomposites. European Polymer Journal (2004) 40:2539-2545.

100. Z. Zhou, H. Zhai, W. Xu, H. Gou, G. Liu, W.P. Peng. Preparation and characterization of PE and PE-g-MAH-styrene/montmorillonite nanocomposites. Journal of Applied Polymer Science (2006) 101:805-809.

101. G. Liang, J. Xu, W. Xu. PE/PE-g-MAH/org-MMT nanocomposites. Π. Nonisothermal crystallization kinetics. Journal of Applied Polymer Science (2004) 91:3054-3059.

102. W. Liu, Y.J. Wang, Z. Sun. Effect of polyethylene-grafted maleic anhydride (PE-g-MA) on thermal properties, morphology, and tensile properties of low density polyethylene (LDPE) and corn starch blends. Journal of Applied Polymer Science (2003) 88:2904-2911.

103. H. Yuan, P. Hu. Study of a compatibilized ultra high molecular weight polyethylene and polyurethane. Journal of Applied Polymer Science (2001) 81:3290-3295.

104. L. Yang, F. Zhang, T. Endo, T. Hirotsu. Microstructure of maleic anhydride grafted polyethylene by high-resolution solution-state NMR and FTIR spectroscopy. Macromolecules (2003) 36:4709-4718.

105. L.U. Bing, T.C. Chung. Synthesis of maleic anhydride grafted polyethylene and polypropylene with controlled molecular structures. Journal of Polymer Science Part A (2000) 38:1337-1343.

106. L. Yang, F. Zhang, T. Endo, T. Hirotsu. Structural characterization of maleic anhydride grafted polyethylene by ^{13}C NMR spectroscopy. Polymer (2002) 43:2591-2594.

107. D. Jianping, Y. Wantai. Surface photografting polymerization of vinyl acetate, maleic anhydride, and their charge-transfer complex. Journal of Applied Polymer Science (2005) 97:2230-2237.

108. D. Jianping, Y. Wantai. Surface photografting polymerization of vinyl acetate, maleic anhydride, and their charge-transfer complex. VIII. Charge-transfer complex (4). Journal of Applied Polymer Science (2006) 99:2710-2720.

109. J.P. Deng, W.T. Yang. Self-initiating performance of maleic anhydride on surface photografting polymerization. Journal of Applied Polymer Science (2001) 39:3246–3249.

110. H. Krump, P. Alexy, A.S. Luyt. Preparation of a maleated Fischer-Tropsch paraffin wax and FTIR analysis of grafted maleic anhydride. Polymer Testing (2005) 24:129-135.

CHAPTER 3

MATERIALS AND METHODS

3.1 Materials

3.1.1 Wax

Oxidized Fischer-Tropsch paraffin wax (A1 wax) was used in this study. A1 wax is an oxidized straight-hydrocarbon chain paraffin wax, average molar mass of 660 g mol^{-1}, density = 0.95 g cm^{-3} (solid) and 0.82 cm^{-3} (liquid) at 25 °C and 110 °C respectively, and melting point 96 °C. It has a thermal decomposition temperature of about 250 °C, C/O ratio 18.8/1, and a flash point of approximately 185 °C. It was supplied by Sasol Wax, Sasolburg, South Africa.

3.1.2 Low-density polyethylene (LDPE)

LDPE was supplied in pellet form by Sasol Polymers, Johannesburg, South Africa. It has an MFI of 7.0 g/10min, a melting point of 106 °C, an average molar mass (MW) of 96000 g mol^{-1}, and a density of 0.918 g cm^{-3}.

3.1.3 O-Xylene

O-xylene was supplied in a liquid form by Laboratory Consumables and Chemical Suppliers, Durban, South Africa. It has a molar mass of 106.7 g mol^{-1}, melting and boiling points of respectively 24 °C and 144°C, and a density of 0.89 g cm^{-3}.

3.1.4 Maleic anhydride (MAH)

MAH was supplied in pellet form by Sigma-Aldrich, Krugersdorp, South Africa. It has a molar mass of 98.06 g mol^{-1} and a melting point of 52 °C.

3.1.5 Acetone

Acetone was supplied in a liquid form by Laboratory Consumables and Chemical Suppliers, Durban, South Africa. It has a molar mass of 58.08 g mol^{-1} and a density of 0.78 g cm^{-3}.

3.1.6 Dicumyl peroxide (DCP)

DCP was supplied in pellet form by Sigma-Aldrich, Krugersdorp, South Africa. It has a molar mass of 270 g mol^{-1} and a melting point of 39 °C.

3.1.7 Tetraethylothosilicate (TEOS)

Tetraethylothosilicate was supplied in a liquid form by Sigma-Aldrich, Krugersdorp, South Africa. It has a molar mass of 208.33 g mol^{-1}, a density of 0.93 g cm^{-3} and a melting point of 164 °C.

3.2 Methods

3.2.1 Preparation of maleic anhydride grafted polyethylene (PE-g-MAH)

LDPE (98.2%), MAH (1%) and DCP (0.8%) were mixed in a 50 mL mixer of a Brabender Plastograph at 130 °C and 30 rpm for 10 min. The reaction product was extruded using a Brabender Plastograph single-screw extruder maintained at 170, 175, 180, 180 °C from the hopper to the die head, and a screw speed of 20 rpm.

3.2.2 Preparation of sol-gel derived nano-silica

The sol-gel derived nano-silica was prepared using a previously reported method [1-3]. 0.76 mL of tetraethylothosilicate was taken as precursor material. To this 3.0 mL of water and 4.0 mL of acetone was added. Tetraethylothosilicate, water and acetone were mixed in a 1:4:4 molar ratio and the mixture were stirred at room temperature for 5-7 hours for hydrolysis and polycondenstaion. The polysilanol precipitates (glassy spherical nanoparticles dispersed in a sol) as nanosilica. The suspension was used, without further treatment, for the preparation of the nanocomposites.

3.2.3 Preparation of nanocomposites and blend nanocomposites

LDPE suspended in xylene was thoroughly mixed with the silica suspension at 130 °C. The solvent was evaporated in fumehood. The resultant nanocomposite was mixed with A1 wax wax in a Brabender Plastograph from Duisburg, Germany with 50 mL internal mixer at 130 °C and 30 rpm for 10 min. The mixed samples were melt-pressed into 1 mm thick sheets at 160 °C for 10 min to form LDPE/silica nanocomposites. LDPE-g-MAH/silica nanocomposites were prepared using the same method. Based on previous research [1-3], where the same molar ratios were used and the nano-silica content quantitatively determined, the nano-silica content in LDPE was accepted to be ~2 phr.

Table 3.1 Sample compositions used in this study

PE/wax/silica (w/w)	PE-g-MAH/ wax/silica (w/w)	PE/wax (w/w)	PE-g-MAH/wax (w/w)
100/0/2	100/0/2	100/0	100/0
95/5/2	95/5/2	95/5	95/5
90/10/2	90/10/2	90/10	90/10
85/15/2	85/15/2	85/15	85/15

3.2.4 Differential scanning calorimetry (DSC)

Differential scanning calorimetry is a technique used to study thermal transitions of a polymer. Thermal transitions are the changes that take place in a polymer when it is heated or cooled at a controlled rate. The melting and crystallization of a crystalline polymer, as well as its glass transition are typical examples of thermal transitions. In DSC systems, two pans containing respectively the polymer sample (1-10 mg) and an inert solid are individually heated or cooled. The DSC measures the difference in electrical power (ΔQ) supplied to the two pans as function of time or temperature.

The DSC used was a Perkin Elmer Pyris-1 DSC from Waltham, Massachusetts, U.S.A. The analyses were performed under flowing nitrogen (20 mL min^{-1}). The instrument was computer controlled and calculations were done using Pyris software. The instument was calibrated using the onset temparatures of melting of indium and zinc standards, as well as the

melting enthalpy of indium. 5-10 mg samples were sealed in aluminium pans, heated from 0 to 160 °C at a heating rate of 10 °C min^{-1}, and cooled at the same rate to 0 °C. For the second scan, the samples were heated and cooled under the same conditions. The onset and peak temperatures of melting and crystallization, as well as the melting and crystallization enthalpies were determined from the second scan.

3.2.5 Thermogravimetric analysis (TGA)

TGA is used mainly for determining the thermal stability of polymers. The most widely used TGA method is based on a continuous measurement of mass on a sensitive balance, called a thermobalance, as the sample temperature is increased in air or in an inert atmosphere. This is referred to as nonisothermal TGA. Data are recorded as a TGA curve of mass or mass % as function of temperature or time. Mass loss may arise from evaporation of residual moisture or solvent, but at higher temperatures it results from polymer decomposition. Besides providing information on thermal stability, TGA may be used to characterize polymers through loss of a known entity, such as HCl from poly (vinyl chloride). TGA is also useful for determining volatilities of plasticizers and other additives.

The TGA used was a Perkin Elmer TGA7 from Waltham, Massachusetts, U.S.A. The analyses were performed under flowing nitrogen at the constant rate of 20 mL min^{-1}. The instrument was computer controlled and calculations were done using Pyris software. Samples (5-10 mg) were heated from 25 to 600 °C at 20 °C min^{-1}.

3.2.6 Dynamic mechanical analysis (DMA)

DMA provides valuable data for characterizing the rheological properties of materials, particularly polymers. DMA measures the amplitude and phase of the displacement of a sample in response to an applied oscillating force. The stiffness of the sample is calculated from this data and converted to a modulus to enable inter-sample comparisons. Tan δ, the loss tangent or damping factor, is also calculated. Dynamic mechanical analysis measures the mechanical properties of materials as a function of time, temperature, and frequency. A temperature scan at constant frequency can generate a fingerprint of the material's relaxational processes and its glass transition temperature (T_g). This technique provides valuable data on polymer viscoelastic properties.

The dynamic mechanical properties of the blends and composites were investigated using a Perkin Elmer Diamond DMA from Waltham, Massachusetts, U.S.A. The settings for the analyses were as follows:

Frequency	1 Hz
Amplitude	20 μm
Temperature range	-140 to 80 °C
Heating rate	5 °C min^{-1}
Preload force	0.02 N
Sample length	20 mm
Sample width	12.0 – 12.5 mm
Sample thickness	1.0 – 1.3 mm

3.2.7 Tensile testing

A tensile test, also known as a tension test, is a measure of material reaction to applied forces. For most materials, the initial relationship between the applied force, or load, and the elongation the specimen exhibits, is linear. In this linear region, the line obeys the relationship defined as "Hooke's Law" where the ratio of stress to strain is a constant, or $\sigma/\varepsilon = E$. E is the slope of the line in this region where stress (σ) is proportional to strain (ε) and is called the modulus of elasticity or Young's modulus. This is a measure of the stiffness of the material, but it only applies in the initial linear region of the curve. Within this linear region, the material will return to its exact same condition if the load is removed. At the point that the curve is no longer linear and deviates from the straight-line relationship, Hooke's Law no longer applies and some permanent deformation occurs in the specimen. This point is called the elastic, or proportional, limit, or the yield point. From this point on in the tensile test, the material reacts plastically to any further increase in load or stress. It will not return to its original, unstressed condition if the load were removed.

A Hounsfield H5KS universal testing machine from Redhill, United Kingdom was used for the tensile analysis of the samples. The dumbbell samples were stretched at a speed of 50 mm min^{-1} under a cell load of 2500 N. The gauge length was 24 mm, the thickness was 1.0 ± 0.1 mm and the width was 4.8 mm. The final mechanical properties were evaluated from 5 different measurements.

3.2.8 Scanning electron microscopy (SEM)

During SEM analysis, electrons from a filament in an electron gun are beamed at the specimen in a vacuum chamber. The beam forms a line that continuously sweeps across the specimen surface at high speed. This beam irradiates the specimen which in turn produces a signal in the form of either x-ray fluorescence, secondary or backscattered electrons. The scan rate for the electron beam can be increased so that a virtual 3-D image of the specimen can be viewed. The image can also be captured by standard photography. SEM images have great depth of field yielding a characteristic three-dimensional appearance useful for understanding the surface structure of a sample.

SEM analyses were carried out in a JEOL WINSEM-6400 scanning electron microscope from Tokyo, Japan. The probe size was 114.98 nm, the probe current 0.02 nA, the noise reduction 64 Fr and the AC voltage 5.0 keV. The surfaces of the samples were coated with gold.

3.2.9 Transmission electron microscopy

TEM is a microscopy technique whereby a beam of electrons is transmitted through an ultra thin specimen, interacting with the specimen as it passes through it. An image is formed from the electrons transmitted through the specimen, magnified and focused by an objective and appears on an imaging screen. The energy of the electrons in the TEM determines the relative degree of penetration of electrons in a specific sample, or alternatively, influence the thickness of material from which useful information may be obtained.

The samples were prepared using cryo-ultramicrotomy. They were mounted on cryo-pins and frozen in liquid nitrogen. Sections were cut at -100 °C using a Reichert FCS (Leica, Vienna, Austria) attached to a Reichert Ultracut S Ultramicrotome. The sections (100-150 nm thick) were collected on copper grids and viewed in a LEO 912 Omega (Carl Zeiss NTS GmbH, Oberkochen, Germany) transmission electron microscope, with an energy filter, operating at 120 kV.

3.2.10 Fourier transform infrared spectroscopy (FTIR)

Infrared is an easy way to identify the presence of certain functional groups in a molecule. It can be used as a unique collection of absorption bands to confirm the identity of a pure compound or to detect the presence of specific impurities or chemicals that are either organic

or inorganic. It can be utilized to quantitate some components of an unknown mixture. It can be applied to the analysis of solids, liquids, and gasses. It deals with the infrared region of the electromagnetic spectrum. It covers a range of techniques, the most common being a form of the absorption spectrum. As with all spectroscopic techniques, it can be used to identify compounds or investigate sample composition.

FTIR spectroscopy was performed using a Perkin Elmer Precisely multiscope from Waltham, Massachusetts, U.S.A. Very thin layers of the samples were placed under the microscope and spectra of the desired areas were collected. The samples were scanned using a Perkin Elmer Spectrum 100 FTIR spectrometer over a 400 - 4000 cm^{-1} wave number range at a resolution of 4 cm^{-1}. The FTIR spectra were recorded in the transmittance mode.

3.3 References

1. A.K. Mishra, A.S. Luyt. Effect of sol-gel derived nano-silica and organic peroxide on the thermal and mechanical properties of low-density polyethylene/wood flour composites. Polymer Degradation and Stability (2008) 93:1-8.
2. H.T. Jeon, M.K. Jang, B.K. Kim, K.H. Kim. Synthesis and characterization of waterborne polyurethane-silica hybrids using sol-gel process. Colloids and Surfaces A: Physicochemical and Engineering Aspects (2007) 302:559-567.
3. V. Raman, G. Bhatia, A.K. Mishra, S. Bhardwaj, K.N. Sood. Synthesis of silica carbide nanofibres from pitch blended with sol-gel derived silica. Materials Letters (2006) 60:3906-3911.

CHAPTER 4

RESULTS AND DISCUSSION

4.1 Attenuated total reflectance Fourier-transform infrared spectroscopy (ATR-FTIR)

Figure 4.1 shows the ATR-FTIR spectra of LDPE, wax, LDPE/wax, and LDPE/wax + 2 phr silica, while Figure 4.2 shows the spectra of LDPE-g-MA, wax, LDPE-g-MA/wax, and LDPE-g-MA/wax + 2 phr silica. Some band assignments are listed in Table 4.1.

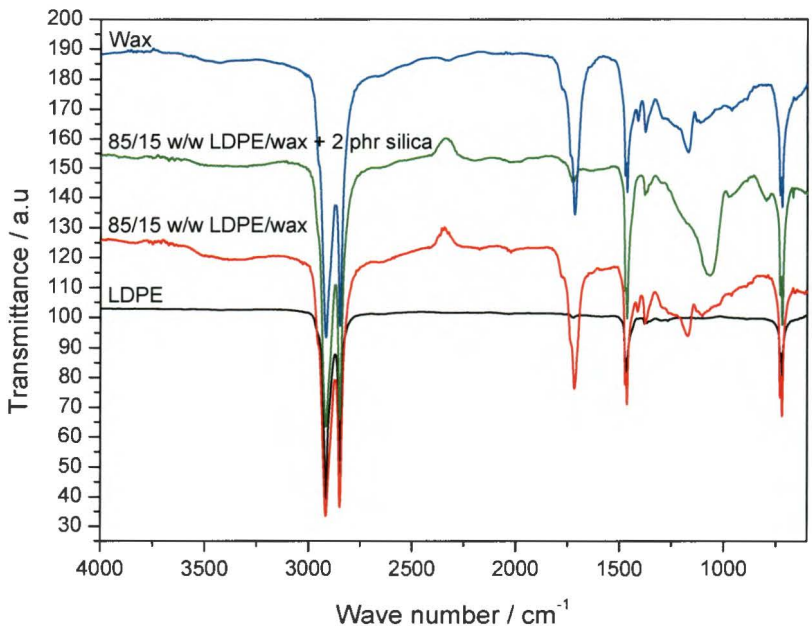

Figure 4.1 FTIR spectra of LDPE, wax, LDPE/wax, and LDPE/wax + 2 phr silica

The FTIR spectrum of 85/15 w/w LDPE/wax shows all the characteristics bands of the two components at the same wavenumbers, with no new peaks being formed. This serves as evidence that LDPE and oxidized wax did not interact in any way. In the spectrum of 85/15 w/w LDPE/wax + 2 phr silica there is a strong absorption at 1069 cm^{-1} attributed to Si-O-Si in polysilanol [2,3], with a shoulder at 1173 cm^{-1} (-C-O- stretching in wax). The C=O stretching vibration in the composite is much less intense than that observed in 85/15 w/w LDPE/wax. This suggests that carbonyl groups in the wax may have formed hydrogen bonding with the OH groups on the silica surfaces.

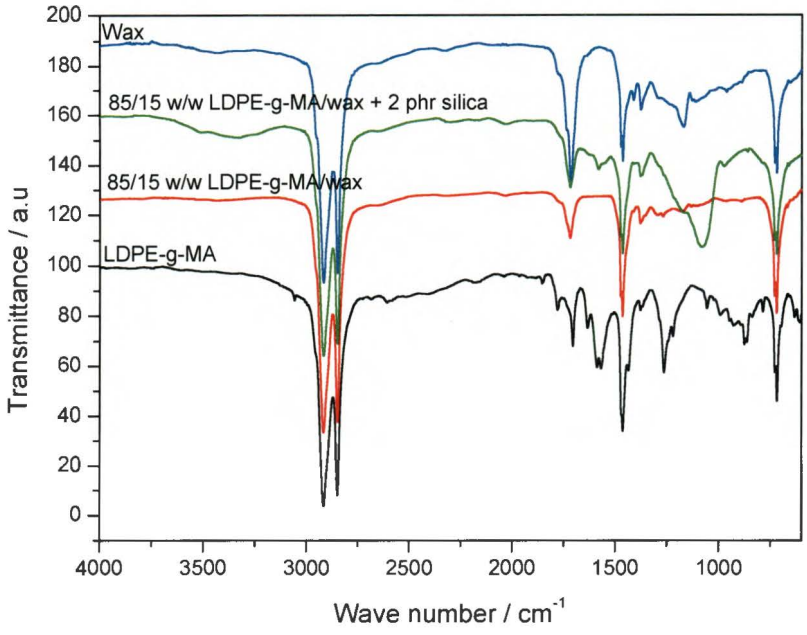

Figure 4.2 FTIR spectra of LDPE-g-MA, wax, LDPE-g-MA/wax and LDPE-g-MA/wax + 2 phr silica

A number of peaks observed in the LDPE-g-MA spectrum are not visible in the spectrum of 85/15 w/w LDPE-g-MA/wax (Figure 4.2), e.g. the unidentified peak at 1578 cm^{-1} and the characteristic absorptions of the cyclic anhydride groups. In the spectrum of 85/15 w/w LDPE-g-MA/wax + 2 phr silica (Figure 4.2) there is an additional strong peak at 1081 cm^{-1} which may be attributed to Si-O-Si of polysilanol. When comparing this spectrum with that of 85/15 w/w LDPE-g-MA/wax, the only obvious differences are a more pronounced OH stretching vibration and the re-appearance of the unidentified peak at 1578 cm^{-1}. Although these differences cannot be directly related to an interaction mechanism between LDPE-g-MA, wax and/or silica, it is clear that there are interactions between LDPE-g-MA and oxidized wax, LDPE-g-MA and silica, and oxidized wax and silica.

Table 4.1 Some important peaks in FTIR spectra of pure LDPE, LDPE-g-MA, wax and LDPE-g-MA + 2 phr silica

Wavenumber / cm^{-1}	Assigned vibrations	Visible in
719	Rocking of sequences of methylene groups	All samples
1081	Si-O-Si vibration	LDPE-g-MA + 2 phr silica
1173	-C-O- stretching	Wax
1215, 1780, 1850	Characteristic absorptions of cyclic anhydride groups	LDPE-g-MA
1463	C-H bending of CH_3 groups	All samples
1578	The source of this peak is presently not clear	LDPE-g-MA
1705	C=O stretching	LDPE-g-MA
1715	C=O stretching vibration from free carboxylic acid and from esters	Wax
2848	C-H stretching	All samples
2914	CH_2 stretching	All samples
3453	-OH stretching	Wax

4.2 Scanning electron microscopy (SEM)

The SEM photographs of the nanocomposites and blends are given in the Figure 4.3. The SEM images of the non-fractured surfaces show white spherical silica nanoparticles uniformly dispersed in the matrices. The sizes of the silica particles were found to be in the range of 10-50 nm, but a few large agglomerates of 100-200 nm were also formed. The larger agglomerates are more visible for all the ungrafted LDPE samples compared to the grafted ones. This is due to weak adhesion between the polymer and silica which improved in the presence of anhydride groups as observed from FTIR. Generally, the SEM images of the fractured surfaces do not show as many nanoparticles. The presence of wax seems to reduce the agglomeration of silica in both the LDPE and LDPE-g-MA/silica nanocomposites, which should lead to improved silica dispersion. This is as a result of the interaction occurred between the components as explained in FTIR.

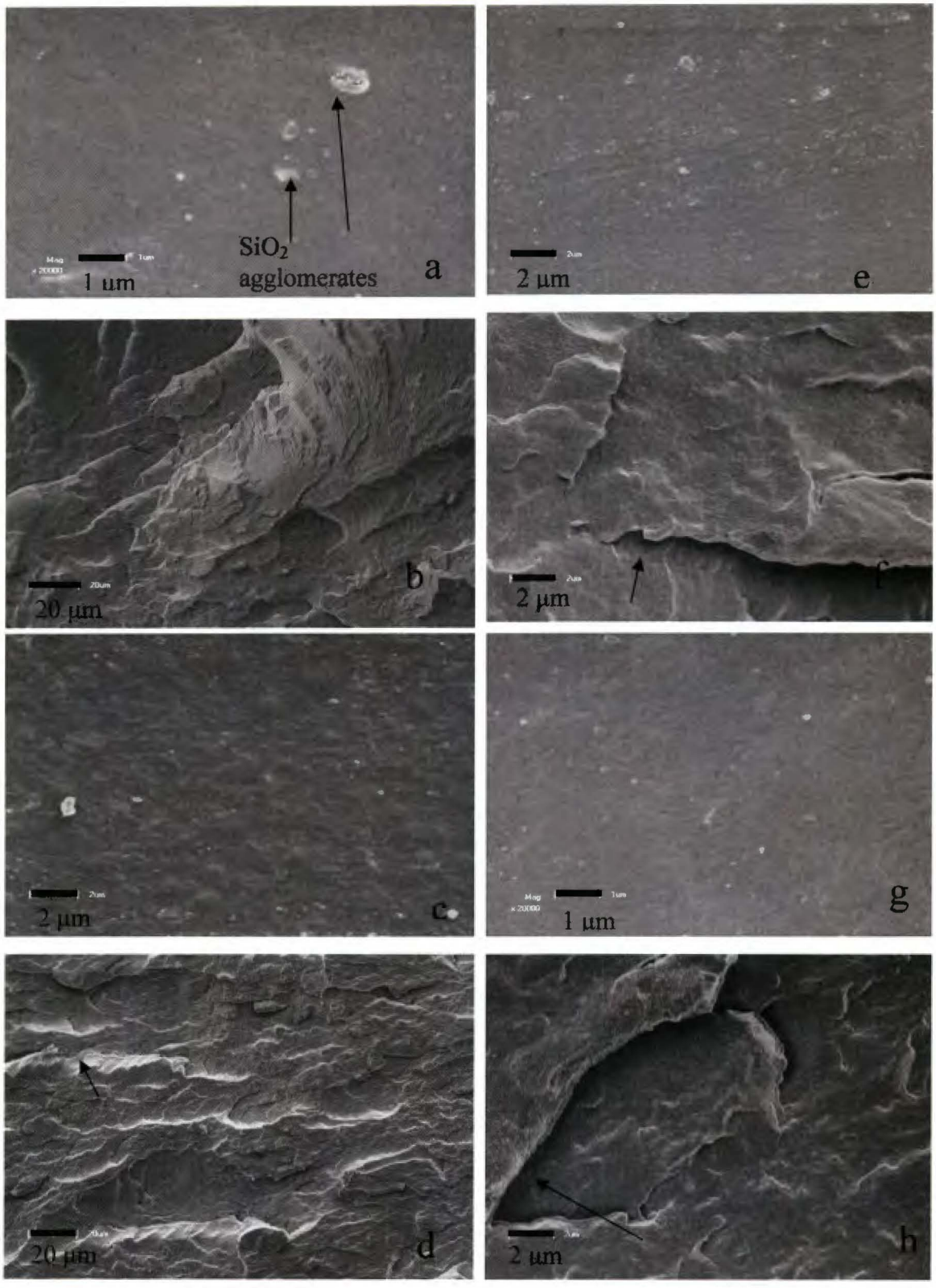

Figure 4.3 SEM images of (a) LDPE + 2 phr silica (surface), (b) LDPE + 2 phr silica (fractured surface), (c) 90/10 w/w LDPE/wax + 2 phr silica (surface), (d) 90/10 w/w PE/wax + 2 phr silica (fractured surface), (e) LDPE-g-MA + 2 phr silica (surface), (f) LDPE-g-MA + 2 phr silica (fractured surface), (g) 90/10 w/w PE-g-MA/wax + 2 phr silica (surface), and (h) 90/10 w/w PE-g-MA/wax + 2 phr silica fractured surface

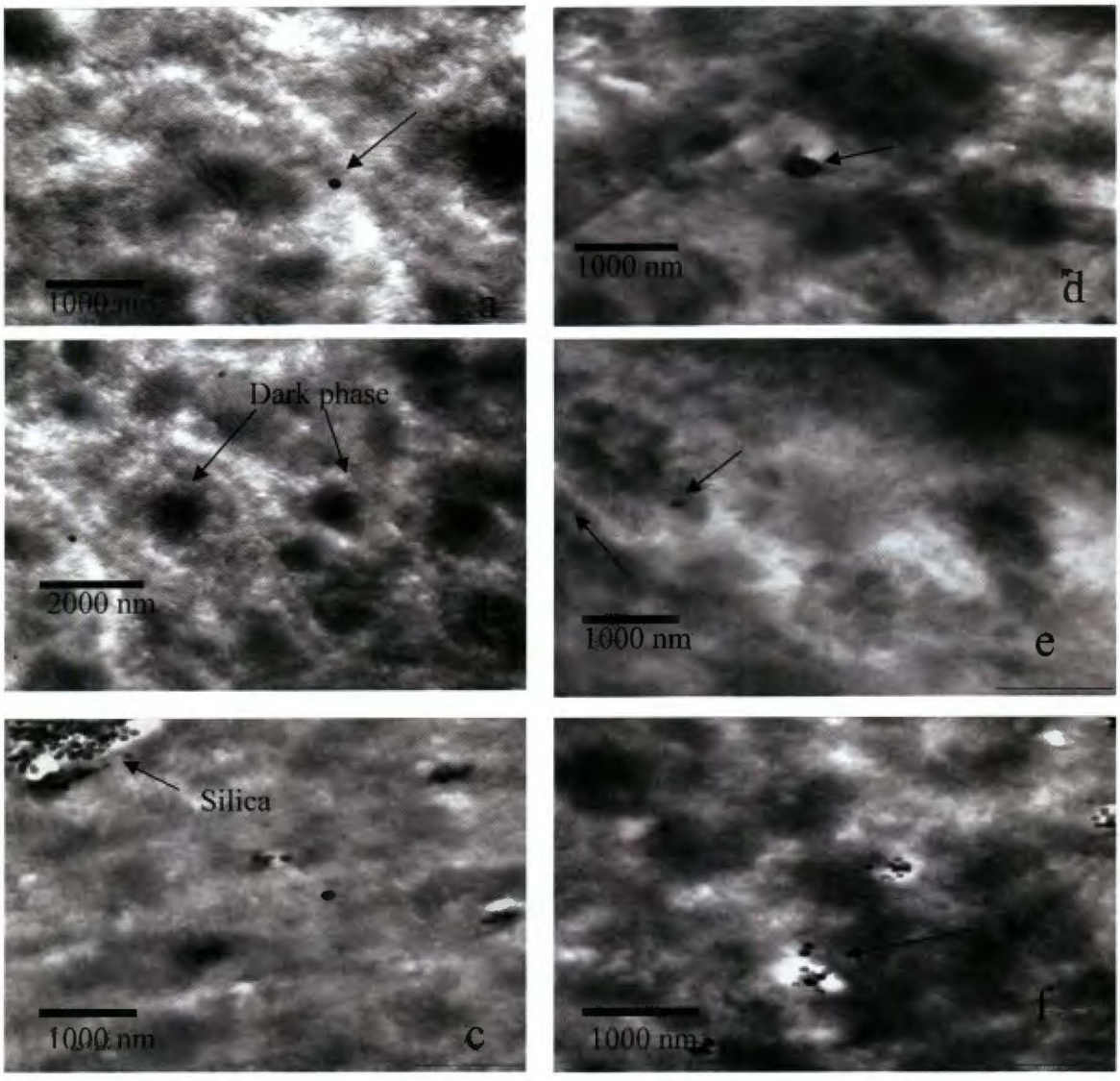

Figure 4.4 TEM micrographs of a) and b) LDPE + 2 phr silica, c) 90/10 w/w LDPE/wax + 2 phr silica, d) LDPE-g-MA + 2 phr silica, e) and f) 90/10 w/w PE-g-MA/wax + 2 phr silica

4.3 Transmission electron microscopy (TEM)

The TEM photographs of the nanocomposites and blends are shown in Figure 4.4. There are dark areas observed in the images which could be attributed to silica clusters surrounded by more crystalline LDPE. In general, these areas are less well distributed in ungrafted LDPE than in the functionalized samples. This may be attributed to poor interaction between the polymer and the filler. In addition to the dark areas, Figure 4.4(b) shows a couple of

nanoparticles approximately 50 nm in diameter. Figure 4.4(c) clearly shows two phases, with the silica concentrated in the one phase as single dispersed particles, as well as small and large agglomerates. Figure 4.4(f) shows mostly particle clusters concentrated in one of the phases, probably the wax. In the presence of wax (Figure 4.4(c) and (f)), the agglomerate sizes seem smaller for the grafted composites compared to the ungrafted ones. Section 4.2 confirms the observation. This is the result of the interactions between the nanoparticles, the oxidized wax and the matrix (see discussion in section 4.1).

4.4 Differential scanning calorimetry (DSC)

The DSC results of all the samples are summarized in Figure 4.5- 4.14. The peak temperatures of melting and crystallization, as well as the melting and crystallization enthalpies, of all the samples are shown in Table 4.2. All the reported DSC heating results were obtained from the second scan to eliminate the effect of the thermal history.

4.4.1 Effect of silica nano-particles and anhydride grafting on the thermal behaviour of LDPE

The DSC curves of pure LDPE and LDPE-g-MA, as well as the LDPE/SiO_2 and LDPE-g-MA/SiO_2 nanocomposites, are presented in Figure 4.5. Only one endothermic peak is observed for all four samples, with very little change in the melting peak temperatures when silica is added to either LDPE or LDPE-g-MA. This indicates that silica does not influence the crystallite sizes of both LDPE and LDPE-g-MA. LDPE-g-MA and its nanocomposites have lower T_m values than LDPE and its nanocomposites. This change in melting temperatures is attributed to the presence of an anhydride group on the matrix backbone. This is in agreement with the findings of Zhou *et al.* [4], where PE-g-MA had a lower melting point, but contrary to the work done by Singh *et al.* [5], where the grafting of maleic anhydride on LDPE increased the melting point. Singh *et al.* [5] related their observations to the presence of polar carboxyl groups. Zhou *et al.* [4] related their observations to an amorphous interaction in the PE phase which could only happen between the anhydride groups of LDPE-g-MAH and the amino groups of an aromatic liquid-crystal poly (ester-co-amide) which was used as filler.

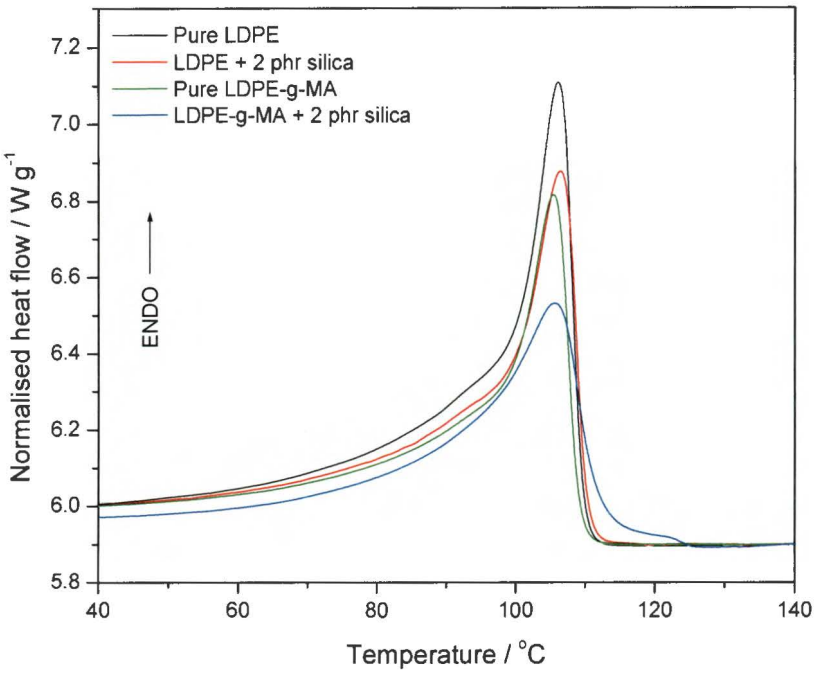

Figure 4.5 DSC heating curves of pure LDPE, pure LDPE-g-MA, and their nanocomposites

The enthalpies of the composites are significantly lower than those of the pure polymers (Table 4.2), which indicates an observable decrease in the crystallinity of the materials. This is confirmed when the measured melting enthalpy values (ΔH_m^{obs}) are compared with the calculated values (ΔH_m^{calc}), where the LDPE and LDPE-g-MA in the composites have significantly lower enthalpy (or crystallinity) values than would be expected if it was assumed that the silica particles had no influence on the LDPE and LDPE-g-MA crystallization behaviour. The ΔH_m^{calc} values were calculated from the melting enthalpies of pure LDPE and pure LDPE-g-MA, and the weight fractions of LDPE and LDPE-g-MA in the respective blends according to additive rule in Equation 4.1.

$$\Delta H_m^{calc} = \Delta H_{m,PE} w_{PE} + \Delta H_{m,w} w_w \qquad (4.1)$$

where $\Delta H_{m,PE}, \Delta H_{m,w}$, ΔH_m^{add} are the specific enthalpies of melting of PE, wax and blends, and w_{PE}, w_w are the weight fractions of PE and wax in the blends. The lower enthalpy values suggest that the presence of the silica restricts the mobility of the polymer chains during crystallization. The difference between ΔH_m^{obs} and ΔH_m^{calc} is more pronounced in the case of

LDPE-g-MA (ΔH_m^{obs} is 18% lower than ΔH_m^{calc}, compared to 13% in the case of LDPE) and this indicates a much stronger interaction between nano-silica and the matrix in the case of the functionalized LDPE.

Table 4.2 Summary of DSC melting and crystallization peak temperatures and enthalpies for all the investigated samples

Sample	Second heating			Cooling	
	$T_{p,m}$ / °C	ΔH_m^{obs} / J g^{-1}	ΔH_m^{calc} / J g^{-1}	$T_{p,c}$ / °C	ΔH_c^{obs} / J g^{-1}
LDPE/SiO_2					
Pure LDPE	106.3	113.7	-	90.1	-117.0
Pure LDPE + 2 phr silica	106.7	98.5	111.4	90.3	-100.1
Pure LDPE-g-MA	105.7	89.0	-	90.6	-90.0
Pure LDPE-g-MA + 2 phr silica	104.7	71.0	87.2	92.4	-92.5
LDPE/wax					
Pure LDPE	106.3	113.7	-	90.1	-117.0
95/5	105.6	101.1	114.1	90.9	-94.5
90/10	105.1	100.4	114.4	90.7	-98.8
85/15	104.5	106.9	114.8	90.0	-98.4
LDPE/wax/SiO_2					
100/2	106.7	98.5	111.4	90.3	-100.1
95/5/2	105.7	96.9	111.8	90.1	-101.8
90/10/2	106.0	100.4	112.1	89.9	-118.5
85/15/2	105.6	112.4	112.5	89.5	-97.0
LDPE-g-MA/wax					
Pure LDPE-g-MA	105.7	89.0	-	90.6	-90.0
95/5	104.9	85.2	90.6	90.1	-91.0
90/10	106.2	87.3	92.2	90.6	-91.0
85/15	105.2	88.1	93.8	90.8	-92.7
LDPE-g-MA/wax/SiO_2					
100/2	104.7	71.0	87.2	92.4	-92.5
95/5/2	105.0	87.7	88.8	91.1	-92.0
90/10/2	104.4	88.7	90.4	90.7	-91.6
85/15/2	104.0	96.1	91.9	91.5	-98.7
Wax					
Oxidized paraffin wax	75.7_a 97.6_b	121.0	-	86.6_a 73.2_b	-112.6

$T_{p,m}$, $T_{p,c}$, ΔH_m^{obs} , ΔH_c^{obs}, ΔH_m^{cal}, are respectively the peak temperature of melting, peak temperature of crystallization, observed melting enthalpy, observed crystallization enthalpy, calculated melting enthalpy, while a and b respectively indicate the first and second peak maxima in the wax melting peak

The DSC cooling curves of pure LDPE and LDPE-g-MA, as well as the LDPE/SiO_2 and LDPE-g-MA/SiO_2 nanocomposites, are shown in Figure 4.6. The results are summarized in Table 4.2. The trends observed from the cooling curves are the same than those observed for melting, and they can therefore be explained in the same way.

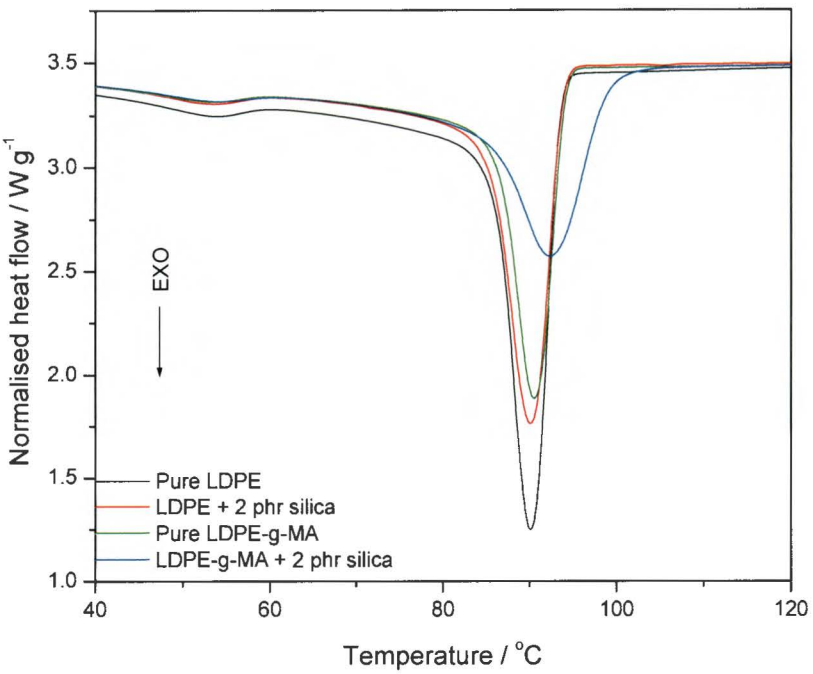

Figure 4.6 DSC cooling curves of pure LDPE, pure LDPE-g-MA, and their nanocomposites

4.4.2 Effect of oxidized wax on the thermal properties of LDPE and its nanocomposites

The DSC heating curves of the LDPE/wax blends and LDPE/wax/silica nanocomposites are shown in Figures 4.7 and 4.8. Only one endothermic peak is observed for the 5 and 10% wax containing samples, but for the 15% wax containing sample a peak appears at lower temperatures. This is the result of a phase separation of the LDPE and wax. The immiscibility of wax and LDPE was observed previously [6], and was explained as being the result of the wax crystallizing separately in the amorphous phase of LDPE. The wax shows two well distinguished separate peaks at 76 and 98 °C. Luyt and Krupa [7] reported that the multiple endothermic peaks of the wax were due to the melting of different molar mass fractions. It can also be seen that there is a slight decrease in T_m values of LDPE with an increase in wax content. This may have been caused by either crystallization of LDPE into thinner lamellae or

plasticization of LDPE by the wax. These results are in line with observations by Djoković *et al.* [8]. The melting temperatures remained fairly constant within experimental error for the silica-containing samples and they differ only slightly from those of the LDPE/wax blends as shown in Table 4.2. This may suggest that silica is preferably covered by the wax. If so, it will give rise to a less effective dispersion of the wax between the LDPE crystallites, which will reduce the plasticizing effect of the wax. The experimental enthalpy values of the LDPE/wax blends are lower than those calculated according to the additive rule (Table 4.2). This may be due to inaccuracies in the analysis of the DSC curves, because it was very difficult to define the correct baseline below the peaks. The values are lower in the presence of silica alone, but they increase with wax content until the experimental value is effectively the same as the calculated value at the highest wax content. Silica, in the absence of wax, seems to influence the polymer crystallization by reducing the mobility of the LDPE chains, giving rise to lower than expected melting enthalpy values. If the wax preferably interacts with the silica, it may crystallize around the silica particles and inhibit interaction between the silica particles and LDPE, giving rise to reduced influence of the silica particles on LDPE crystallization.

The DSC cooling curves of the LDPE/wax blends and the blend nano-composites are shown in Figure 4.9 and 4.10. The results are summarized in Table 4.2. The trends observed from the cooling curves are the same than those observed for melting, and they can therefore be explained in the same way.

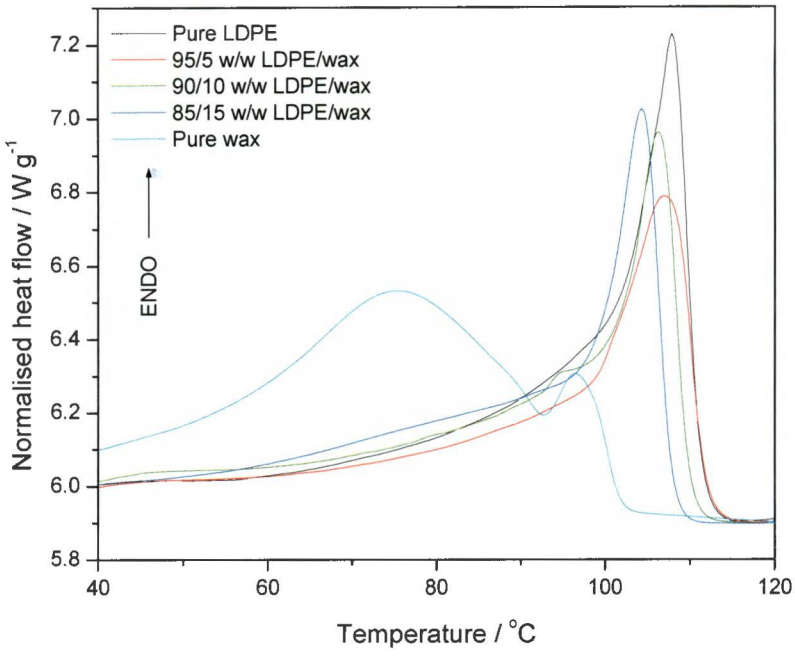

Figure 4.7 DSC heating curves of pure LDPE, oxidized wax, and the LDPE/oxidized wax blends

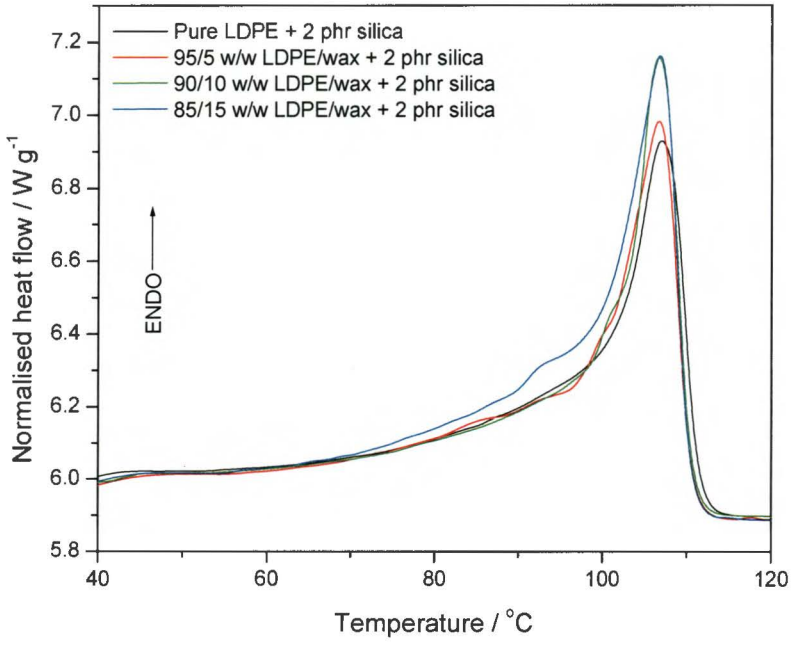

Figure 4.8 DSC heating curves of the LDPE nanocomposite and the LDPE/wax blend nanocomposites

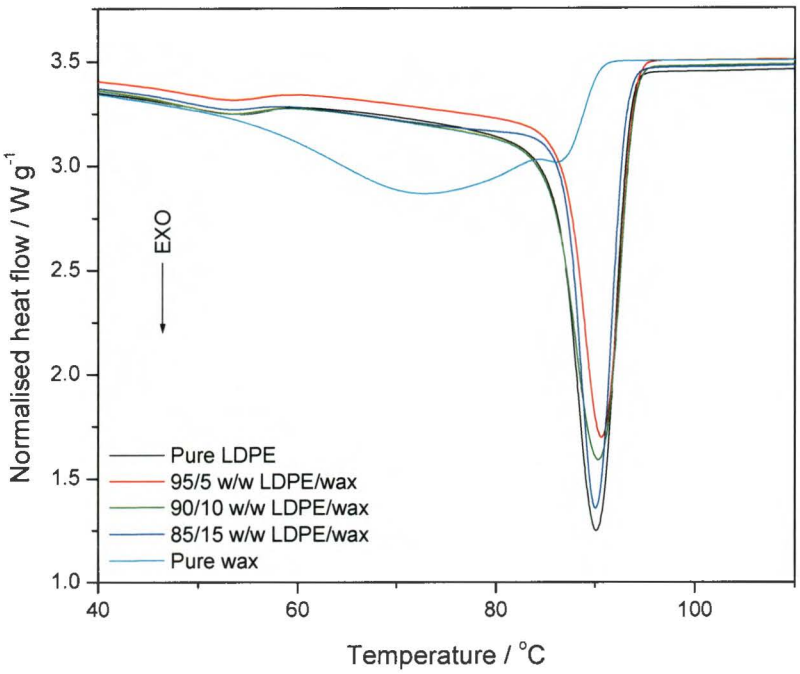

Figure 4.9 DSC cooling curves of pure LDPE, oxidized wax, and the LDPE/oxidized wax blends

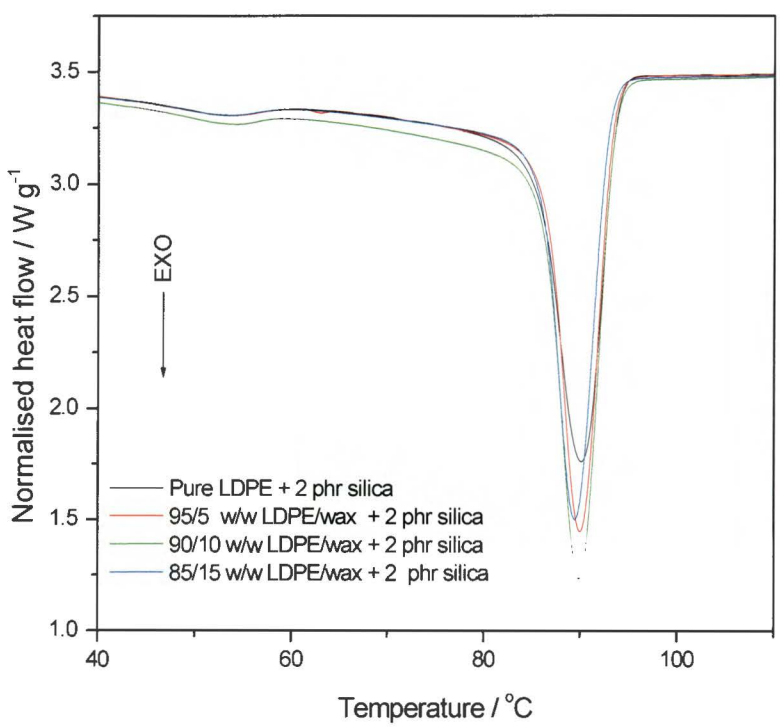

Figure 4.10 DSC cooling curves of the LDPE nanocomposite and the LDPE/wax blend nanocomposites

4.4.3 The effect of oxidized wax on the thermal properties of LDPE-g-MA and its nanocomposites

The DSC heating curves of the LDPE-g-MA/wax blends and the LDPE-g-MA/wax/silica nanocomposites are shown in Figure 4.11 and 4.12. Generally, only one endothermic peak is observed, except for the 85/15 w/w LDPE-g-MA/wax + 2 phr silica nano-composite, which shows the formation of a peak at a lower temperature. This indicates that the LDPE-g-MA and the wax are (at least partially) miscible in the crystalline phase. In contrast with the 85/15 w/w LDPE/wax blend which shows a peak at lower temperatures, the equivalent LDPE-g-MA/wax blend does not show any peak at lower temperatures. In the case of the LDPE-g-MA/wax blend, the functional groups in the wax interact with the anhydride groups in LDPE-g-MA, which will promote co-crystallization. From Table 4.2 it can be seen that the melting temperatures for all the samples are the same within experimental error. The melting enthalpies of the LDPE-g-MA/wax samples follow the same trend with increasing wax content as those of the LDPE/wax samples (Table 4.2), but the differences between the experimentally observed and theoretically calculated values are smaller. The reason for this is probably that there is more efficient co-crystallization of the LDPE-g-MA and the wax because of stronger interaction between their respective functional groups. The melting temperatures of the LDPE-g-MA/wax blend composites are slightly lower than those of the LDPE-g-MA/wax blends. Wax seems to have no influence on the melting and crystallization temperature values (within experimental uncertainty) of the LDPE-g-MA/wax blends and their respective composites. For pure LDPE-g-MA + 2 phr silica the observed enthalpy value is significantly lower than the calculated value, at lower wax contents the values are almost the same, and at the highest wax content it is higher. The presence of silica alone reduces the crystallinity of the material as explained in the case of LDPE, and hence the melting enthalpy values are lower. At low wax contents the wax is probably more concentrated around the silica, if it can be accepted that the silica interacts more strongly with the wax than with the LDPE-g-MA, which may reduce the influence of the silica on the polymer crystallization. At the highest wax contents, some of the wax probably co-crystallized with the LDPE-g-MA (because of the interaction between the two components) and, because of the higher crystallinity of the wax, the matrix crystallinity increased to values higher than expected.

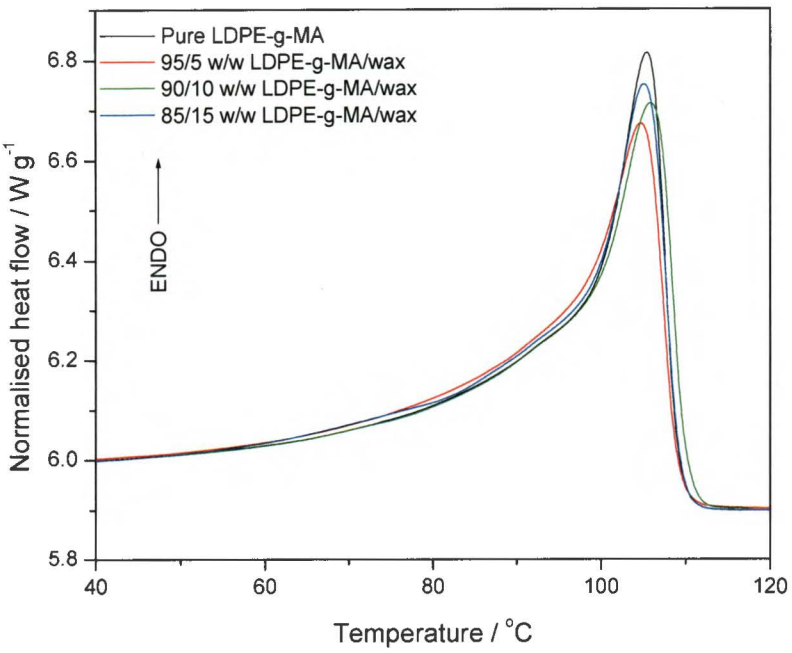

Figure 4.11 DSC heating curves of pure LDPE-g-MA and the LDPE-g-MA/oxidized wax blends

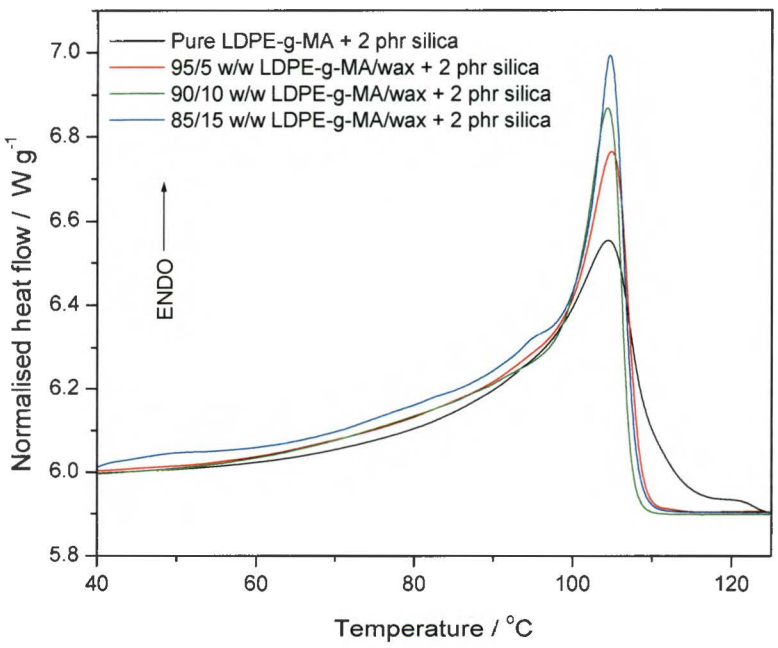

Figure 4.12 DSC heating curves of the PE-g-MA nanocomposite and the PE-g-MA/wax blend nanocomposites

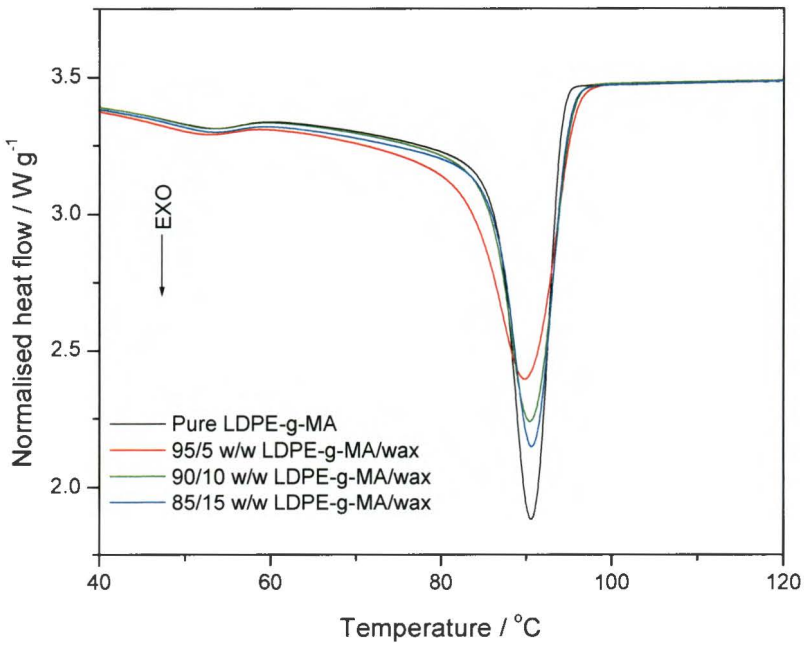

Figure 4.13 DSC cooling curves of pure LDPE-g-MA, oxidized wax and the LDPE-g-MA/oxidized wax blends

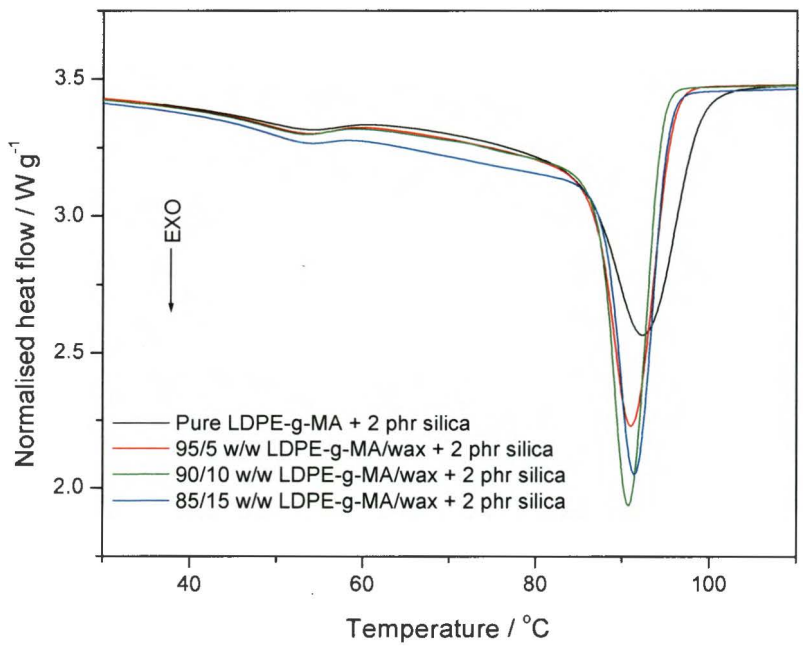

Figure 4.14 DSC cooling curves of the PE-g-MA nanocomposite and the PE-g-MA/wax blend nanocomposites

The DSC cooling curves of the LDPE-g-MA/wax blends and the blend nano-composites are shown in Figure 4.13 and 4.14. The results are summarized in Table 4.2. It can be seen that the crystallization trends are the same as those observed for melting, and they can therefore be explained in the same way.

4.5 Thermogravimetric analysis

The results of the TGA measurements of all the blends and nanocomposites are summarized in Figures 4.15- 4.19. The thermal stabilities of all the samples are summarized in Table 4.3 in terms of the onset temperature and the temperature at 30% mass loss. The TGA curves of all the samples show a single mass loss step.

4.5.1 Effect of silica nano-particles and anhydride grafting on the thermal stability of LDPE

Figure 4.15 shows that the silica nano-particles have a negligible effect on the thermal stability of both ungrafted and grafted LDPE, but that the maleic anhydride grafting improves the thermal stability of LDPE. The improvement in the thermal stability is associated with the disturbed degradation mechanism in the presence of anhydride functional groups. Random scission is the primarily degradation pathway in PE and it can also result in branching [9]. It is possible that there may be a strong interaction between the anhydride groups which may hinder to some extend the evaporation of monomers. These results are in line with observations of Wang *et al.* [10] and Zhai *et al.* [11], but they differ from those found by Singh *et al.* [5], who observed that the presence of the anhydride groups on the LDPE chains does not influence the thermal stability.

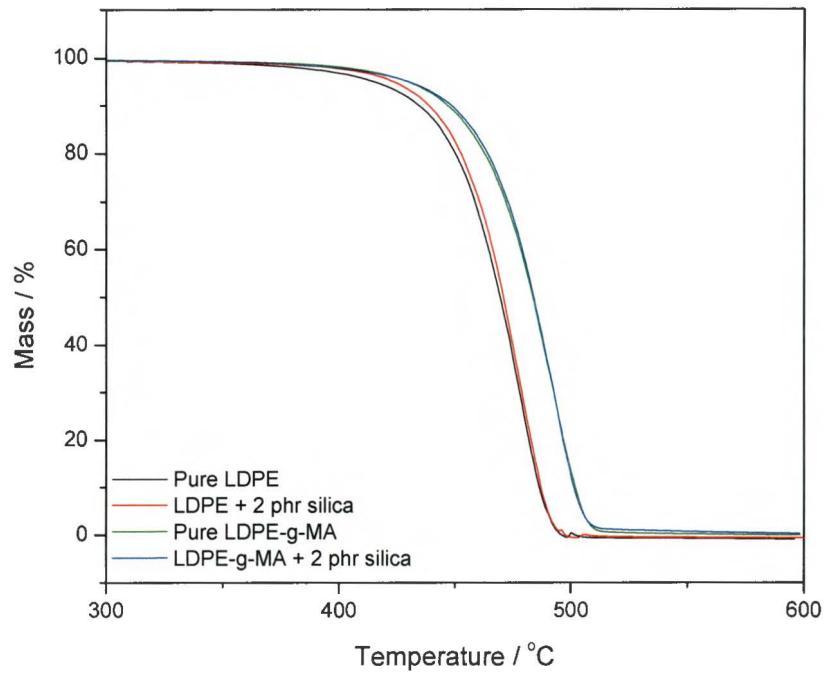

Figure 4.15 TGA curves of pure LDPE, pure LDPE-g-MA, and their silica nano-composites

4.5.2 Effect of oxidized wax on the thermal stability of LDPE and its nanocomposites

The TGA curves of the LDPE/wax blends and their silica nanocomposites are shown in Figures 4.16 and 4.17. The thermal stabilities of both the blends and blend composites decrease with an increase in wax content as a consequence of the lower thermal stability of the wax. Similar behaviour was found by Djoković *et al.* [8] and Krupa *et al.* [12], who respectively investigated LDPE/oxidized wax and LLDPE/oxidized wax blends. In general, it seems as if the LDPE/wax blends have lower thermal stabilities than the respective composites (Table 4.3). This may be due to the synergistic effects of the silica and the wax, since there is strong interaction between the oxygen groups on the wax chains and the OH groups on the silica (see section 4.1), which may have caused reduced chain mobility (see also discussion of DSC results above). It is also possible that the presence of the silica particles inhibits the evolution of volatile degradation products.

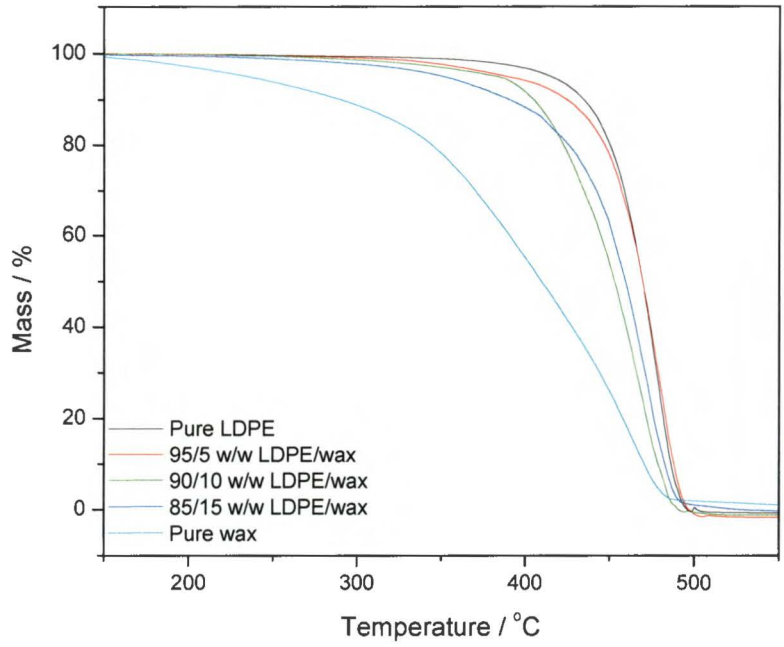

Figure 4.16 TGA curves of pure LDPE, pure wax and LDPE/wax blends

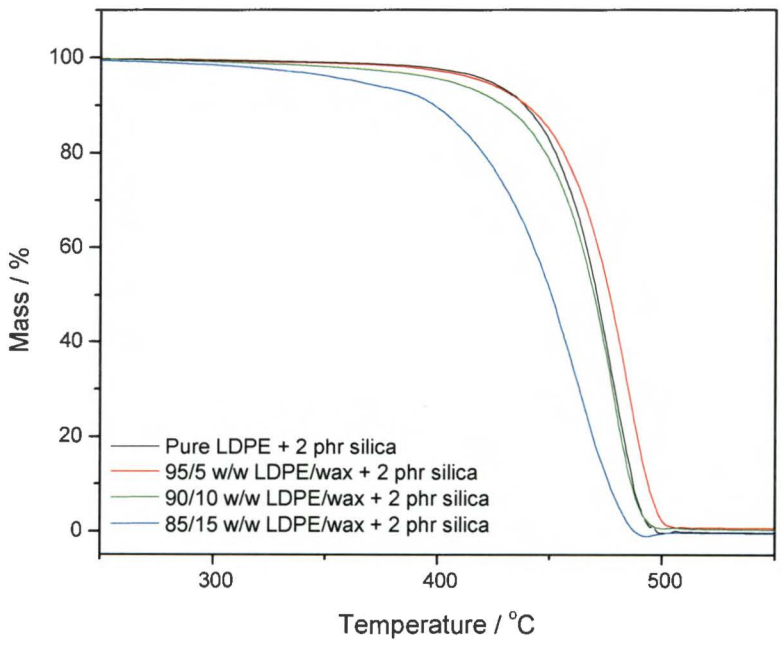

Figure 4.17 TGA curves of the LDPE and LDPE/wax nano-composites

Table 4.3 Summary of TGA results for all the investigated samples

Sample	T_{onset} / °C	T_{30} / °C
LDPE/SiO_2		
Pure LDPE	446.2	458.1
Pure LDPE + 2 phr silica	449.7	460.2
Pure LDPE-g-MA	460.5	471.4
Pure LDPE-g-MA + 2 phr silica	460.7	472.4
LDPE/wax		
Pure LDPE	446.2	458.1
95/5	444.8	456.2
90/10	418.1	434.4
85/15	417.3	441.2
LDPE/wax/SiO_2		
100/2	449.7	460.2
95/5/2	453.4	464.6
90/10/2	447.2	457.7
85/15/2	420.1	433.0
LDPE-g-MA/wax		
Pure LDPE-g-MA	460.5	471.4
95/5	461.6	474.8
90/10	463.0	473.8
85/15	459.5	468.5
LDPE-g-MA/wax/SiO_2		
100/2	460.7	472.4
95/5/2	465.8	477.7
90/10/2	463.1	474.6
85/15/2	439.2	453.5
Wax	354.5	369.9

T_{onset} = onset temperature of degradation; T_{30} = temperature at 30% mass loss.

4.5.3 Effect of oxidized wax on the thermal stability of LDPE-g-MA and its nanocomposites

The TGA curves of the LDPE-g-MA/wax blends and their silica nanocomposites are shown in Figures 4.18 and 4.19. All the PE-g-MA/wax blends and nanocomposites have higher temperature values for both the onset and 30% degradation temperatures than the LDPE/wax blends and nanocomposites. This is because LDPE-g-MA itself is more thermally stable than LDPE. It does not seem as if the wax or the silica has a major influence on the degradability of PE-g-MA.

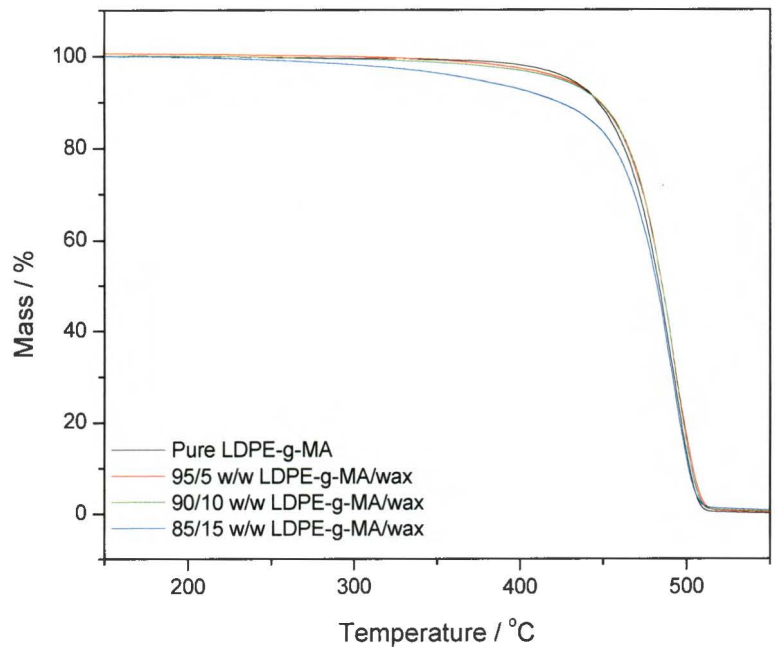

Figure 4.18 TGA curves of pure LDPE-g-MA and LDPE-g-MA/wax blends

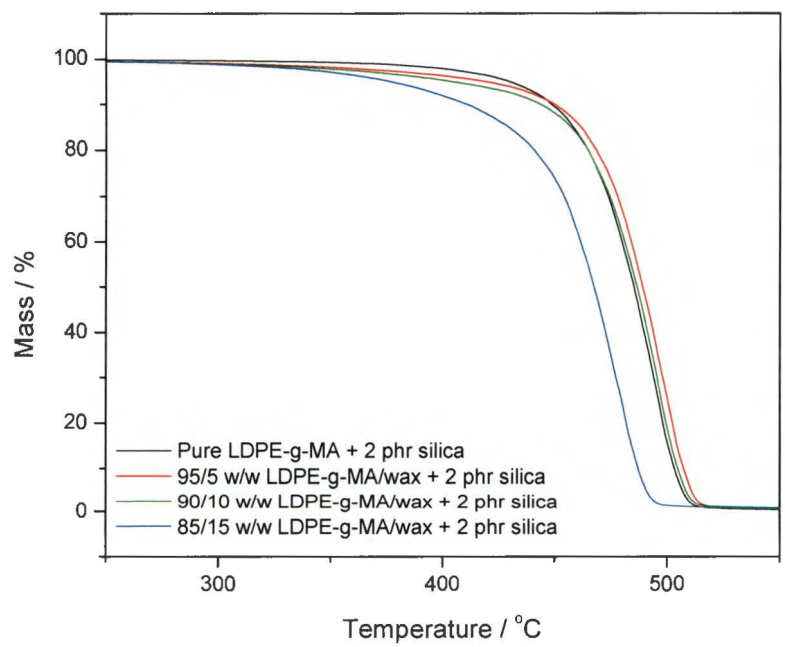

Figure 4.19 TGA curves of the LDPE-g-MA and LDPE-g-MA/wax nano-composites

4.6 Tensile properties

The stress and strain at yield, stress and strain at break, and Young's modulus of all the samples are summarized in Table 4.4. The influence of wax content on the modulus of the different blends and nanocomposites are shown in Figure 4.20. All the grafted LDPE samples show a higher modulus for all wax contents than the ungrafted LDPE samples. All the samples show a slight increase in Young's modulus with an increase in wax content up to 10% for the LDPE/wax blend nanocomposites. Similar trends were observed by Krupa and Luyt [12], and it was attributed to the higher degree of crystallinity of the material in the

Table 4.4 The mechanical properties of polyethylene blends and the nanocomposites

Sample	$\varepsilon_y \pm S\varepsilon_y$ / %	$\sigma_y \pm S\sigma_y$ / MPa	$\varepsilon_b \pm S\varepsilon_b$ / %	$\sigma_b \pm S\sigma_b$ / MPa	E ± SE / MPa
LDPE/SiO_2					
Pure LDPE	9.2 ± 0.4	8.8 ± 0.2	51 ± 1.0	9.5 ± 0.6	145 ± 3.8
Pure LDPE + 2 phr silica	7.6 ± 0.3	9.5 ± 0.3	21 ± 1.2	9.6 ± 0.3	149 ± 3.1
Pure LDPE-g-MA	5.2 ± 0.7	7.0 ± 0.6	141 ± 13.1	8.1 ± 0.5	184 ± 11.1
Pure LDPE-g-MA + 2 phr silica	5.2 ± 0.8	7.7 ± 0.4	114 ± 22.3	8.7 ± 0.6	201 ± 4.0
LDPE/wax					
Pure LDPE	9.2 ± 0.4	8.8 ± 0.2	51 ± 1.1	9.5 ± 0.6	145 ± 4.0
95/5	9.9 ± 0.5	7.0 ± 0.2	21 ± 2.3	10.4 ± 0.8	158 ± 6.8
90/10	6.6 ± 0.8	6.3 ± 0.3	18 ± 1.1	11.0 ± 1.1	182 ± 2.7
85/15	6.7 ± 0.5	6.1 ± 0.3	19 ± 1.3	6.8 ± 0.3	298 ± 4.1
LDPE/wax/SiO_2					
100/2	7.6 ± 0.3	9.5 ± 0.3	21 ± 1.0	9.6 ± 0.3	149 ± 3.1
95/5/2	6.8 ± 0.8	9.4 ± 0.2	20 ± 1.4	10.0 ± 0.3	163 ± 8.8
90/10/2	6.3 ± 0.3	9.5 ± 0.6	19 ± .07	11.5 ± 0.2	172 ± 16.0
85/15/2	6.2 ± 0.4	9.1 ± 0.6	18 ± 0.6	9.8 ± 0.6	161 ± 12.1
LDPE-g-MA/wax					
Pure LDPE-g-MA	5.2 ± 0.7	7.0 ± 0.6	141 ± 13.1	8.1 ± 0.5	184 ± 11.1
95/5	6.1 ± 1.1	7.3 ± 0.7	32 ± 1.9	8.0 ± 0.6	188 ± 29.0
90/10	3.4 ± 0.3	8.3 ± 0.5	16 ± 6.9	8.3 ± 0.6	276 ± 21.9
85/15	3.6 ± 0.3	9.4 ± 0.6	10 ± 1	9.5 ± 0.4	309 ± 8.7
LDPE-g-MA/wax/SiO_2					
100/2	5.2 ± 0.8	7.7 ± 0.4	114 ± 21.7	8.7 ± 0.6	201 ± 3.6
95/5/2	4.1 ± 0.4	7.7 ± 0.3	27 ± 1.3	7.9 ± 0.3	223 ± 10.9
90/10/2	4.1 ± 1.1	7.9 ± 0.4	26 ± 0.8	8.4 ± 0.4	233 ± 15.7
85/15/2	3.2 ± 0.3	9.7 ± 0.3	9 ± 0.1	10.3 ± 0.4	370 ± 9.0

ε_y ,σ_y, ε_b, σ_b and E are elongation at yield, yield stress, elongation at break, stress at break and Young's modulus of elasticity. $S\varepsilon_y$,$S\sigma_y$, $S\varepsilon_b$, $S\sigma_b$ and S_E are their respective standard deviations

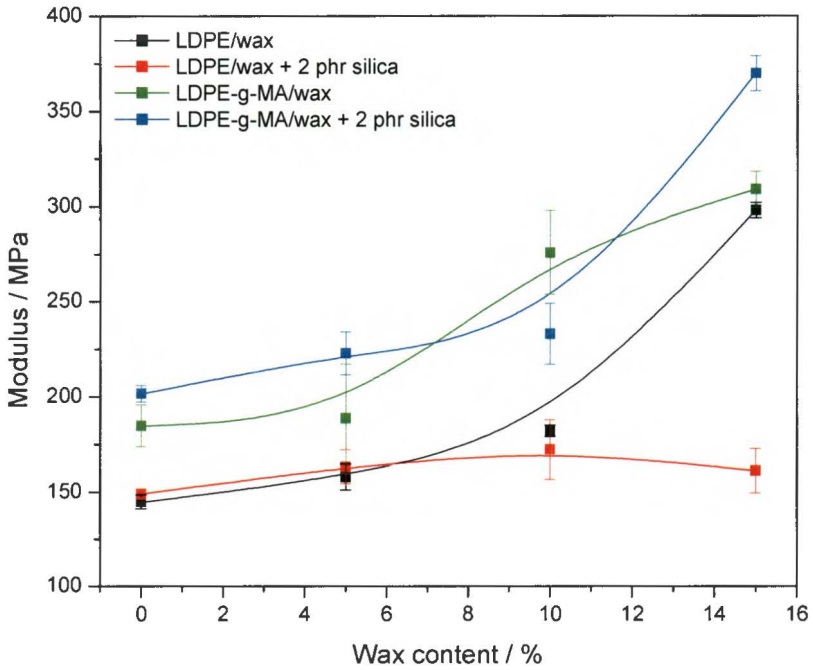

Figure 4.20 Young's modulus of LDPE/wax and LDPE-g-MA/wax blends and blend composites

presence of wax. At 15% wax content, a slight decrease in Young's modulus is observed for the LDPE/wax blend nanocomposites. This is associated with the phase separation of the wax and the polymer at the highest wax content (see section 4.1), or by plasticization of the polymer by the wax (see section 4.4). The phase separation may be the result of the presence of silica which inhibits the co-crystallization of the wax with the polymer, because the wax seems to concentrate around the silica (see previous discussion). In the case of the PE-g-MA/wax blends and PE-g-MA/wax blend nanocomposites the opposite behaviour is observed, where Young's modulus increase further for 15% wax content for both the blend and the nanocomposite. This is probably the result of the stronger interactive forces between the polymer, wax and nanoparticles (as discussed previously). The presence of silica alone did not increase the Young's modulus of LDPE, but it increased the Young's modulus of LDPE-g-MA by 9%. This is probably due to the good interface between the components as a result of the interaction between the functional group in the polymer and the silica nanoparticles (see section 4.1).

The yield stress of both the LDPE/wax and LDPE-g-MA/wax blends and their nano-composites are shown in Figure 4.21. An increase in yield stress (measure of the resistance to plastic deformation) for all the LDPE-g-MA/wax blends and their composites with an increase in wax content is observed. This may be attributed to intermolecular interaction of the LDPE-g-MA and oxidized wax in the case of the blends (see section 4.1), and also an increase in the degree of crystallinity in the case of the composites (see Table 4.2).

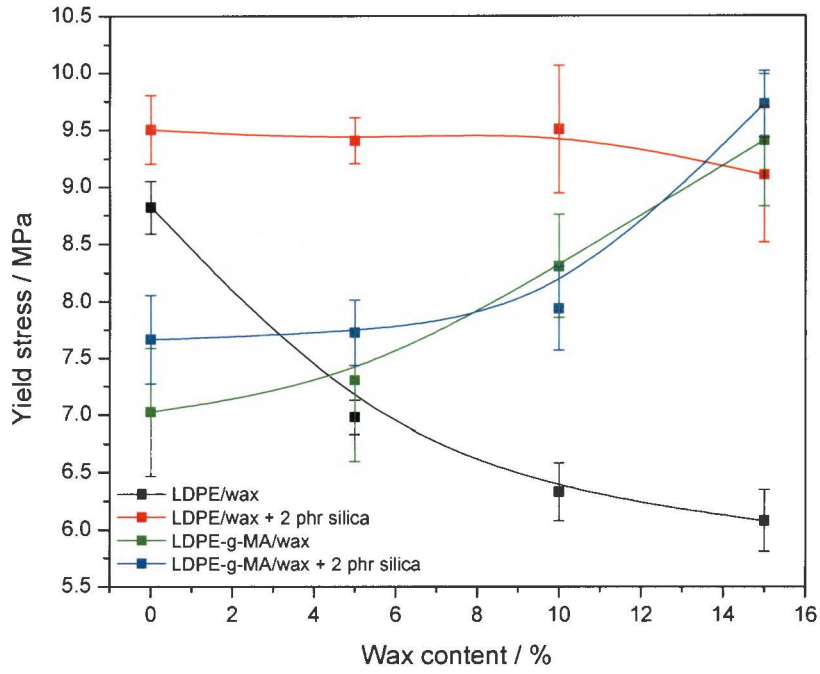

Figure 4.21 Stress at yield of LDPE/wax and LDPE-g-MA/wax blends and blend nano-composites

A significant decrease in yield stress is observed for the LDPE/wax blends with an increase in wax content, while the yield stress for the LDPE/wax blend nano-composites did not change significantly. The decrease in the absence of silica is probably the result of the shorter, more extended chains of the wax that are fairly uniformly dispersed in the polymer matrix. When silica is present, the wax seems to be more concentrated around the silica particles. This, and the observed increase in crystallinity (see Table 4.2), may be the reasons for the negligible change in yield stress. The presence of silica alone slightly increases the yield stress in both polymers. It is generally known that during yielding, there is irreversible movement of polymer chain segment and slippage of crystallites. The higher yield stress could be attributed to the silica reducing the mobility of the polymer chains, with a resultant higher stress needed

before yielding occurs. The presence of the maleic anhydride functional group decreases the yield stress of LDPE-g-MA and LDPE-g-MA + 2 phr silica (Table 4.4). This is the result of the plasticization effect by the functional group (maleic anhydride increases the amorphous phase of the material).

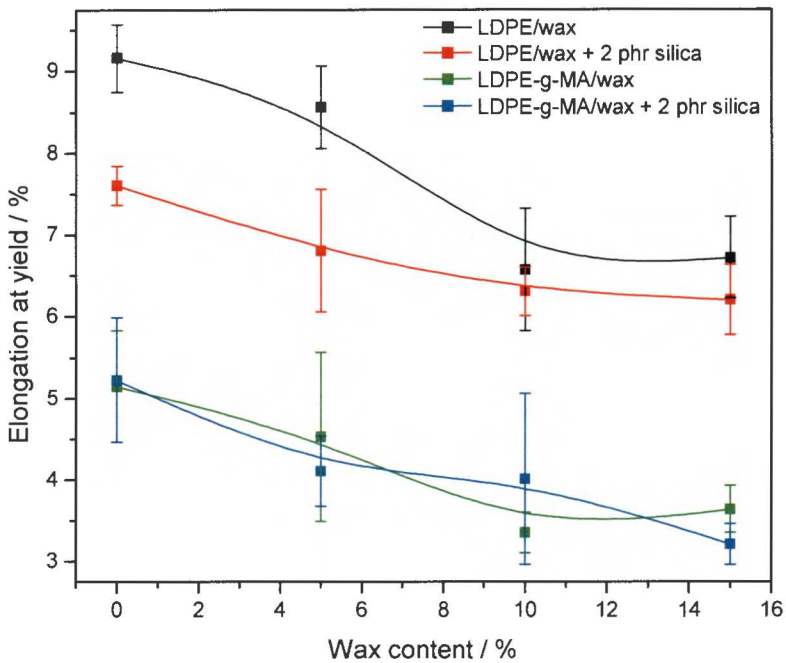

Figure 4.22 Elongation at yield of LDPE/wax and LDPE-g-MA/wax blends and blend composites

The effect of wax content on the elongation at yield of the samples is shown in Figure 4.22. The elongation at yield decreases with an increase in wax content for all the investigated samples. This could be associated with the presence of short wax chains in the amorphous phase of the polymer. In the presence of the short (and linear) chains, due to their lower viscosity, structural rearrangements of the amorphous phase prior to the macroscopic yield point will be easier. This effect and the effect of a reduction in the amorphous phase in the case of the composites (as a result of the increase in crystallinity) will induce the beginning of plastic deformation at lower strains. The influence of the presence of silica nano-particles depends on the type of polymer in the system. Firstly, the presence of silica reduces the elongation at yield of LDPE, but the influence is smaller at higher wax contents. This is probably related to the influence of silica on the polymer chain mobility, and the reduction of this influence in the presence of the wax because of the preferable crystallization of the wax around the silica nano-particles. Secondly, the presence of silica had very little influence on

the elongation at yield of LDPE-g-MA and its blends at all wax contents. The reason for this is not entirely clear, but a complex set of interactions between the grafted polymer, the functionalized wax and the silica probably contributes to this observation.

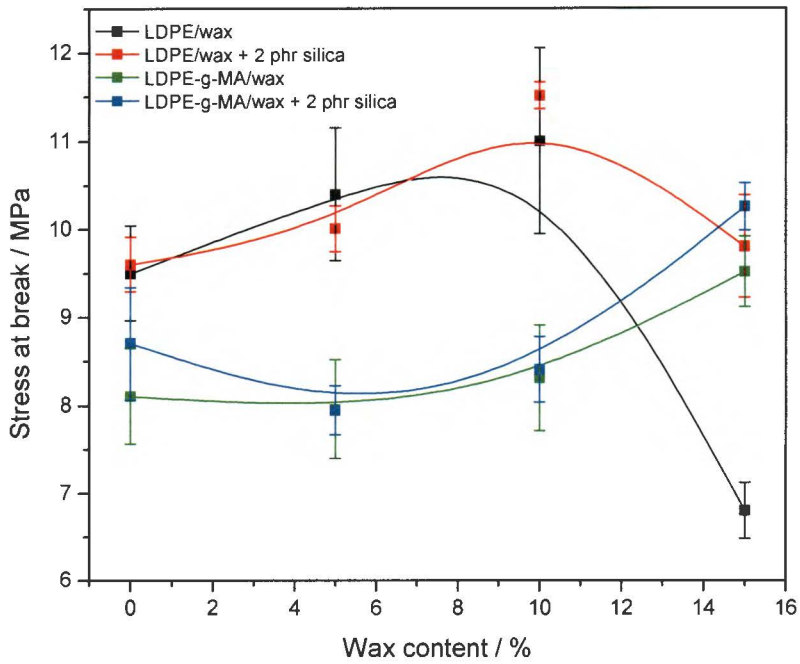

Figure 4.23 Stress at break of LDPE/wax and LDPE-g-MA/wax blends and blend composites

The effect of wax content on the tensile strength is shown in Figure 4.23. For both LDPE and its nano-composite, the tensile strength initially increases with increasing wax content, but it decreases for the highest wax content. The initial increase can be attributed to the co-crystallization of the LDPE and the wax. At the highest wax content, the observed decrease can be attributed to the phase separation of the LDPE and wax, where the separate wax crystals in the amorphous phase act as defect points. The presence of silica alone has little influence on the tensile strength of LDPE (Table 4.4). This can be attributed to the quantity of silica used that showed an insignificant influence on stress transfer. The decrease in tensile strength at higher wax contents is more significant in absence of silica. This can again be related to the fact that, in the absence of silica, the wax crystallizes in the amorphous phase of the LDPE and the wax crystals form defect points that induce stress cracking at lower stresses. The LDPE-g-MA samples initially show little change in tensile strength with increasing wax content, but there is an obvious increase for the highest wax content. The presence of silica slightly improves these values. This may be explained by the fact that, at all

wax concentrations there was no phase separation of the wax and the polymer. The stronger interaction between the wax and the polymer causes the general increase in tensile strength with increasing wax content. In the case of the nano-composites, the presence of silica strengthened the matrix, probably due to strong interfacial interaction between the components. A good interface will restrict the deformation of the polymer and wax chains around the silica, hence a higher tensile strength.

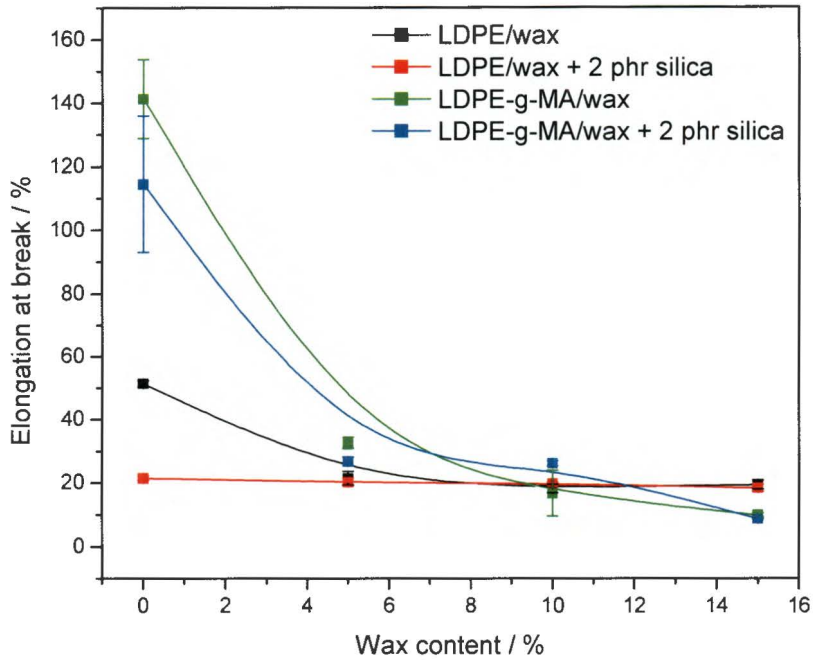

Figure 4.24 Elongation at break of LDPE/wax and LDPE-g-MA/wax blends and blend composites

The effect of wax content on the elongation at break is shown in Figure 4.24. In the presence of silica, the elongation at break of both LDPE and LDPE-g-MA reduces, although the effect is less significant in the case of LDPE-g-MA. This is probably the result of the reinforcement effects of silica, because the material becomes stronger, but the mobility of the chains is changed and they lose the ability to absorb the energy that results from the changing conformation. The effect is less significant in the case of LDPE-g-MA because of the increase in the amorphous fraction after grafting. The presence of wax had little influence on the elongation at break of LDPE + 2 phr silica, because the elongation at break is already low as a result of the silica nano-particles acting as defect points. In the case of LDPE the elongation at break in the absence of wax is higher, while crystallization of the wax in the amorphous phase of the LDPE leads to reduced elongation at break values. There is a significant decease in

elongation at break with increasing wax content for both LDPE-g-MA and its nano-composite. The reason for this is probably the more efficient co-crystallization of the wax with LDPE-g-MA and the resultant decrease in number of tie chains [13].

4.7 Dynamic mechanical analysis (DMA)

The storage modulus is the component of the applied normal stress which is in phase with the normal strain, divided by the strain. It is approximately similar to the Young's or elastic modulus, or stiffness. The loss modulus is a measure of the energy absorbed due to relaxation and it is useful in clarifying the mechanism of internal motion. The damping factor (tan δ) is the ratio of the loss modulus to the storage modulus. It may also be obtained as the ratio of the real part to the imaginary part of the complex viscosity.

4.7.1 Effect of silica and anhydride grafting on the viscoelastic properties of LDPE

The effect of silica and anhydride grafting on the storage modulus, loss modulus and damping factor of LDPE is shown in Figures 4.25 to 4.27. There is a decrease in storage modulus with increasing temperature for all the samples, and there are changes in the rate of decrease around -29 °C. The storage modulus starts increasing around 25 °C with the formation of a peak at about 50 °C. This is not a typical observation for storage modulus as function of temperature, but it was observed for all the investigated samples, and currently the only explanation is that it is related to the melting of the thinnest lamellae. The loss modulus curves show peaks around -29 °C and 70 °C (Figures 4.26). These transitions may be attributed to the β- and α-relaxations. Polyethylenes generally show three transitions, namely γ-, β- and α-transitions, before melting. The γ-relaxation occurs in the amorphous phase around -120 °C and some authors attribute it to the glass transition [14,15]. The β-transition between 0 and -50 °C is attributed to the movement of very loose folds and relatively non-extended chains, and some authors attribute this transition to glass transition [16,17]. The α-relaxation in the temperature range 50 to 100 °C is associated with an interlamellar shear process in the crystalline phase and to inhomogeneous crystallinity in the sample.

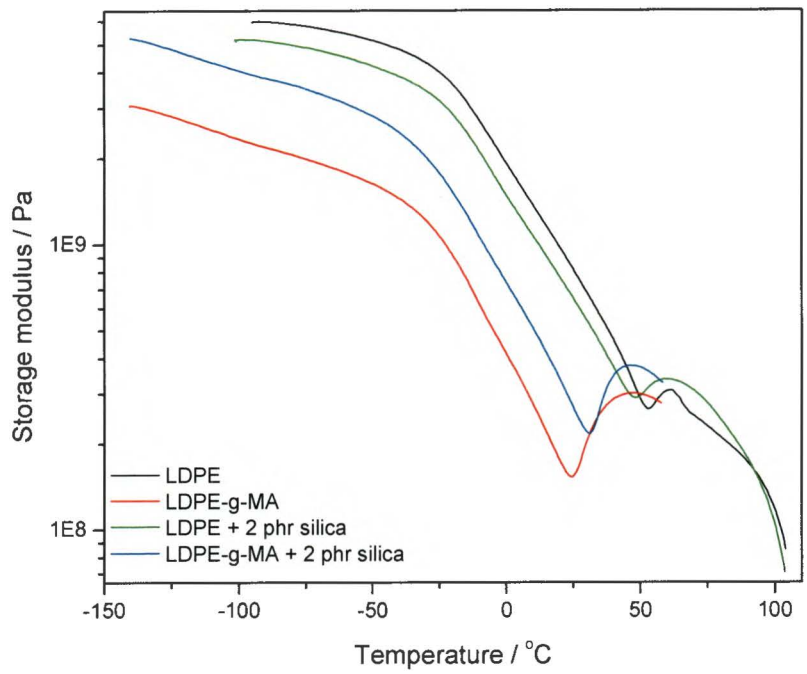

Figure 4.25 DMA storage modulus curves of LDPE, LDPE-g-MA, LDPE + 2 phr silica and LDPE-g-MA + 2 phr silica

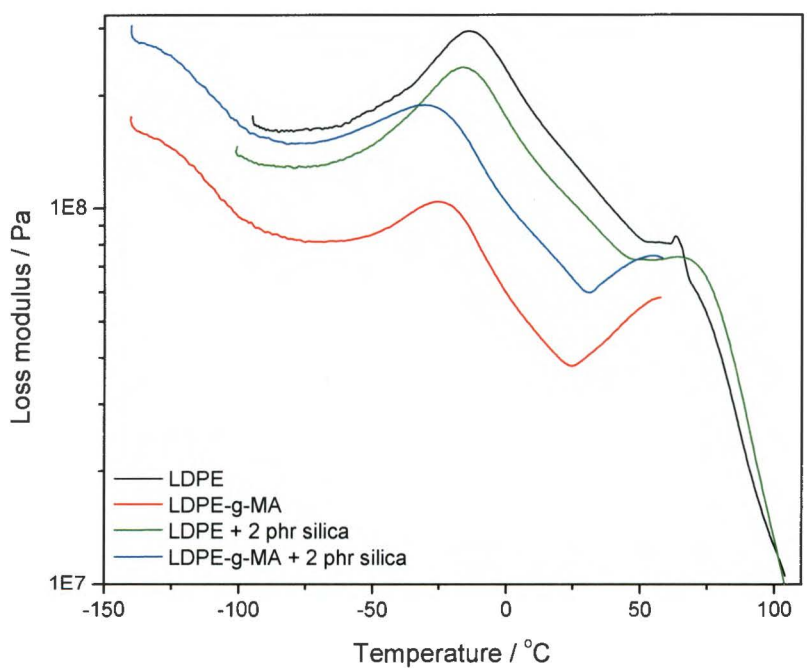

Figure 4.26 DMA loss modulus curves of LDPE, LDPE-g-MA, LDPE + 2 phr silica and LDPE-g-MA + 2 phr silica

The presence of silica alone does not seem to significantly influence the storage modulus of LDPE (the storage modulus curves of LDPE and LDPE + 2 phr silica in Figure 4.25 are very close to each other), but at temperatures below that of the α-transition, the presence of silica causes an increase in the storage modulus of LDPE-g-MA. This increase is probably due to the good interfacial adhesion between the polymer and the silica particles as a result of the maleic anhydride grafting, and is in line with changes in the Young's modulus (see section 4.6). LDPE-g-MA has a lower storage modulus than LDPE, LDPE + 2 phr silica and LDPE-g-MA + 2 phr silica at all temperatures. This could be attributed to an increased amorphous phase as a result of the presence of maleic anhydride functional groups.

The influence of maleic anhydride grafting and the presence of silica on the loss modulus are shown in Figure 4.26. The storage and loss moduli follow the same trend, and therefore they could be explained in the same way. β-transition peaks of the grafted samples appeared at lower temperatures compared to the ungrafted ones. This could be attributed to the increased amorphous phase as a result of the presence of the functional group.

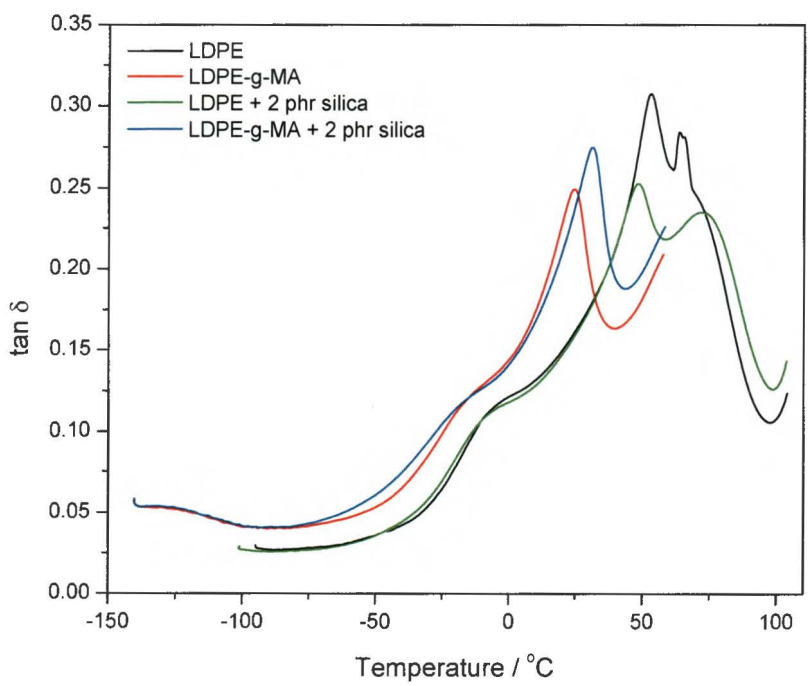

Figure 4.27 DMA damping factor curves of LDPE, LDPE-g-MA, LDPE + 2 phr silica and LDPE-g-MA + 2 phr silica

Figure 4.27 compares the damping factor (tan δ) curves of LDPE, LDPE-g-MA and their nano-composites. All the samples show a peak shoulder between 0 and -25 °C, which is the result of the β-relaxation. As in the loss modulus curves, these peaks are at a lower temperature for the maleic anhydride grafted samples. The well-defined peaks at higher temperatures are, however, difficult to interpret as a result of the apparent melting of thin lamellae which starts around 50 °C. The observed multiple peaks are therefore a mixture of transitions related to interlamellar shear and melting of thin crystallites occurring in the same temperature region.

4.7.2 The effect of oxidized wax on the viscoelastic properties of LDPE and its nanocomposites

The effect of the wax content on the storage modulus, loss modulus and damping factor of the LDPE/wax blends is shown in Figures 4.28 to 4.30, and those of the LDPE/wax blend composites in Figures 4.31 to 4.33. From Figure 4.28 it is difficult to establish a trend for the influence of wax content on the storage modulus of LDPE, because the curves for LDPE and LDPE with respectively 10 and 15% wax are almost the same below 50 °C, while the presence of 5% wax gave rise to significantly higher values at all temperatures. This may be the result of the miscibility (co-crystallization) of LDPE and wax at low wax contents.

The values of the loss modulus show the same trend (Figure 4.29), and the β- and α-transitions are clearly visible for all the samples. There is an obvious shift of the β-transition to lower temperatures after introduction of the wax, which can be attributed to the plasticizing effect of the wax in the amorphous fraction. The presence of wax or wax content does not seem to have any influence on the damping characteristics of the samples at temperatures below the α-transition (Figure 4.30), but the presence of wax clearly has an influence on the energy dissipation around the α-transition, which seems to decrease with increasing wax content.

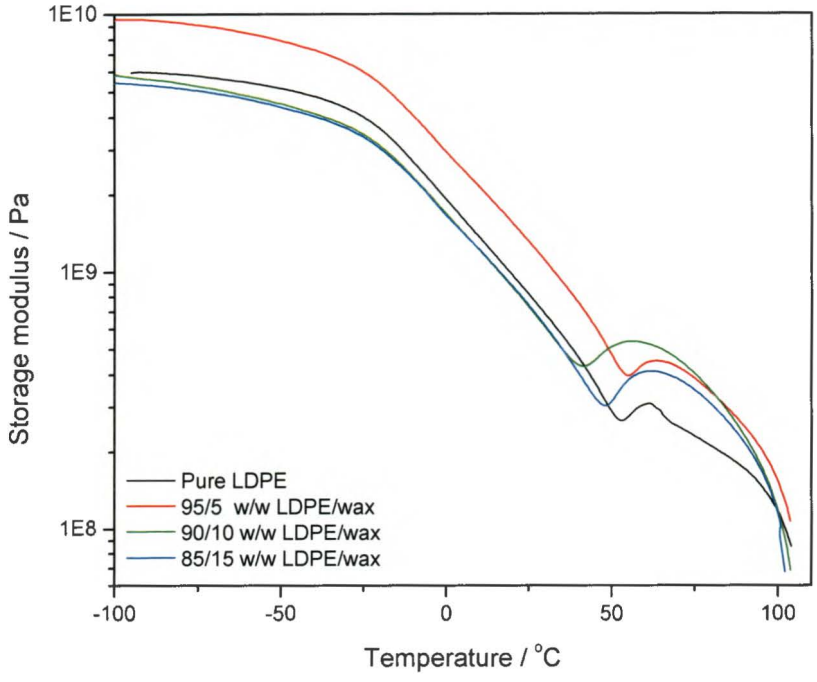

Figure 4.28 DMA storage modulus curves of pure LDPE and the LDPE/oxidized wax blends

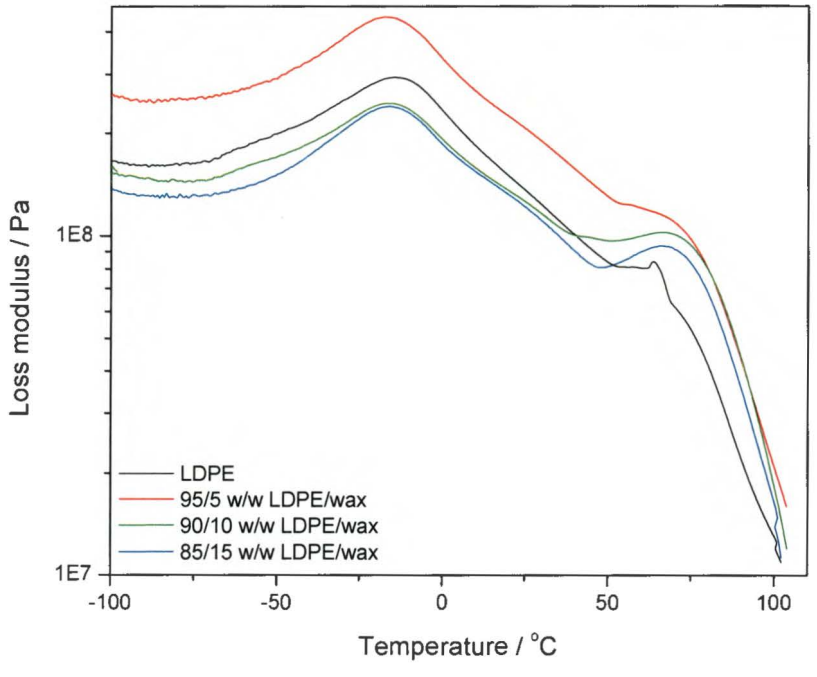

Figure 4.29 DMA loss modulus curves of pure LDPE and the LDPE/wax blends

There are observable transitions at -25 °C (β-relaxation) and 25-75 °C (Figure 4.30). The presence and content of wax do not seem to influence the temperature of the β-relaxation. Again the multiple peaks around 50 °C are difficult to interpret, but it is interesting that the lower-temperature peak moves to even lower temperatures, while the higher-temperature peak moves to even higher temperatures with an increase in wax content. It seems as if the presence and content of wax have an influence on both the melting of thin crystallites and interlamellar shear in LDPE. However, the exact nature of this influence is not clear.

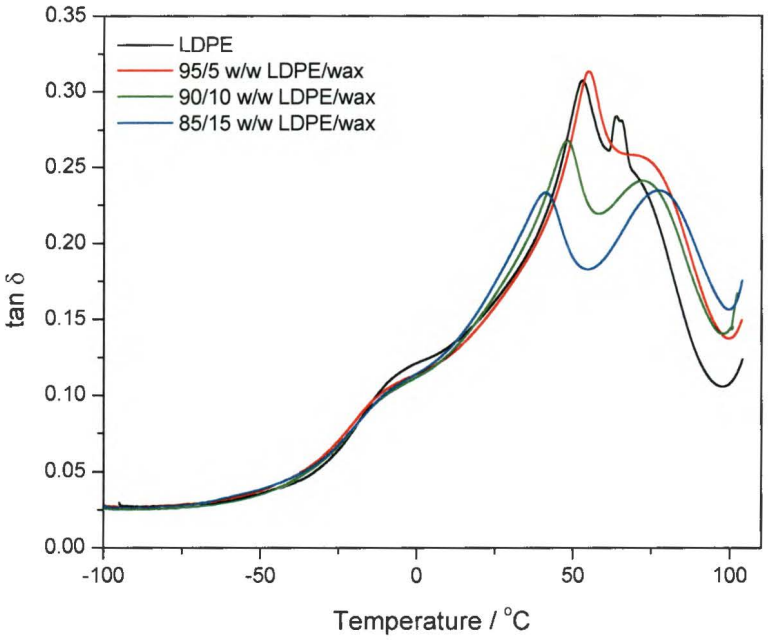

Figure 4.30 DMA damping factor curves of LDPE and the LDPE/wax blends

Although the LDPE/wax blend composites also do not show a specific trend of increase or decrease in storage modulus with increasing wax content (Figures 4.31), it is interesting in this case that the values are lower for the 5% wax containing sample. Although the reason for this is not entirely clear, it is clear that the presence of silica nanoparticles and the stronger interaction between these particles and the wax have an observable influence on the sample morphology and chain mobility of the polymer chains. The loss modulus curves in Figure 4.32 also do not show a specific trend with respect to the amount of wax in the samples, and the β- and α-relaxation peaks look similar an may be explained in a similar way to those of the LDPE/wax blends (Figure 4.29).

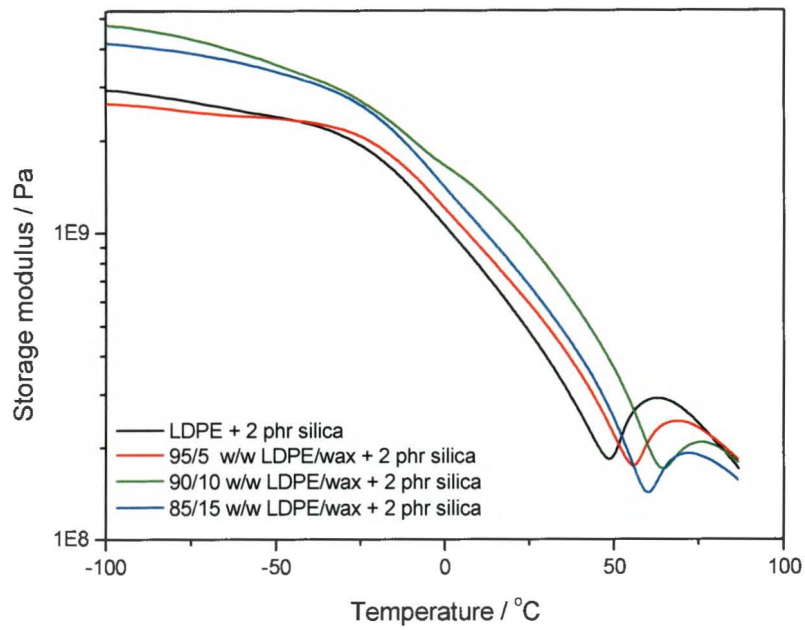

Figure 4.31 DMA storage modulus curves of the LDPE nanocomposite and the LDPE/wax blend nanocomposites

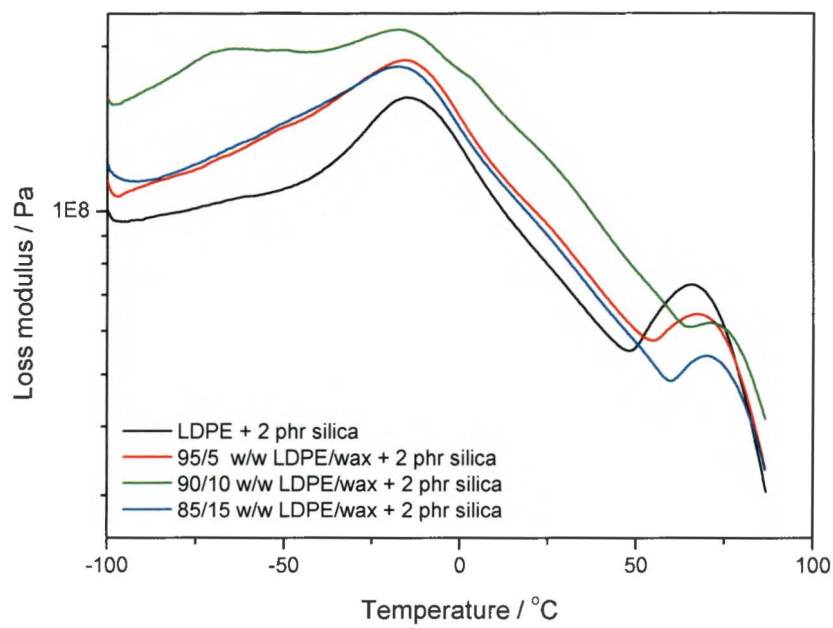

Figure 4.32 DMA loss modulus curves of the LDPE nanocomposite and the LDPE/wax blend nanocomposites

The damping factor curves (Figure 4.33), however, show different behaviour from those of the LDPE/wax blends (Figure 4.30). In this case the lower-temperature peak in the α-relaxation temperature region moves to a higher temperature with increasing wax content, while the higher-temperature peak does not seem to change with increasing wax content, so that the higher-temperature peak seems to disappear because of merging of the two peaks. It is thus clear that the presence of silica nano-particles causes the wax to have a different influence on the melting of thin crystallites and interlamellar shear in LDPE, probably because of the stronger interaction between the wax and the nano-particles which gives rise to a different sample morphology.

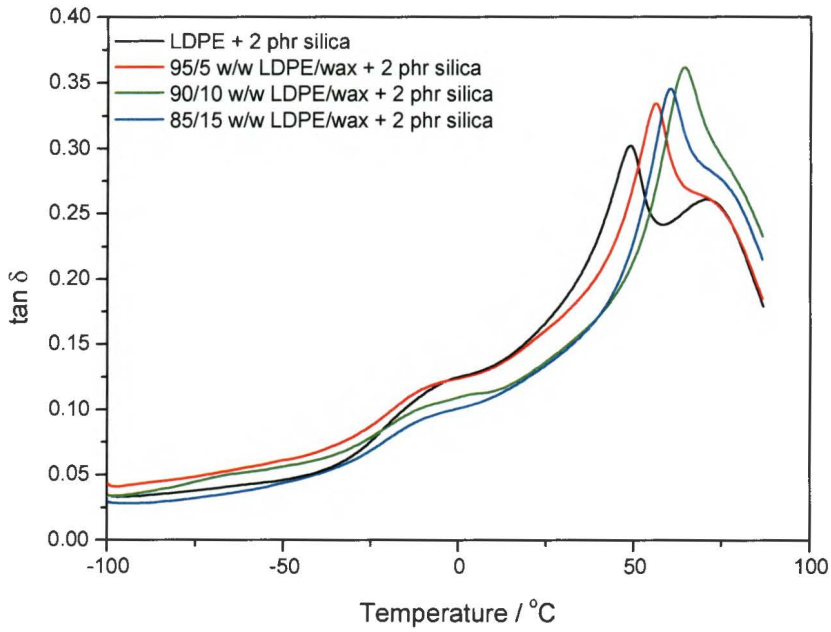

Figure 4.33 DMA damping factor curves of the LDPE nanocomposite and the LDPE/wax blend nanocomposites

4.7.3 The effect of oxidized wax on the viscoelastic properties of LDPE-g-MA and its nanocomposites

The effect of the wax content on storage modulus, loss modulus and damping factor curves of the LDPE-g-MA/wax blends is shown in Figures 4.34 to 4.36, and on those of the LDPE-g-MA/wax blend composites in Figure 4.37 to 4.39. The observations are similar to those for the LDPE/wax blends and LDPE/wax/silica composites, except that the wax does not seem to have such a big influence on the tan δ peaks in the α-relaxation temperature region. This is

most probably the result of the much stronger interaction between the maleic anhydride grafted LDPE, the oxidized wax and the silica nano-particles.

The β-transition temperatures of the wax-containing samples of the LDPE-g-MA/silica nanocomposites (Figure 4.38) are higher than that of the LDPE-g-MA/silica nanocomposite. This behaviour is the different from that of the LDPE/silica nanocomposites (Figure 4.32), where wax does not have any influence on the position of the β-transition. The stronger interaction between the oxidized wax and the MA grafted polymer could account for the shift in the β-transition, because the wax crystals can immobilize the LDPE-g-MA chains.

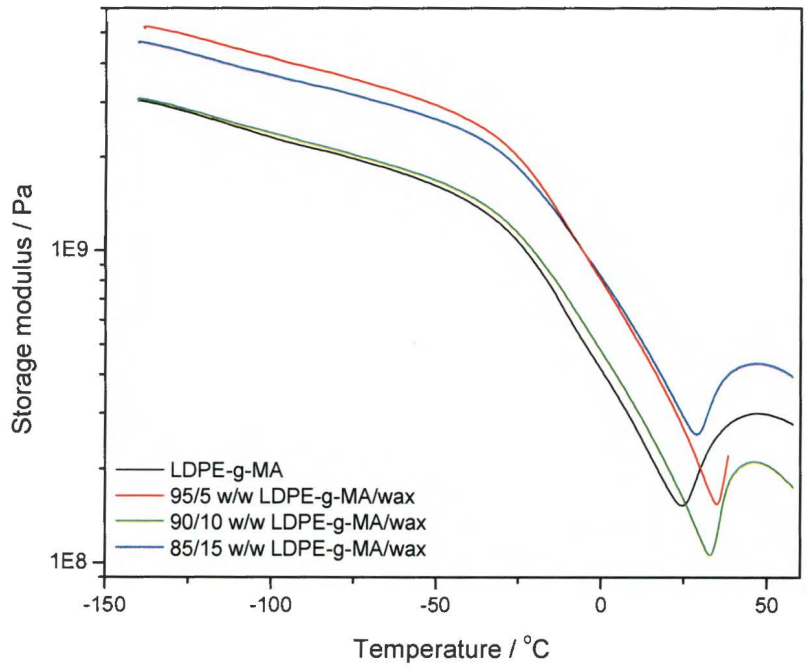

Figure 4.34 DMA storage modulus curves of pure LDPE-g-MA, and the LDPE-g-MA/ wax blends

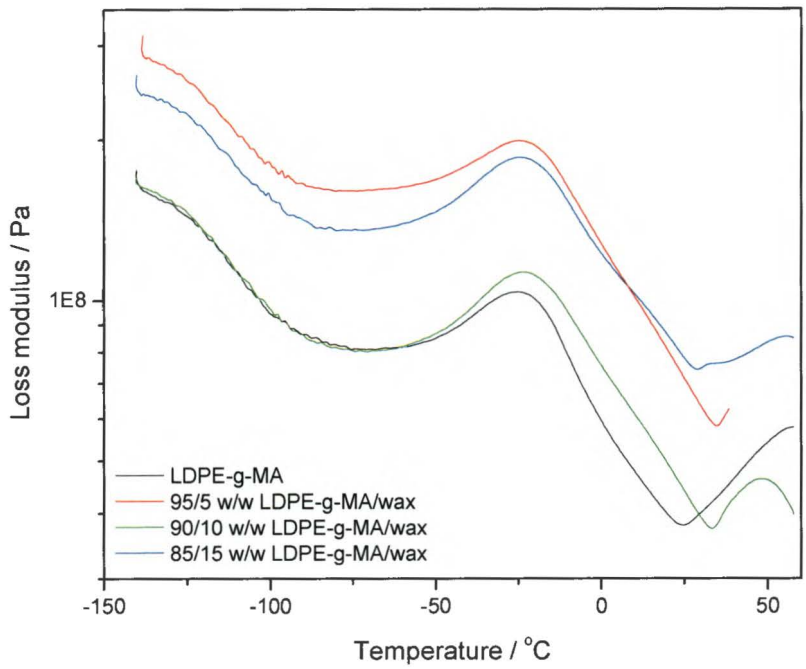

Figure 4.35 DMA loss modulus curves of LDPE-g-MA and the LDPE-g-MA/wax blends

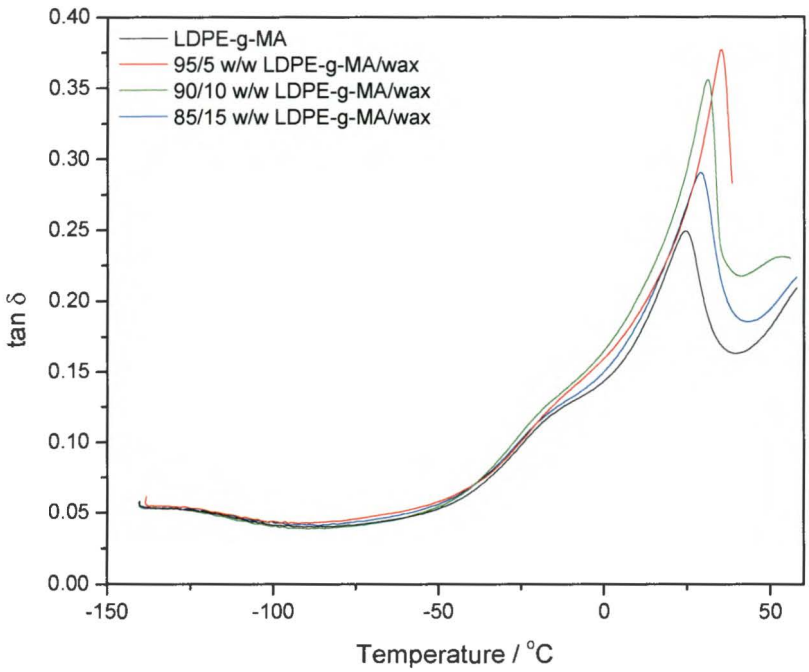

Figure 4.36 DMA damping factor curves of LDPE-g-MA and the LDPE-g-MA/wax blends

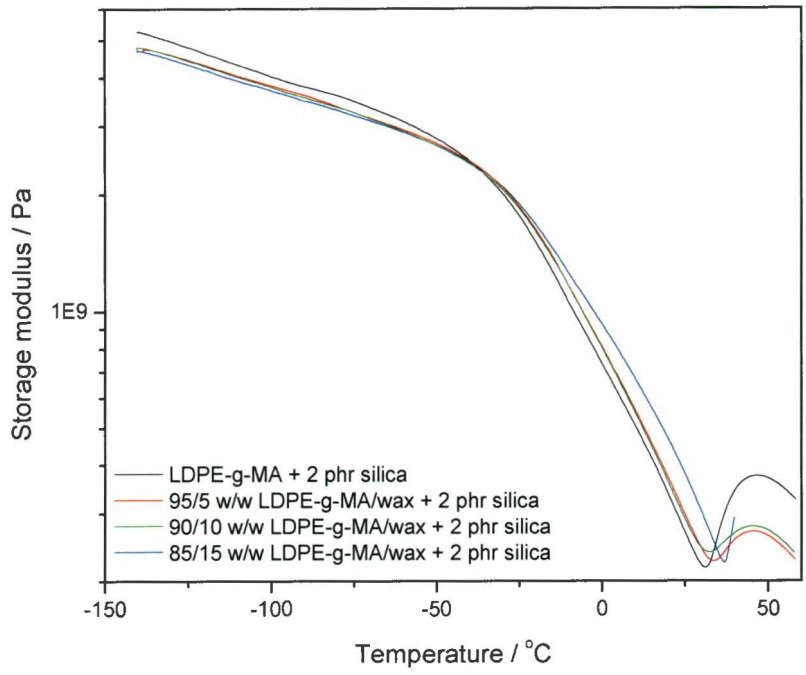

Figure 4.37 DMA storage modulus curves of the LDPE-g-MA nanocomposite and the LDPE-g-MA/wax blend nanocomposites

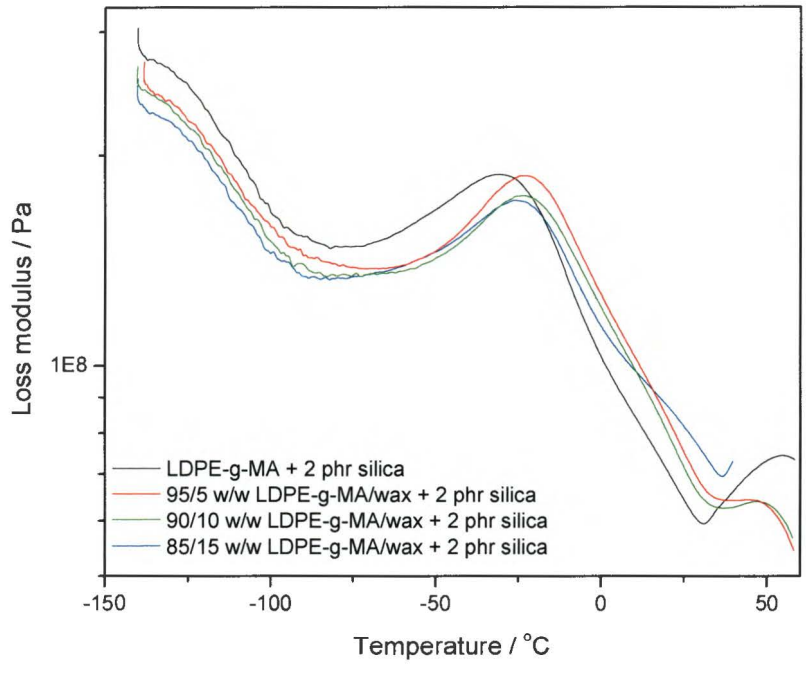

Figure 4.38 DMA loss modulus curves of the LDPE-g-MA nanocomposite and the LDPE-g-MA/wax blend nanocomposites

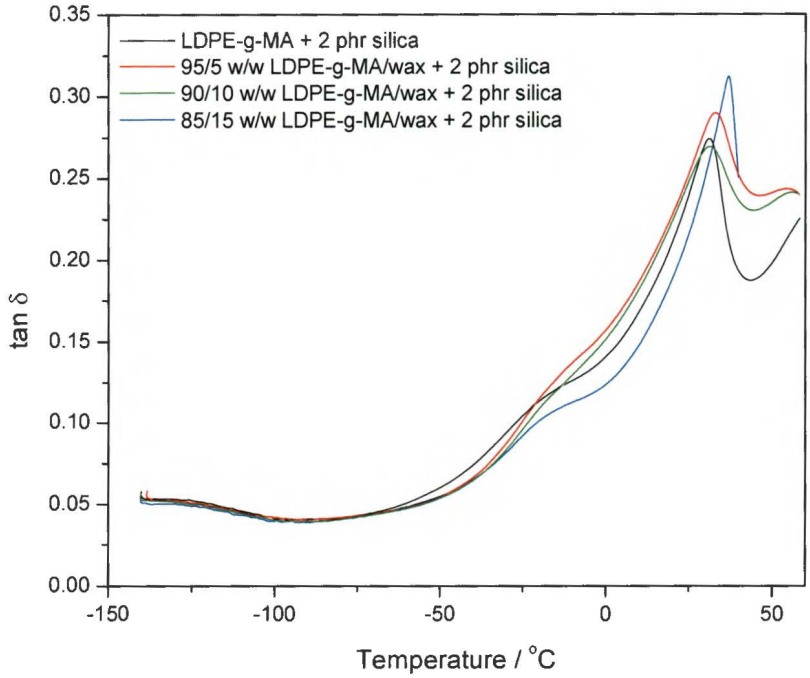

Figure 4.39 DMA damping factor curves of the LDPE-g-MA nanocomposite and the LDPE-g-MA/wax blend nanocomposites

4.7 References

1. J.C.Z. Hernández, M.S. Sánchez, J.L.G. Ribelles, M.M. Pradas. Polymer-silica nanocomposites prepared by sol-gel technique: Nanoindentation and tapping mode AFM studies. European Polymer Journal (2007) 43:2775-2783.
2. K.H. Nitta, A. Tanaka. Dynamic mechanical properties of metallocene catalyzed linear polyethylenes. Polymer (2001) 42:1219-1226.
3. L.C. Simon, R.F. de Souza, J.B.P. Soares, R.S. Mauler. Effect of molecular structure on dynamic mechanical properties of polyethylene obtained with nickel-diimine catalysts. Polymer (2001) 42:4885-4892.
4. Z. Zhou, H. Zhai, W. Xu, H. Gou, G. Liu, W.P. Peng. Preparation and characterization of PE and PE-g-MAH-styrene/montmorillonite nanocomposites. Journal of Applied Polymer Science (2006) 101:805-809.
5. S.K. Singh, S.P. Tambe, A.B. Samui, V.S. Raja, D. Kumar. Maleic acid grafted low density polyethylene for thermally sprayable anticorrosive coatings. Progress in Organic Coatings (2006) 55:20-26.

6. A.S. Luyt, R. Brüll. Investigation of polyethylene-wax blends by CRYSTAF and SEC-FTIR. Polymer Bulletin (2004) 52:177-183.
7. A.S. Luyt, I. Krupa. Thermal behaviour of low and high molecular weight paraffin waxes used for designing phase change materials. Thermochimica Acta (2008) 467:117-120.
8. V. Djoković, T.N. Mtshali, A.S. Luyt. The influence of wax content on the physical properties of low-density polyethylene-wax blends. Polymer International (2003) 52:999-1004.
9. D.J. Peterson, S. Vyazovkin, C.A. Wight. Kinetics of thermal and thermo-oxidative degradation of polysterene, polyethylene and poly(propylene). Macromolecular Chemistry and Physics (2001) 2002:775-784.
10. Y. Wang, F.B. Chen, K.C. Wu. Effect of the molecular weight of maleated polypropylenes on the compounding of polypropylene/organoclay nanocomposites. Journal of Applied Polymer Science (2005) 97:1667-1680.
11. H. Zhai, W. Xu, H. Gou, Z. Zhou, S. Shen, Q. Song. Preparation and characterization of PE and PE-g-MAH/montmorillonite nanocomposites. European Polymer Journal (2004) 40:2539-2545.
12. I. Krupa, A.S. Luyt. Physical properties of blends of LLDPE and an oxidized paraffin wax. Polymer (2001) 42:7285-7289.
13. S.P. Hlangothi, I. Krupa, V. Djokovic, A.S. Luyt. Thermal and mechanical properties of cross-linked and uncross-linked polyethylene-wax blends. Polymer Degradation and Stability. 2003: 79(1):53-59.
14. A. Pegoretti, M. Ashkar, C. Migliaresi, G. Marom. Relexation process in polyethylene fibre reinforced polyethylene. Composites Science and technology (2000) 60:1181-1189.
15. M. Matsuo, L.M.M. Azuma, H. Chunqing, T. Suzuki. Characteristic of ultradrawn polyethylene films as function of temperature estimated by the positron annihilation lifetime method. Macromolecules (2002) 35:3059-3065.
16. Y. Alone, G. Marom. On the β Transition in high density polyethylene: the effect of transcrystallinity. Macromolecular Rapid Communication (2004) 25:1387-1391.
17. M.L. Cerrada, R. Benavente, E. Pérez. Effect of short glass fiber on structure and mechanical behavior of an ethylene-1-octene copolymer. Macromolecular Chemistry and Physics (2001) 202:2686-2695.

CHAPTER 5

CONCLUSIONS

The purpose of the study was to investigate the influence of sol-gel prepared silica on the thermal and mechanical properties of low-density polyethylene (LDPE) and maleic anhydride grafted LDPE (LDPE-g-MA), as well as the influence of an oxidized paraffin wax as possible compatibilizer between the polymer and filler.

As expected, the FTIR analyses of LDPE and the LDPE/silica composite showed that there was no interaction between the matrix and the filler. The silica was also not well dispersed in the LDPE matrix. However, despite the lack of interaction and the poor dispersion of silica nano-particles in the LDPE matrix, the silica had a significant influence on the LDPE crystallization behaviour. The total crystallinity of the LDPE (as indicated by the melting enthalpy) was about 10% lower than expected for the sample mixed with silica nano-particles. The presence of the silica nano-particles had little influence on the thermal stability and tensile properties of LDPE, except for the elongation at break which was significantly reduced. Both the storage and loss modulus of LDPE were slightly reduced over the whole investigated temperature range in the presence of silica, which is probably the result of the weak interaction between the LDPE and filler.

There was also no interaction between the LDPE and the oxidised wax, and the wax seemed to be miscible with the LDPE up to 10% wax content. The melting temperature of LDPE slightly decreased with increasing wax content, probably because of the plasticizing effect of the molten wax. Up to 10% wax in LDPE reduced the sample crystallinity, but the crystallinity increased for the 15% wax containing sample, probably because of the formation of separate wax crystals in the amorphous phase of the polymer. The thermal stability of the LDPE/wax blends decreased with increasing wax content. The stress and strain at yield, as well as the elongation at break were lower for the wax containing samples, but wax content did not seem to significantly influence these properties. The tensile strength increased with increasing wax content up to 10% wax content, but decreased for the 15% wax containing sample, probably because of the presence of wax crystals in the amorphous phase of LDPE that acted as defect points. The co-crystallization of LDPE and wax at low wax contents, the

separate crystallization of part of the wax at higher wax contents, and the plasticizing effect of the wax on the LDPE matrix were all reflected in the DMA results.

FTIR analysis of LDPE/wax/silica composites showed that there was an interaction between oxidised wax and silica. Despite the poor dispersion of wax in the LDPE/wax/silica composites, the presence of wax reduced the agglomeration of silica. In contrast to the LDPE/wax blends, the melting temperatures remained fairly constant for the silica containing samples, which suggests that the silica was preferably covered by wax. At the lowest wax content in the composite the sample crystallinity was lower, but it increased with an increase in wax content. The thermal stability of the composites decreased with increasing wax content, but the composites have higher thermal stabilities than their comparable blends. The tensile strength and modulus increased with increasing wax content up to 10% wax content, but decreased for the 15% wax containing sample, probably because of the presence of silica which inhibited the co-crystallization of the wax with the polymer. The DMA results of the LDPE/wax/silica composite samples show that the presence of silica nanoparticles and the stronger interaction between these particles and the wax have an observable influence on the sample morphology and chain mobility of the polymer chains.

Because of the presence of the cyclic anhydride groups there was an interaction between the polymer and the silica particles. This could account for the smaller silica agglomerates. The total crystallinity of the LDPE-g-MA (as indicated by the melting enthalpy), for the sample mixed with silica nano-particles, was about 20% lower than expected. This was attributed to the interaction between the nano-silica and the matrix, which reduced the polymer chain mobility and inhibited crystallization. The presence of the silica nanoparticles had little influence on the thermal stability of the samples, probably because of the low filler content. Young's modulus, yield stress and tensile strength of LDPE-g-MA improved in the presence of silica nano-particles, probably because of the better interaction between the polymer and the silica particles. This improved interaction also gave rise to slightly higher storage and loss moduli over the whole investigated temperature range.

There was also interaction between the LDPE-g-MA and oxidised wax, and the wax seemed to be miscible with the grafted polymer at all the investigated concentrations. This is probably due to the interaction between the polymer and wax that promoted co-crystallization. The crystallinity and thermal stability of these blends followed the same trend with increase in

wax content as those of the LDPE/wax samples. Strain at yield and break decreased with increasing wax content, probably because of the more efficient co-crystallization of the wax with LDPE-g-MA and the resultant decrease in number of tie chains. Tensile strength, modulus and yield stress increased with increasing wax content, which was explained as being the result of the interaction between the functionalised polymer and wax. The DMA results also reflected this interaction.

FTIR and TEM analyses of the LDPE-g-MA/wax/silica nano-composites showed that there was an interaction between the different components and a reduction in silica agglomeration. The wax seemed to be miscible with the polymer up to 10% wax content. At 15% wax content a second endotherm appeared in the wax melting temperature region, which was attributed to partial miscibility of the LDPE-g-MA and wax in the crystalline phase. The melting temperatures of the LDPE-g-MA/wax blend composites remained fairly constant, and were slightly lower than those of the LDPE-g-MA/wax blends. The crystallinity increased with an increase in wax content compared to their respective blends, and this was attributed to more efficient co-crystallization of the LDPE-g-MA and the wax. Neither the wax nor the silica had a major influence on the degradability of LDPE-g-MA. The presence of silica nano-particles in LDPE-g-MA/wax had little influence on the tensile and dynamic mechanical properties.

To summarise, all the LDPE properties were observably influenced by the presence of silica nanoparticles, maleic anhydride grafting and/or the presence of oxidised wax. The strongest influence was observed in the samples where there were interactions between functional groups on LDPE-g-MA, oxidised wax and/or nano-silica. Future research in this field may concentrate on the use of different amounts of nano-silica, different types of polyethylenes, and different MA grafting levels. It may also be a worthwhile exercise to establish the exact nature of the interactions between the different functional groups.